VTT Technical Research Centre of Finland

Constrained Thermochemistry for Process Digitalization

Nappa, Marja; Koukkari, Pertti; Pajarre, Risto; Penttilä, Karri; Nappa, Marja; Blomberg, Peter; Roth, Andreas; Kangas, Petteri; Koukkari, Pertti

Published: 15/06/2021

Document Version
Publisher's final version

[Link to publication]

Constrained Thermochemistry for Process Digitalization

Editors: Marja Nappa, Pertti Koukkari

Authors: Risto Pajarre, Karri Penttilä, Marja Nappa, Peter Blomberg, Andreas Roth, Petteri Kangas†, Pertti Koukkari

Confidentiality: Public

Report's title	
Constrained Thermochemistry for Process Digitalization	
Customer, contact person, address	**Order reference**
Janne Viemerö, Business Finland; Antti Roine, Outotec; Matias Hultgren, Outotec; Camilla Karlemo, Valmet; Sonja Enestam, Valmet; Kaisa Kiipula, Suomen malminjalostus; Jani Kiuru, Suomen Malmijalostus; Teuvo Kekko, Sulfator; Risto Aurola, Sulfator; Erkki Räsänen, Langis; Eero Antikainen, Savonia	
Project name	**Project number/Short name**
DeepCleanTech	118887 DeepCleanTech
Author(s)	**Pages**
Risto Pajarre, Karri Penttilä, Marja Nappa, Peter Blomberg, Andreas Roth, Petteri Kangas†, Pertti Koukkari	83/
Keywords	**Report identification code**
ChemSheet, constraint free energy (CFE), thermodynamics, multi-phase chemistry, sulphate reducing bacteria, reaction constraints, Gibbs energy minimization, affinity, extent of reaction (EOR), phase diagrams, partial equilibria, supersaturation, oxidation-reduction potentials, lime kiln, LIFAC, neural networks	VTT-R-01210-20

Summary

The report summaries a set of computational studies applying process digitalization in terms of thermodynamics, biological modelling and artificial intelligence. The approach is based on computational chemical thermodynamics with special emphasis on advanced applications of VTT's unique Constrained Free Energy (CFE) method, the use of which in VTT's ChemSheet and KilnSimu software is shortly reviewed.

The present work introduces systematic and automated method to add several reaction constraints to thermodynamic multicomponent system and thus widens the applicability of CFE in *e.g.* biochemical systems, which often have multiple reactions to be constrained. The developed methodology can be applied also inversely to the addition of equilibrium reactions to kinetic reaction systems. In addition, the tools of modelling bioprocesses combined with CFE modelling have been tested using Sulphate Reducing Bacteria (SRB) reactor as an example process. Moreover, a CFE related constraint deduced from the saturation index is used to calculate supersaturation conditions in aqueous solutions. The reaction constraint is further applied for computing oxidation-reduction potentials in non-equilibrium redox systems.

An additional new development of CFE method is its usage to produce phase diagrams for time-dependent reactive systems using extents of reaction as diagram axis. Applying such diagrams, the dynamic reaction conditions can be analysed graphically without doing elaborate and time-consuming kinetic experiments. Moreover, the simulation of time dependent features related to VTT's KilnSimu has been advanced with an application example for lime kiln in kraft recovery process.

Several new thermodynamic mixing models have been implemented to VTT's ChemSheet software. These include LIQUAQ and LIFAC electrolyte models to allow for coupling of electrolyte modelling with various vapour-liquid-liquid and solid phase systems. In addition, a new approach for computing highly concentrated aqueous solutions is presented by connecting the Pitzer activity model with the adsorption theory to enable modelling of aqueous multiphase multicomponent systems covering the range from dilute solutions to the hydrated salt instead of earlier applicability on diluted or medium concentrated solutions.

Machine learning (two-layer feed-forward neural network model) are applied for predicting mean activity coefficients for ion pairs in concentrated aqueous solutions. Further, the

methods applying neural networks in process modelling are investigated and different approaches to replace the first principle based process models partially or as a whole, are tested targeting at faster calculation and better predictions in systems with scarce data.

The developed models and methods are targeted to be used in chemical and process engineering tools and work. In the wider perspective the deep-tech digitalization is facilitating more efficient process operation and design and thus enable better product quality with lower consumption of energy and pristine raw materials in an environmentally friendly and more economic processes.

Confidentiality	Public

Espoo 15.6.2021

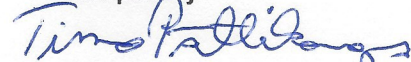| Written by	Reviewed by	Accepted by
Marja Nappa, Senior Scientist	Pertti Koukkari, Research Professor	Timo Pättikangas, Team leader

VTT's contact address

VTT Technical Research Centre of Finland Ltd, Tietotie 4E, 02044 VTT Espoo, Finland

Distribution

Project's steering group, Business Finland, VTT

Preface

This report contains the results from Constrained Thermochemistry for Process Digitalization research at VTT (DeepCleanTech Project 2018-2020). The focus of the study has been in process digitalization by applying means of computational thermodynamics, biological modelling and artificial intelligence. The technological approach is based on VTT's long term experience in multiphase chemical thermodynamics with special emphasis on new applications of the internationally awarded Constrained Free Energy method. The report contains 7 chapters and multiple subchapters which all share the common goal of using advanced modelling methods to support process industry in deep tech digitalization and further on to support development of fossil free, environmentally friendly processes with resilient practices in raw material and energy use. The authors acknowledge Business Finland – the Finnish Funding Agency for Innovation, the VTT Technical Research Centre of Finland, Outotec, and Valmet for funding and support this DeepCleanTech project. In addition, authors would like to acknowledge the support within the steering group from Finnish Minerals Group, Savonia, Sulfator and Langis.

Espoo 15.6.2021

Authors

Petteri Kangas (1976-2019) in memoriam

This report is dedicated to our beloved colleague Petteri Kangas. We miss you.

Petteri Kangas had a long and prosperous career at VTT in different positions: Senior Scientist, Team leader and most recently Research Manager. He experienced great respect amongst his colleagues. Petteri was widely known, and he was valued within VTT as well as outside of VTT. We miss Petteri and his professionalism and friendliness, his sense of humour as well his supportive and warm attitude toward others.

Contents

1. Introduction

Process digitalization is central to today's industrial strategy. In most Finnish industrial companies' computational expert systems, such as process advisers, digital twins, training simulators and extended databases are progressively advanced and used. As a key part of this development chemical modelling is increasingly utilised for technology improvement, process operation, customer services and marketing.

Cleantech business boosts the need to create methods for chemical recycling, management of non-process elements in process streams and response to the tightening environmental conditions. During the last two decades a great number of new elements (*e.g.* technology metals in the ICT sector) have been introduced in both industry and in consumer products while the material property data of their compounds and mixtures is missing or inadequate. At the same time the exponential growth of computer power has introduced new possibilities for data processing and generation by using means of computational science.

The research hypothesis in DeepCleanTech project was that by combining the deep understanding of first principle chemical thermodynamic models and modern computational techniques one can create new hybrid approaches which entails the benefits from both systems. The investigated research challenges included among the others the development of advanced methods for modelling aqueous systems for industrial and mining waters to cover concentration ranges from dilute solutions to precipitation limits; applying dynamic features in multiphase process modelling systems to exploit the delays in varying time scales; exploration of biochemical phenomena as a part of thermodynamic system; and investigate how the novel artificial intelligence techniques can be utilised in process modelling.

The report consists of seven chapters describing the adopted methods, based on advanced computational thermodynamics with key focus on contemporary problems in multiphase process chemistry. In the background chapter, the development history of the advanced thermodynamic algorithms and software of VTT is briefly reviewed. In Chapter 3 dynamic chemical systems are considered with three new applications of the Constrained Free Energy (CFE) technique. Use of CFE to reduction-oxidation (REDOX) potentials in time dependent systems is introduced and the saturation index (SI) is used as a new constraint in CFE modelling. It also implies the method to produce phase diagrams for time dependent reactive systems using the extent of reaction and the non-equilibrium driving force as diagram axis. In addition, the chapter includes a dynamic lime kiln model as an extension to the steady-state rotary drum simulator KilnSimu.

Chapter 4 considers modelling of highly concentrated aqueous solutions and brines with new added data in VTT's advanced aqueous database. It introduces the combination of adsorption models (BET, GAB) and Pitzer technique, which enables the modelling of aqueous solutions from infinitely diluted conditions to highly concentrated (precipitating) systems. It also presents the coupling of electrolyte models (LIQUAQ and LIFAC) and thermochemical multicomponent system, which can be utilized to solve vapour/liquid/liquid equilibrium (VLLE) including complex chemical reactions, solids dissolution and precipitation.

In Chapter 5 biochemical systems in thermodynamic calculations are considered. An optimization-based algorithm for accelerating the systematic generation of sparse constraints method is introduced, particularly valuable in biochemistry where multiple reactions need to be constrained. In addition, the modelling of sulphate reducing bacteria process with its pre-treatments has been addressed. Finally, Chapter 6 bestows the usage of artificial intelligence combined with thermodynamic modelling. The prediction of unknown elemental properties by means of machine learning is suggested and the usage of surrogate models in flowsheet simulation is presented as a case study.

2. Background

Mastering of complex chemical and physical interactions is a continuing challenge in process and materials technology. For the process industries, optimal functionality, saving raw materials and energy and reducing the environmental impacts are the pertinent goals. In materials development, their physical and chemical relations are utilised for the purposes of developing the appropriate structural and operational properties and controlling the durability under various conditions.

The complexity of contemporary process and materials development is most efficiently managed by computational technologies. The systematic structure and firm mathematical basis of chemical thermodynamics is well suited for the computer and data processing, while the extensive databases of thermochemical and -physical properties of materials offer a first principles basis for the digitalization. Reliable in-scale models of the real process, often also called digital twins, can be created by using modern computational thermodynamics.

Conventionally thermodynamic calculation methods are focused on phase changes and on products of chemical reactions as function of temperature and pressure. The methods in wide international use are specifically suited for predicting multiphase chemical equilibrium compositions and for drawing diagrams describing multicomponent phase equilibria. Both approaches have been extensively used for several decades in chemical technology and materials science.

In practical processes full equilibria are, however, seldom attained. On the other hand, the composition of the material being processed is often affected also by other than purely chemical factors. VTT has developed new breaching algorithms which make use of the constrained Gibbs free energy (CFE) method and allow for the time dynamics of the chemical reactions and inclusion of various physical preconditions while performing the multiphase thermodynamic calculation (Koukkari and Pajarre, 2006; Pajarre et al., 2016).

2.1   *Ratemix*-algorithm

The coupled kinetic-thermodynamic simulation method provides a unique approach for quantification of the behaviour of chemical processes in multiphase systems. Its characteristic feature is the ability to make use of the thermochemical state functions during the (time) course of a multiphase process by applying dynamic constraints in the free energy minimizing procedure. In a single algorithm one may deal with all significant factors of the thermodynamic natural process, describing the dynamic behaviour of a multi-component system with its complete extensive and intensive state properties. Thus, the virtues of reaction kinetic methods are combined with those of multicomponent thermodynamics, which conventionally had been applied but to static (equilibrium) conditions.

With the coupled method, chemical reactors are simulated as time-dependent thermochemical systems by using sequential constrained minimization of Gibbs free energy, which combines the known reaction kinetics, reactor-specific mass and heat transfer and thermodynamic data of the multicomponent reaction mixture. As the first industrial application, a reactor scale-up at the **Kemira Inc** titanium dioxide pigment plant, located in Savannah, United States was performed and the respective algorithm was published (Koukkari, 1993).

The novel simulation technique was further presented by Koukkari, (1995) as doctoral thesis. The general applicability of the method presented in the thesis lead to its registration as a trademark by **Kemira Oy**, which was enlisted in Finland as *Ratemix*® (Reg,nr. 129743) and as computer code copyright in the United States (Reg.nr TXu000603111 / 1993-06-03. Kemira Inc.).

Since 1995 the development work continued in VTT, leading soon to publishing and commercialisation of *ChemSheet* and *KilnSimu* software, both of which may apply the *Ratemix* algorithm, see Figure 1, (Ketonen et al., 1997; Koukkari et al., 2000). In 1997, the rights of *Ratemix®* were transferred from Kemira to **VTT Chemical Technology**.
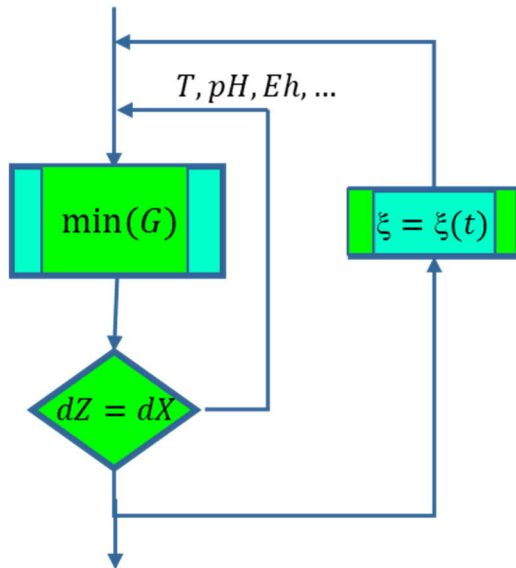
Figure 1. Flowsheet of the Ratemix® algorithm

2.2 The thermochemical simulation method

The use of the Gibbs energy approach gives a possibility to utilise the driving force of a chemical system towards equilibrium in dynamic process models. In Figure 2, a volume element of a continuous reaction system, interacting with its surroundings is shown. The system is affected by its thermal conditions (temperature and pressure) as well as by the chemical processes, which take place within the volume element. In addition, for an inclusive thermochemical treatment of the system, the heat and mass transfer across the boundaries of the volume element need to be considered. The governing equations of the continuous thermochemical system are concisely presented in the Figure 2.

When the process simulation is performed in terms of the chemical potentials of the constituents of the system (*i.e.*, in terms of minimum Gibbs energy), the obvious advantage of the method is that one receives the results of the calculation in the form of the thermochemical state properties. Thus, instead of concentration-volume data, which is characteristic to conventional equation-of-state or mechanistic models, one gets as a result consisting of the comprehensive set of state properties, by which the volume element becomes characterised. Thus, one may follow *e.g.* the amounts of minor and non-process compounds or a measurable property such as the oxygen potential in terms of time or in terms of some other intensive variable, such as temperature or pH value. The state properties, being scalable homogeneous functions of 1st degree, also allow for robust in-scale variation when using the model.

Result Option	Unit
Activity	
Amount	*e.g.* mol
Chemical potential	*e.g.* J/mol-K
Enthalpy	*e.g.* J
Entropy	*e.g.* J
Gibbs energy	*e.g.* J/K
Heat capacity	*e.g.* J/K
Volume change	*e.g.* dm3
Enthalpy/amount	*e.g.* J/mol
Entropy/amount	*e.g.* J/mol-K
Gibbs energy/amount	*e.g.* J/mol
Heat capacity/amount	*e.g.* J/mol-K
Incoming amount	*e.g.* mol
Pressure	*e.g.* bar
Temperature	*e.g.* K
Volume	*e.g.* dm3

Within the figure:
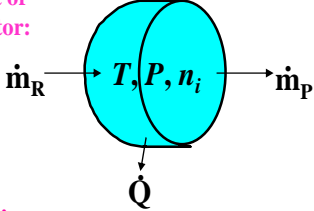
Volume element of a chemical reactor:

$$\dot{m}_R \rightarrow T, P, n_i \rightarrow \dot{m}_P$$

$$\dot{Q}$$

The heat balance:

$$-\operatorname{div} \mathbf{J}_Q = \frac{C_P}{V}\left[\frac{\partial T}{\partial t} + \mathbf{v}\operatorname{grad} T\right] + \sum_r \sum_k H_k\, \upsilon_{kr}\, b_r$$

The chemical reaction rate:

$$b_r = \frac{1}{V}\left[\frac{d\xi_r}{dt}\right] = k[A]^a[B]^b ... [M]^m$$

$$\text{where } \ln(k) = \ln(\mathbf{A}) - \frac{\mathbf{E_a}}{RT}$$

The Gibbs energy:

$$G = G(T, P, n_i)$$

$$G = \sum_\alpha \sum_i n_i^\alpha \left(\mu_i^{\circ\alpha}(T) + RT \ln a_i^\alpha\right)$$

$$\Longrightarrow \quad \min(G) \text{ at equilibrium}$$

Figure 2. The volume element of a thermochemical system with its governing equations. The table gives a list of the state properties, which can be calculated in ChemSheet and KilnSimu software (Koukkari, 2009)*.*

2.3 Generalisation to other complex systems

The continued research on the *Ratemix* algorithm soon led to more general approach with the dynamic constraints applied to other than purely chemical factors, which often have a major influence on chemical and phase changes (Koukkari and Pajarre, 2006; Pajarre et al., 2016). The *Constrained Free Energy* (CFE) method makes use of the *Ratemix* approach by generalizing the thermodynamic free energy calculation for systems subdued to different physical or dynamic work factors (Pajarre, 2016). The incorporation of reaction constraints into the free energy minimization procedure was also mathematically formalised (Blomberg and Koukkari, 2011). With CFE it then became possible to handle both time-dependent kinetics and various physical constraints in the classical thermodynamic calculation routines, and thus significantly expand the scope of their applications. The published CFE applications already cover largely the wide field of chemical thermodynamics, ranging from supercritical and high temperature processes to ambient and sublime conditions and from nanoscale phenomena to complex industrial systems.

In 2007, Professor Koukkari and Senior Scientist Risto Pajarre were given the Best Paper Award of the CAPLHAD Journal for publication of the constrained Gibbs energy minimization method. In 2002, the trademark *ChemEner* (Reg,nr. 225151) was adapted to cover the usage of the method in industrial applications.

Customers for VTT's advanced thermochemical modelling represent a wide range of industrial fields including energy and power production, pulp and paper manufacturing, chemical, metallurgical and steel industries. Many of the technologies have been designed at a time when advanced computer techniques were not yet available. Modelling has been found to be a tool of paramount importance when developing new Best Available level Technologies (BAT) and pursuing for maximum efficiency with minimal environmental and climate impacts. The unique in-scale features of the *Ratemix* approach effectively support both performance improvement of existing processes, refurbishing operational strategies and development of entirely new process concepts.

The usage of CFE methods has also produced several new openings in material sciences. In materials technology, the challenge is in most cases the mastering of the structure-property-performance chain. Advanced thermodynamics often helps to reach practical solutions by its predictions of work functions in various material combinations, which now can effectively be simulated by using the generalised *Ratemix* algorithm.

The computational programs (see Table 1), ChemSheet, KilnSimu and ChemBalas, developed by VTT have been commercialised in collaboration with the German SME **GTT Technologies GmbH**, which markets and distributes thermodynamic calculation software and databases worldwide. VTT's ChemSheet software has been a part of this product family since 1999 with the latest release of ChemSheet2 at 2020[1]. ChemSheet and the simulation tool for industrial rotary kiln systems (KilnSimu) are being used in more than 20 countries by both research and industry. In Japan the programs are represented by the Tokyo-based SME **Research Center of Calculational Mechanics**, **RCCM**. In addition, VTT steady state process simulation software Balas®, developed at VTT over the last 20 years and which many paper mills, engineering companies and equipment manufacturers currently use, is featured with multiphase chemical calculations possibilities.

Table 1. Multi-phase thermodynamic software from VTT

Program / Application	Publishing year	Main field of application	Co-operation partner
ChemSheet	1998	Generic thermodynamic software as Ms-Excel Add-in	GTT Technologies RCCM
KilnSimu	1996	Dynamic and steady state simulation of counter-current and co-current rotary kilns	RCCM GTT Technologies Elomatic*
ChemBalas	2005	Steady state flowsheet simulation software Balas®, supplemented with add on for multiphase chemical calculations	GTT Technologies Kemira
CROM-Simulator	2017	Dynamic and steady state simulation of smelting furnaces and shafts	GTT Technologies

*Successor of Process Flow Ltd with the specific coupling of CFD-technology (Fluent-KilnSimu)

---

[1] The use of the dynamic CFE constraints has been implemented into the latest release of FactSage (version 8.1, May 2021, see www-factsage.com). The program now permits constrained free energy calculations in its modules EQUILIB, PHASE DIAGRAM, COMPOUND and SOLUTION.

3. Dynamic and Constrained Thermochemical Systems

3.1 Oxidation - reduction potentials in multicomponent non-equilibrium free energy models

Risto Pajarre, Pertti Koukkari, Marja Nappa

The oxidation-reduction potential (ORP) is the measurable variable that is frequently used for follow-up of the conditions in aqueous systems. ORP is dependent on the redox state of the system and thus a function of *e.g.* gas composition and temperature. ORP is an intensive variable that, alongside with solution pH can be locally measured and typically is also followed during the time course of the chemical and phase changes occurring in the solution. Conventionally the equilibrium state ORP is defined in terms of the activities (partial pressures) of oxygen, hydrogen and the solvent water and calculated for a known redox pair with the Nernst equation, while there has not been a thermodynamically consistent approach to define the ORP during the time dependent dynamic conditions. By using the constrained Gibbs energy method, it is however possible to formulate the Nernst equation to include the contribution from the extent of the known redox reaction so that the ORP can be calculated. In the following the CFE theory for the time dependent redox system is briefly outlined with a schematic calculation example.

Consider a typical redox reaction for a metal cation Me^{z+} in aqueous media, such as

$$Me^{3+} + e^- \rightarrow Me^{2+} \tag{1}$$

The respective redox potential as function of composition is received with the Nernst equation

$$E = E^0 + \frac{RT}{nF} ln\left(\frac{a_{Me^{3+}}}{a_{Me^{2+}}}\right) \tag{2}$$

where $(n = 1)$:

$$E° = -\frac{\Delta G°}{F} \tag{3}$$

with

$$\Delta G^0 = \mu^0(Me^{2+}(aq)) - \mu^0(Me^{3+}(aq)) - \mu^0(e^-(aq)) \tag{4}$$

where $\mu^0(e^-(aq))$ follows from the hydrogen ion convention

The Gibbs energy of the redox reaction is:

$$\Delta G = \mu_{Me^{2+}} - \mu_{Me^{3+}} - \mu_{e^-} \tag{5}$$

Using activities and formally assuming electron as an aqueous species

$$\Delta G = \Delta G^0 + RTln\left(\frac{a_{Me^{2+}}}{a_{Me^{3+}} a_{e^-}}\right) \tag{6}$$

$$\Delta G = \Delta G^0 + RTln\left(\frac{a_{Me^{2+}}}{a_{Me^{3+}}}\right) - RTlna_{e^-} = -E \cdot F - RTlna_{e^-} \tag{7}$$

At equilibrium $\Delta G = 0$ and thus

$$E = -\frac{RT}{F}lna_{e^-} \qquad (equilibrium) \tag{8}$$

For the non-equilibrium condition, one has respectively

$$E = \frac{-\Delta G}{F} - \frac{RT}{F}lna_{e^-} \qquad (non\_eq.) \tag{9}$$

Now, the ΔG equals the affinity (driving force) of the redox process and becomes computed as the respective constraint potential π_R. Using component potentials (π_j for each component j) for ΔG there is:

$$\Delta G = \pi_{Fe} - 2\pi_{e^-} + \pi_R - (\pi_{Fe} - 3\pi_{e^-} + \pi_{e^-}) = \pi_R \tag{10}$$

The constraining component R has thus been applied onto the Me^{2+} species (actually on all respective species containing divalent Me in the multicomponent system) and appears as one component in its chemical potential. At equilibrium π_R equals zero.

Finally, the redox potential from the constrained Gibbs energy calculation then is

$$E = \frac{-\pi_R}{F} - \frac{RT}{F}lna_{e^-} \qquad (non\_eq.) \tag{11}$$

One should note that the activity of aqueous electrons also depends on the changing internal state of the system during the redox process and thus corresponds the constant ORP-value determined for each intermediate state in the constrained Gibbs energy calculation. As both terms for such intermediate states become calculated in the CFE method it becomes viable to predict non-equilibrium redox potentials and produce respective (phase) diagrams by using appropriate Gibbs energy minimization routines.

By using the concurrent phase diagram software, such as FactSage, equilibrium diagrams for the multicomponent aqueous systems can be drawn. In such diagrams the constant values of pH and ORP as Eh can be presented in the form of iso-pH and iso-Eh lines. The redox potential as Eh is calculated by using the convention that $E(H^+ | H_2) = 0$ at all temperatures (*e.g.* Pelton & al 2018):

$$Eh = -\frac{RT}{F}lna_{e^-} = \left(\frac{2.303RT}{F}\right)\left(0.25logP(O_2) - pH - 0.5\,logK + loga(H_2O)\right) \tag{12}$$

where

$$K = P(H_2)P(O_2)^{\frac{1}{2}}/a(H_2O) \tag{13}$$

The respective nonequilibrium redox potential can further be received by using equations (11) and (12). The solution allows for *e.g.* contour T, x -diagrams with E or pH as parameter (ξ being the extent of the redox reaction, see Figure 3). Respectively, the aqueous phase diagrams can be presented with ξ as the axis variable as shown in Figure 4. The schematic

diagram is calculated by using the phase diagram module of FactSage software. While the thermodynamic data available for the new CFE calculations in FactSage is not fully consistent, the Y-axis (partial pressure of oxygen) is normalised to present an arbitrary range $-1.5 < y < 1$. However, the schematic diagram shows both the iso-Eh lines calculated by equation (12) and the isoactivities of the reduction component (R). As the potential π_R can directly be deduced from the latter, the diagram could also be used to present the ORP-values as iso-E lines when superposing the two iso-factors by equation (11). Practical introduction of such diagrams will yet require appropriate databases to be developed for the present day phase diagram software, so that the said ORP variables may be included in the calculation as a typical conjugate pair of the intensive and extensive properties (Pajarre et al., 2021, to be published).
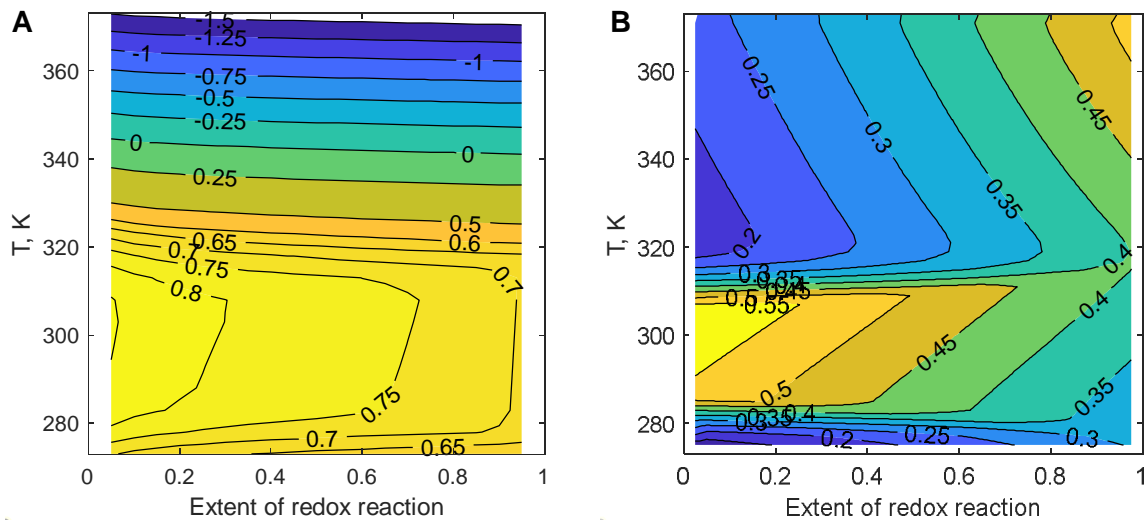
Figure 3. Aqueous phase: Scheme calculation of ORP (A) and pH values (B) in a Me^{3+}, Me^{2+}-redox system as function of temperature and extent of the redox-reaction. EOR related to equilibrium reduction.
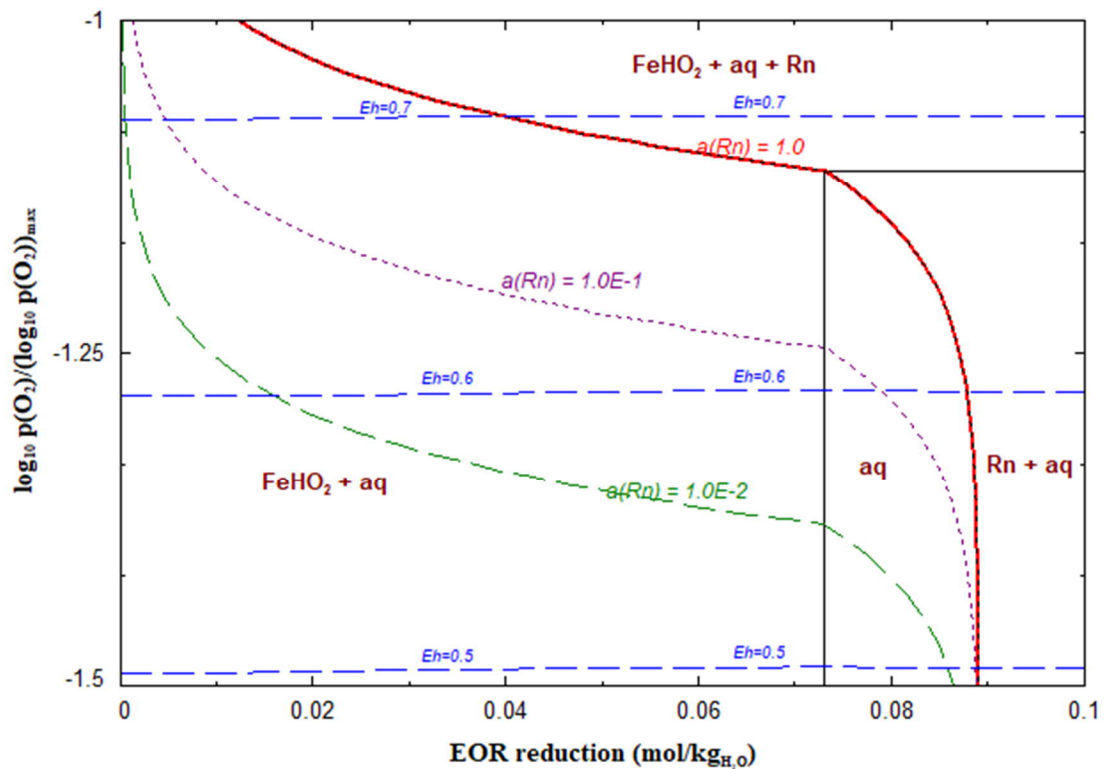
Figure 4. Aqueous phase diagram (50 °C; schematic) drawn for a constrained Fe^{3+}, Fe^{2+} redox system in 1.5 mol/kg$_{H_2O}$ sulfuric acid with extent of the reduction reaction as X-axis, Y-axis normalised not-to-scale. Content of Fe ca. 0.09 mol/kg$_{H_2O}$ and Na_2SO_4 0.05 mol/kg$_{H_2O}$. Iso-Eh-lines calculated by FactSage, iso-activities of the constraining reduction component are also shown. The continuous red line indicates the phase boundaries at redox equilibrium with the condition $a(Rn) = 1$, $a(Rn)$ being the activity of the virtual reduction component. The red line also limits the physical range of the diagram set by the requirement that $a(Rn) \leq 1$.

3.2 SI as constraint in thermodynamic modelling – supersaturation in respect to gypsum

Marja Nappa, Pertti Koukkari, Risto Pajarre, Petteri Kangas†

Undesired scaling on equipment surfaces and heat exchangers is often a persistent problem in industrial water systems, such as petroleum production line or cooling water systems (Abd-El-Khalek et al., 2019). Fouling and scaling is the most serious challenge for widespread implementation of membrane processes, desalination processes as well on membrane treatment of mine water (Guo et al., 2012; Kyllönen et al., 2016) causing higher operating and membrane replacing costs. Calcium forming $CaCO_3$ or $CaSO_4$ scale is one of the cations that account for most of the precipitates (Guo et al., 2012). Scaling is a general problem in NF and RO filtration, but it is especially a problem at metal sulphide mines where the amount of sulphate in downstream processes is high (Kyllönen et al., 2016).

The understanding of fouling phenomena is the key to control and solve the fouling problems. The fouling is affected by aqueous solution characteristics, such as temperature, pH and composition. One successful method for handling scales is pH control, but not for the control of gypsum scaling due to weak pH dependence of gypsum solubility. Scale inhibitors, *i.e.* antiscalants have been used widely to control gypsum scaling (Kyllönen et al., 2016). Commonly used antiscalants, such as organic polymers, surface active reagents, organic phosphonates and phosphates, interfere with the kinetics of crystal nucleation, formation and growth (Shenvi et al., 2015).

In contact with water three phases of calcium sulphate can crystallise: gypsum, anhydrite, and hemihydrate. Solubility curves modelled with Chemsheet of these three phases are shown in Figure 5. At the given temperature the solid phase with lowest solubility represents the stable phase. However, due to slow crystallization kinetics the solubility of a certain phase can be extended into the metastable temperature, when there are no nuclei of stable phase present (Freyer and Voigt, 2003).

Thermodynamic equilibrium calculations, generally, allow the calculation of thermodynamic equilibrium based on minimization of Gibbs energy. In calculation programs (*e.g.* ChemSheet, FactSage) phases can be excluded from calculations, which can be used to prevent certain solid phase to form. The constrained Gibbs free energy method enables the reaction to proceed upto certain desired extent. CFE method makes use of complementary conservation conditions for selected immaterial properties in addition to the conservation of molar amounts of the physical system components (Koukkari et al., 2018; Pajarre et al., 2018).

The methodology to utilise the reaction affinities of constraining reaction as part of the constrained thermodynamic model is presented by (Koukkari et al., 2018) and applied successfully on methanation process by (Kangas et al., 2017). In aqueous solutions, a typical measure of deviation from equilibrium is saturation index (SI). The aim of this study is to provide a practical approach to model supersaturation of minerals in industrial waters by using the similar approach for supersaturation of calcium sulphate than (Kangas et al., 2017) uses in high temperature problems. Simultaneously, the study illustrates the methodology for utilizing SI (saturation index) as part of constrained thermodynamic model.

3.2.1 Methods

The modelling approach is based on the constrained free energy technique (CFE), which is extending the calculation of thermodynamic equilibria by introducing additional virtual constraints to the chemical system. Saturation index (*SI*) is used as a basis for constraints with similar approach than presented for thermodynamic affinity (Kangas et al., 2017;

Koukkari et al., 2018). CFE method is used within ChemSheet to calculate the local equilibrium state. The equilibrium data is based on VTT's advanced aqueous database (Pajarre et al., 2018).

Reaction equations of precipitation of gypsum and anhydrite formation are as follows:

$$Ca^{2+} + SO_4^{2-} + 2H_2O \leftrightarrow CaSO_4 \cdot 2H_2O \qquad (r_1)$$

$$Ca^{2+} + SO_4^{2-} \leftrightarrow CaSO_4 \qquad (r_2)$$

Thermodynamic equilibrium is defined by equilibrium constant K. For gypsum dissolution that is

$$K = \frac{a_{eq,Ca^+} a_{eq,SO_4^{2-}} \left(a_{eq,H_2O}\right)^2}{a_{eq,CaSO_4 \cdot 2H_2O}} \qquad (14)$$

Where a indicate activity in saturation state. Thus, the activity of solid phase is one, the solubility product can be written:

$$K_{SP,gypsum} = a_{eq,Ca^+} a_{eq,SO_4^{2-}} \left(a_{eq,H_2O}\right)^2 \qquad (15)$$

When the solution is not in equilibrium, ion activity product can be calculated respectively to solubility product.

$$IAP_{gypsum} = a_{Ca^+} a_{SO_4^{2-}} \left(a_{H_2O}\right)^2 \qquad (16)$$

Saturation Index (SI) is a criterion to see if the solution is unsaturated SI < 0, saturated SI =0 or supersaturated SI > 0. Saturation ratio (SR) is the ratio of ion activity product to solubility product. Solubility product is obtained in the saturation state of system and ion activity product in the real state of system. (Doubra et al., 2017)

$$SI = log\,SR = log\frac{IAP}{K_{SP}} \qquad (17)$$

To the anhydrite K_{SP} and IAP are following

$$K_{SP,anhydrite} = a_{eq,Ca^+} a_{eq,SO_4^{2-}} \qquad (18)$$

$$IAP_{anhydrite} = a_{Ca^+} a_{SO_4^{2-}} \qquad (19)$$

The constrained gypsum formation is elaborated here in more detail. The main species included in the modelled system are H_2O, $CaSO_4$, Ca^{2+}(aq), SO_4^{2-}(aq), $CaSO_4 \cdot 2H_2O$ and $CaSO_4$, hemihydrate is set dormant. This simplified chemical system is then expressed in a form of a stoichiometric matrix, A. However, the system is not in equilibrium, and thus an additional constraint is added to the matrix. This enables the calculation of local equilibrium and resulting as the extended stoichiometric matrix shown in equation (20). The system components (Ca, S, O, H) and virtual component (constraint) c_1 and the applied constituents and virtual phase (reaction of gypsum formation) r_G are illustrated beside the matrix for clarity.

$$A = \begin{array}{c} \\ Ca \\ S \\ O \\ H \\ c_1 \end{array} \begin{array}{cccccc} Ca^{2+} & SO_4^{2-} & H_2O & CaSO_4 \cdot 2H_2O & CaSO_4 & r_G \\ \left[\begin{array}{cccccc} 1 & 0 & 0 & 1 & 1 & 0 \\ 0 & 1 & 0 & 1 & 1 & 0 \\ 0 & 4 & 1 & 6 & 4 & 0 \\ 0 & 0 & 2 & 4 & 0 & 0 \\ 0 & 0 & 0 & 1 & 0 & 1 \end{array}\right] \end{array} \tag{20}$$

The Gibbs energy change of reaction r can be written

$$\Delta_r G = \Delta G° + RT \, ln(Q_r) \tag{21}$$

or for aqueous solution

$$\Delta_r G = \Delta G° + RT \, ln(IAP) \tag{22}$$

where $\Delta_r G$, $\Delta G°$, R, T and Q_r are Gibb's energy change due to reaction, molar gas constant 8.314 JK^{-1}mol^{-1}, temperature, and reaction quotient, respectively.

In equilibrium Gibbs energy change $\Delta_r G = 0$ and $IAP = K_{SP}$, and thus $\Delta G° = -RT \, ln \, K_{SP}$

$$\Delta_r G = -RT \, ln(K_{SP}) + RT \, ln(IAP) = RT \, ln(IAP/K_{SP}) \tag{23}$$

The reactions r_1 and r_2 were defined in opposite direction to the solubility and ion activity product, thus Gibbs energy change for precipitation reaction is

$$\Delta_r G = RT \, ln\left(\frac{1}{IAP}\Big/\frac{1}{K_{SP}}\right) = RT \, ln(K_{SP}/IAP) \tag{24}$$

Affinity of a reaction is given with opposite sign of the Gibbs energy change.

$$\mathbb{A} = -\Delta_r G = RT \, ln(IAP/K_{SP}) = RT \, ln(SR) \tag{25}$$

Affinity can be also defined based on chemical potentials of components and chemical potentials of the virtual components.

$$\begin{aligned} \mathbb{A} &= \pi_{Ca} + \pi_S + 4\pi_0 + 4\pi_H + 2\pi_O - \pi_c - \pi_{Ca} - (\pi_S + 4\pi_0) - (4\pi_H + 2\pi_O) = -\pi_c \\ &= -\Delta_r G \end{aligned} \tag{26}$$

Using the minimization of Gibb's energy to solve π_c and defining the virtual constituents to have zero standard chemical potential at all temperatures ($\mu_r^o \equiv 0$), it follows that the affinity and saturation index of particular reaction is connected to chemical activity a_r of virtual phase for respective constrained reaction r,

$$\mathbb{A} = -RT \, ln(a_r) = RT \, ln(SR) \, ; \quad a_r = 1/10^{SI} \tag{27}$$

The chemical activity of virtual phases defined above can conveniently be used as an input parameter of ChemSheet models (Kangas et al., 2017) where constraints are applied for calculating the constrained local thermodynamic equilibrium.

3.2.2   Results and Discussion

As the first example for the calculation of *SI* to be used as constraint in thermodynamic calculation the metastable state of anhydrite and gypsum were studied. The solubility of

gypsum and anhydrite is shown in Figure 5. Above the transition temperature (~45°C) gypsum is metastable and its solubility is higher than that of anhydrite. Below the transition temperature anhydrite is metastable and its solubility is higher than that of gypsum. The system is also illustrated by using true aqueous phase diagram produced using the methodology presented in (Pelton et al., 2018). In this example it is assumed that there is no precipitation between the solubility lines and SI for stabile phase is calculated from equations (15), (16) and (17) using VTT:s aqueous database. The calculated SI_G values for gypsum below transition temperature and SI_A values for anhydrite above transition temperature are shown in Figure 7. Similar procedure is performed for above transition temperature where the anhydrite is assumed to be in metastabile state and not precipitate before gypsum solubility line. The linear model is fitted for $SI = a\ T\ [°C] + b$ with good agreement. R value is over 0.99 for both SI_G and SI_A. Table 2 illustrates the SI model parameters.
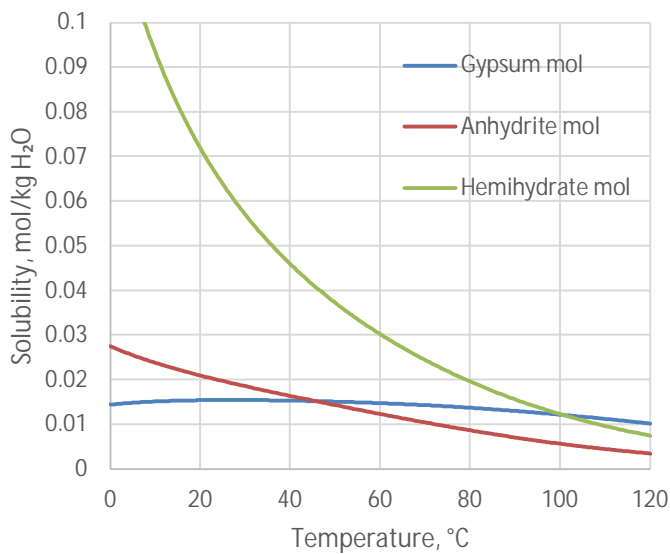
Figure 5. Gypsum, anhydrite and hemihydrate solubilities between 0 and 120 °C.

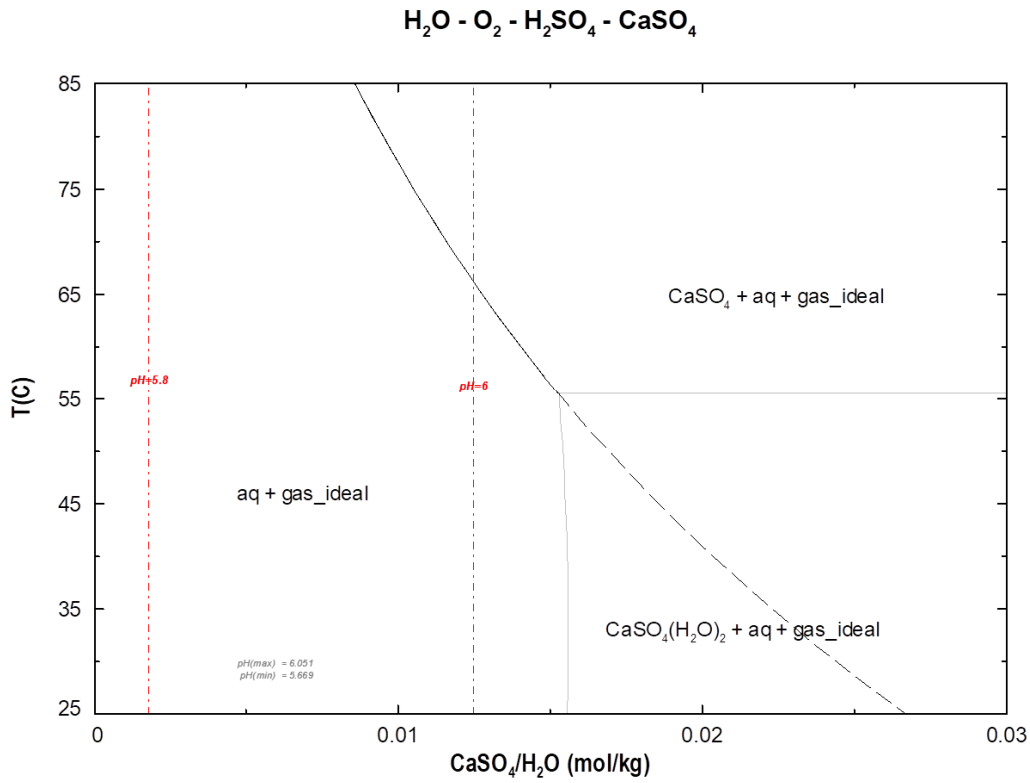**H$_2$O - O$_2$ - H$_2$SO$_4$ - CaSO$_4$**

Figure 6. Phase diagrams of CaSO$_4$-water system. Solid lines: the equilibrium conditions including gypsum-phase and dashed lines: the metastable solubility limit of CaSO$_4$ anhydrite (no gypsum-phase).
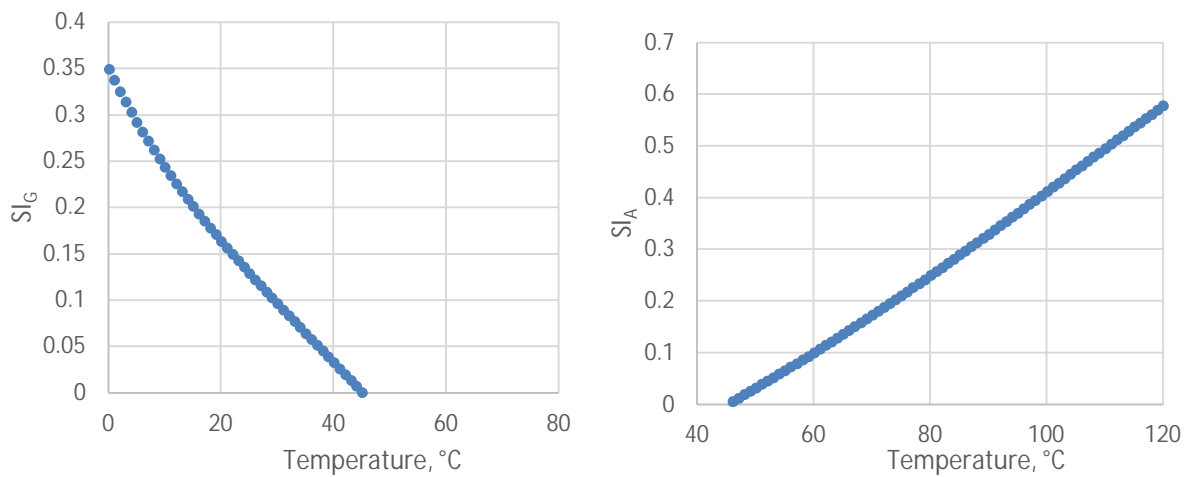
Figure 7. Saturation index (SI) as a function of temperature.
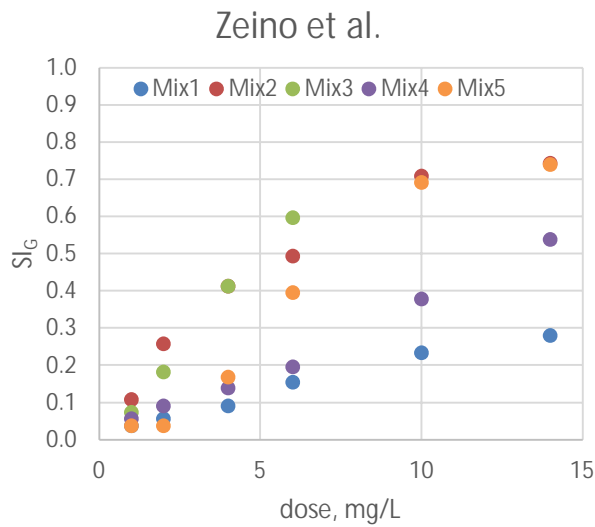
Figure 8. Saturation index as a function of different antisclant dose. (data from Zeino et al., 2018)

Table 2. Applied constraints and their model parameters.

		Model equation	a	b	c	R^2-value
ChemSheet		$SI_G = ax + b$	-0.00744	0.3230	-	0.991
ChemSheet		$SI_A = ax + b$	0.00781	-0.3687	-	0.999
Zeino et al.	mix 1	$SI_G = ax$	0.0219	-	-	0.971
Zeino et al.	mix 2	$SI_G = ax$	0.0645	-	-	0.828
Zeino et al.	mix 3	$SI_G = ax$	0.0996	-	-	0.996
Zeino et al.	mix 4	$SI_G = ax$	0.0378	-	-	0.992
Zeino et al.	mix 5	$SI_G = ax$	0.0580	-	-	0.950
ChemSheet		$SI_{G2} = ax2 + bx + c$	5.65E-5	-9.98E-3	0.342	0.999

When comparing the predicted values by the SI-models and experimental values from the literature and those generated by ChemSheet, there were good agreement for the aqueous Ca. The relative error of measured vs. modelled points is in all cases under 10%, as illustrated in Figure 9

The first model for SI was a simple linear fit, however for more accurate results the more detailed model may be used. *E.g.* by using polynomial fit for SI_G (SI_{G2}, Table 2) the results are more accurate (see Figure 9), R^2 value is 0.999 compared to earlier 0.991, however also a new model parameter is introduced.

The Ca^{2+} molality as a function of temperature is printed in Figure 10, while using produced SI_G as a constraint. The curve agrees well with results which can be calculated by setting gypsum as dormant phase in ChemSheet. Experimental data for the figure is taken from (Møller, 1988). Illustration of the use of SI_A is also shown in Figure 10 producing the curve corresponding situation where anhydrite is set as dormant.

The data related to different antiscalant usage are often hidden information measured by antiscalant manufacturers, however with a wider dataset the SI model could take into account both temperature changes and the antiscalant addition would be possible to fit.
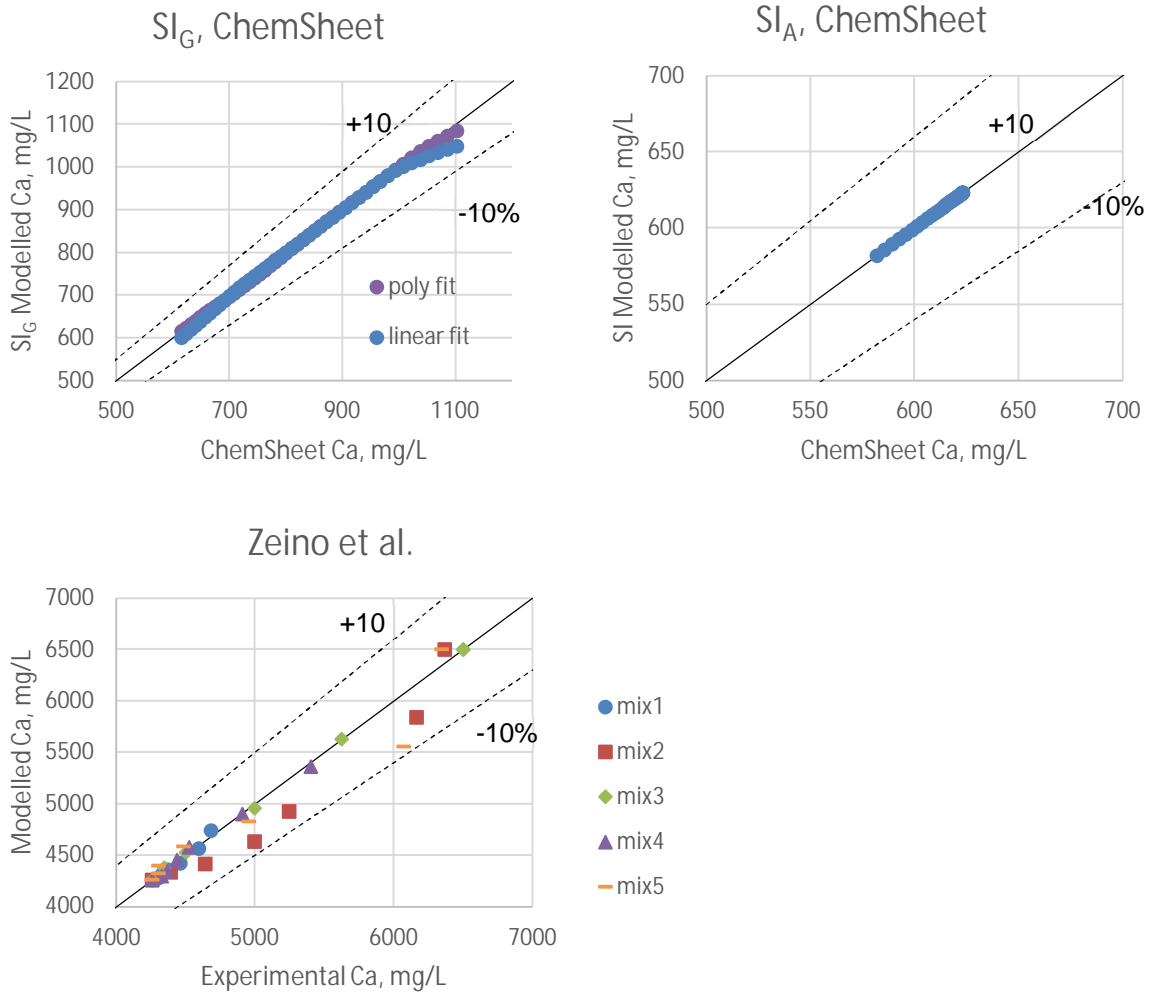
Figure 9. Aqueous Ca^{2+}, ChemSheet calculation of solubility of metastabile form (CaSO$_4$ or CaSO$_4$·2H$_2$O) or measured value vs. SI modelled value.
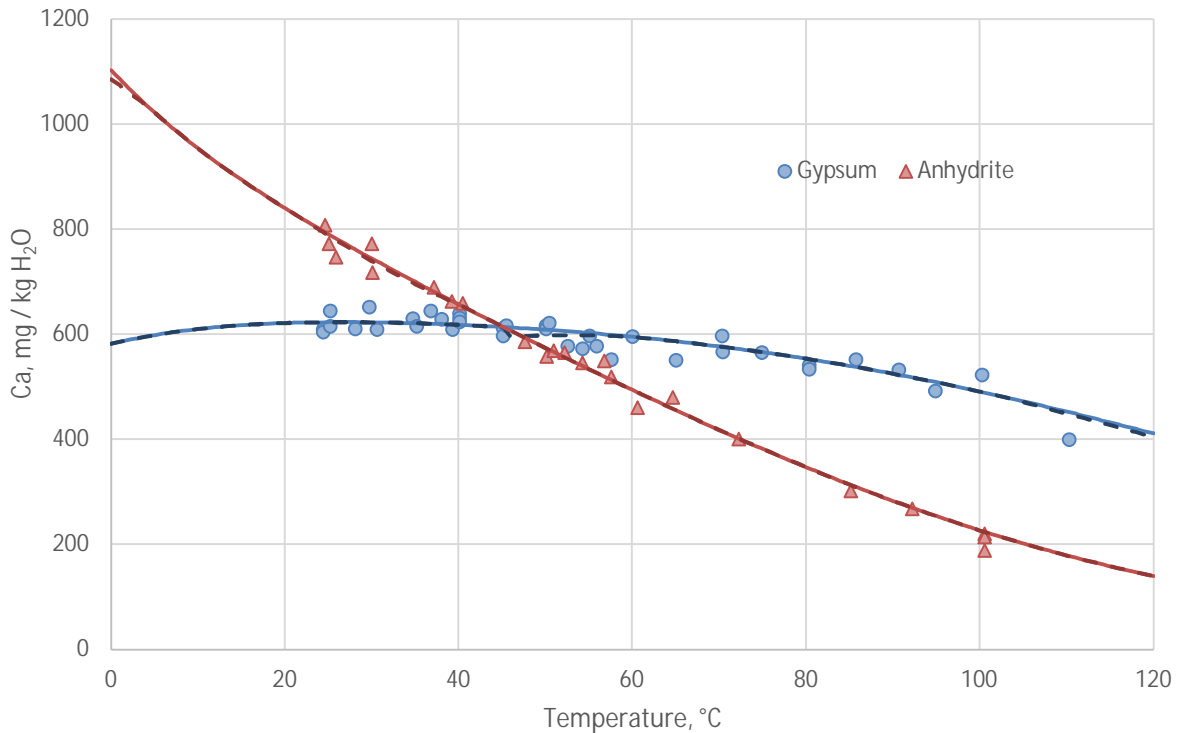
Figure 10. Dissolution of gypsum (blue) and anhydrite (red). Dashed lined SI-model results, solid lines ChemSheet results while other forms of calcium sulphate are set dormant. Experimental data is obtained from (Møller, 1988). *Polynomial fit for SI_{G2} is used.*

3.2.3   Conclusions

The applicability of methodology presented for modelling supersaturation in aqueous solutions is evaluated against theoretic data and literature data. The usage of saturation index *SI* as constraint in CFE calculations for modelling the supersaturation of aqueous solutions process seems feasible. When comparing the predicted values by the *SI*-constrained models and experimental values from the literature or values calculated with ChemSheet, relatively good agreement for dissolved calcium is obtained.

The developed method may provide a practical and relative straightforward method to model *e.g.* mine waters, where there are some natural inhibitors for scale formation or when commercial antiscalants are used. If the certain mine water SI is known or modelled as function of *e.g.* antiscalant dose the composition of the solution can be calculated using the presented methodology.

3.3 Dynamic lime kiln model

Karri Penttilä

Rotary kilns are used in several industries. The rotary kiln provides an efficient means for both heat and mass transfer in the processing of slurries and other condensed mixtures. Pigment and cement manufacturing industries among others are using rotary kilns for the thermal treatments of various materials. In the chemical recovery of Kraft pulping rotary kilns are applied for lime recycling.

A steady-state rotary drum simulator KilnSimu developed in VTT has been successfully used for these and other chemical systems (Meyer et al., 2016). KilnSimu is a versatile simulation software that can handle several different kinds of rotary kiln applications with chemical systems consisting of hundreds of phases and species. Optimization of rotary kilns will benefit from appropriate simulation models, which include accurate description of the chemical and physical processes inside.

As a steady-state simulator, KilnSimu is suitable tool for solving energy and mass balances of the kiln for known feed rates and compositions to find out the distribution of elements between the outgoing bed and gas flows. For example, it can be used to study how switching from traditional fossil fuel to alternative fuel would affect the internal chemical reactions as additional alkali elements in the new fuel can and in many cases will cause unwanted accumulation and enrichment of alkali sulphates and chlorides into the process. However, there is also a demand to study the delay between the changes in the model inputs and outputs. Residence times of the bed in kilns are typically from tens of minutes to several hours and longer time-delay in a process increases the difficulty of controlling it. Controlling such processes with high order dynamics and large time constants and time-delays might require a predictive control strategy using an accurate model of the process. Ultimately, a dynamic version of KilnSimu could be used for such a model. It could also be used as a teaching tool for the process operators.

3.3.1 Model

In KilnSimu, heat and mass transfer are assumed to occur in radial direction. An axial plug flow model is used for both the bed and gas flows. The unknown variables are the temperatures of the bed, gas, inner and outer wall, and the flow rates of the bed and gas species. The volume elements of the bed and gas are described as open thermochemical systems, which transform heat and mass with each other. The equilibrium states of the volume elements are calculated by minimizing their Gibbs energy and by taking into account the heat and mass transfer between the elements and their surroundings. The time-dependent reactions in the bed and the gas flow are considered in the Gibbs energy minimization by constraining the fractions of phases taking part in the equilibrium calculation (*e.g.* inert and reactive parts). The Gibbs energy minimization is done by calling routines in the ChemApp library (Petersen and Hack, 2007).

The unknown variables are determined at discrete reference points called calculation cells or nodes. Each cell represents a certain volume, and its temperature and composition are a measure of the average properties of that volume. The counter-current flow system in the kiln comprises a so-called two-point boundary value problem with a fixed boundary. It is solved iteratively until the composition and the temperature profiles of the bed and gas flows converge within a given tolerance.
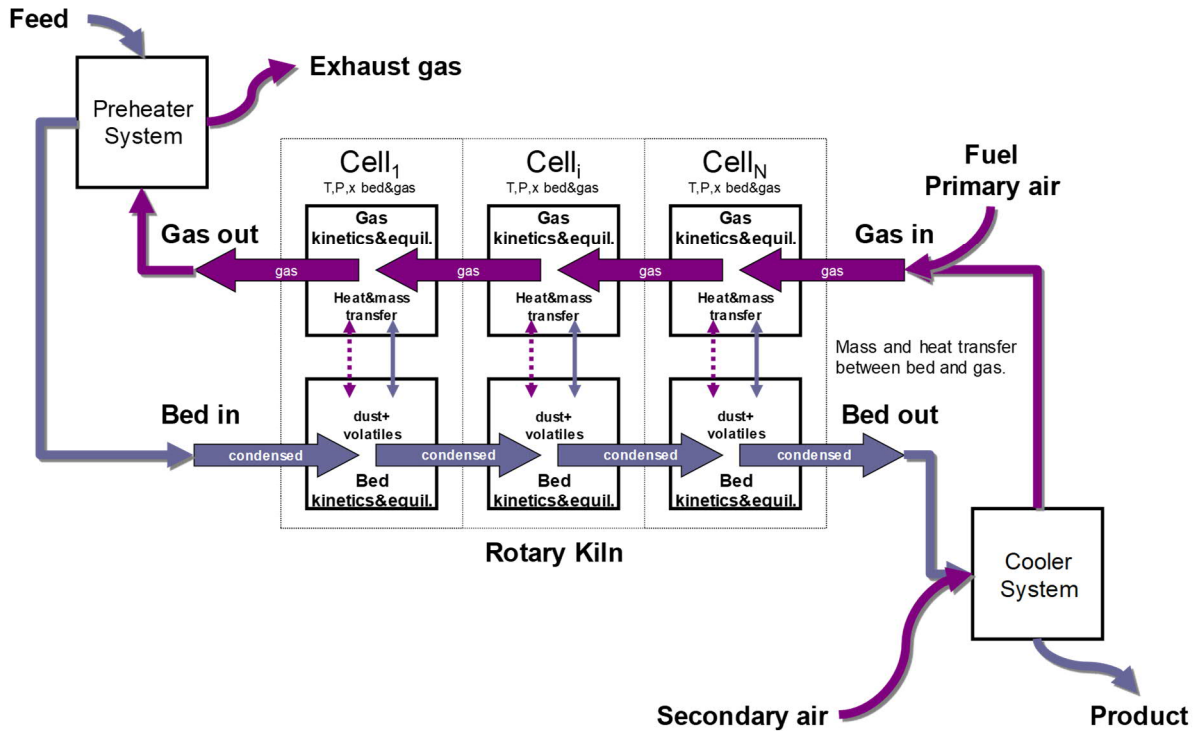
Figure 11. General KilnSimu flowsheet.

The dynamic version of KilnSimu uses similar approach and same set of heat transfer equations as the steady-state version (Meyer et al., 2016). The main difference being the switch from steady-state solver to a dynamic one. Also, the kinetic model have been updated and a new particle model has been added in order to include several potentially different raw materials represented as discrete particles not being able to interact with each other until reaching higher temperatures and formation of melt phase.

3.3.1.1 Kinetic Model

Kinetics controls how fast individual phases are allowed to react to products and equilibrium calculation determines what these products are. In KilnSimu, for each time step reaction kinetics is used to determine the fractions of each phase that are allowed to react (reactive part). These are then taken into equilibrium calculation to determine the reaction products. Other part of phases are kept inert (inert part). After the equilibrium calculation, reactive and inert parts are combined again as one. General differential equation for the conversion is given as:

$$\frac{d\alpha}{dt} = kf(\alpha) = A_0 e^{-E_a/RT} f(\alpha) \tag{28}$$

where k is the reaction rate coefficient calculated with Arrhenius equation and α is the conversion of the reactant/phase:

$$\alpha = 1 - \frac{c_t}{c_0} \tag{29}$$

where c_0 is the initial/maximum mass of the reactant/phase and c_t is its current/local mass. Several kinetic models are supported (see Table 3).

Table 3. Examples of supported kinetic models.

• Kinetic Model		$f(\alpha)$	
• Power law	P2	$2\alpha^{1/2}$	
• Power law	P3	$3\alpha^{2/3}$	
• Power law	P4	$4\alpha^{3/4}$	
• Avrami-Erofeyev	A2	$2(1-\alpha)[-\ln(1-\alpha)]^{1/2}$	
• Avrami-Erofeyev	A3	$3(1-\alpha)[-\ln(1-\alpha)]^{2/3}$	
• Avrami-Erofeyev	A4	$4(1-\alpha)[-\ln(1-\alpha)]^{3/4}$	
• Contracting area	R2	$2(1-\alpha)^{1/2}$	$k' = k/R$
• Contracting volume	R3	$3(1-\alpha)^{2/3}$	$k' = k/R$
• 1-D diffusion	D1	$1/2\alpha$	$k' = k/R^2$
• 2-D diffusion	D2	$-1/\ln(1-\alpha)$	$k' = k/R^2$
• 3-D diffusion	D3	$3(1-\alpha)^{2/3}/[2(1-(1-\alpha)^{2/3})]$	$k' = k/R^2$
• First-Order	F1	$(1-\alpha)$	
• Second-order	F2	$(1-\alpha)^2$	
• Third-order	F3	$(1-\alpha)^3$	

3.3.1.2   Particle Model

The particle simulation model can include one or more particles (1 to 5), all of which have same set of size classes (1 to 15). Size class refers to particle size between fixed minimum and maximum diameters (average being the value in the middle). Particle size distribution (PSD) is then represented as mass fractions of these particle size classes. Furthermore, each particle can contain any set of phases and compositions. Constrained equilibrium is calculated separately for each particle including interaction with the surrounding gas. Growing and shrinking models allows changes in the particle size distribution. Sintering model allows particles to interact with each. For example, formation of clinker nodules out of lime, silica and oxide melt in the cement production.

3.3.1.3   Dynamic Algorithm

Rotary kiln is divided axially into calculation nodes for the bed and gas sides - one node for both the bed and the gas in any axial position.

A. At start the kiln is filled with charge with given composition and temperature, for example at room temperature for simulating a cold start of the kiln.

B. For each subsequent time step (optimally same as bed residence time in node):

1. Starting from gas feed end: bed, gas and wall temperatures and bed and gas compositions are solved iteratively. Solved gas outlet flow from the node is taken as inlet to the gas side in the next node so effectively gas side is assumed to obtain steady state during each time step. This simplification can be justified as

the residence time of the gas inside the node is normally more than 100 times less than that of the bed.

2. Only after all nodes are solved, bed is moved forward to the next node (and last node is moved out of the kiln.)

3. Go to next time step (B.1) until end time / maximum number of time steps has been reached.

3.3.2 Lime Kiln Application

Recausticizing is part of the recovery process in a kraft pulp mill. In the recovery process, cooking chemicals NaOH and Na_2S are regenerated. The process involves a reaction turning $CaCO_3$ to CaO, which occurs in the lime kiln. The reaction is endothermic and requires a significant amount of energy. To provide this energy, a fuel must be burned in the kiln.
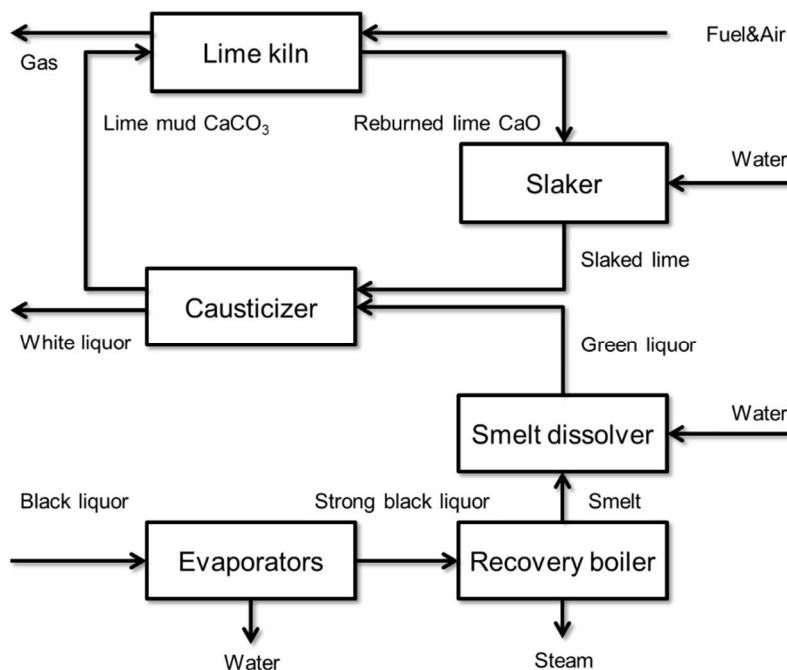
Figure 12. Chemical recovery process and lime kiln.

Lime kilns are often the last place in a pulp mill where fossil fuels are used, but recently, it has become more common to use fossil-free options in the lime kilns as well, making pulp mills completely fossil-free. Some alternatives to methane and fuel oil are wood powder, biomass-based oil and biomass-based gas (Francey et al., 2009).

NPEs are elements not directly associated with the recovery reactions. In a pulp mill, most of the NPEs originate from the wood raw material, but a part of these elements may also originate from the alternative fuel as the bark gasification gas. Especially phosphorus, magnesium, and silicon are suspected to increase in burned lime if a bark-based product gas is fired in the lime kiln, although some of the ash in bark is removed from the gasifier through its bottom ash. The NPEs are unwanted, because they may enrich in the recausticizing cycle and cause different problems, such as a decrease in causticizing efficiency and lime mud dry solids content.

This first version of the dynamic model is used for solving the temperatures and reactions for the main components in the lime mud feed. However, in the future the dynamic algorithm will

be improved so that also number of minor NPEs could be included (without increasing the overall simulation time too much) so that their enrichment could also be studied as function of time (for period of several days). Moreover, other low temperature, aqueous processes in the recovery cycle such as smelt dissolving, slaker and causticizer could be included.

3.3.3 Simulation Results

Simulations have been made for a general lime kiln. The selected lime mud composition contains only the main components to make the simulations faster. Altogether nine elements are included. Thermodynamic data-file contains 83 chemical species composed of these nine elements (60 in gas phase and 33 pure condensed phases). Table 4 shows the used input parameters.

Table 4. Model input parameters

Total length	60	m
Inner diameter	4	m
Wall thickness	0.25	m
Lime mud feed	50	t/h
Temperature	25	C
$CaCO_3(s)$	92	m-%
$MgCO_3(s)$	1	m-%
$Ca_5(PO_4)_3(OH)(s)$	1	m-%
$Na_2S(s)$	0.6	m-%
$NaOH(s)$	0.4	m-%
$H_2O(l)$	5	m-%
Number of particles	1	Lime
Number of particle size classes	4	#
25 μm	0	m-%
100 μm	50	m-%
400 μm	50	m-%
1600 μm	0	m-%
Fuel feed	3.2	t/h
Temperature	25	C
$CH_4(g)$	99	m-%
$N_2(g)$	1	m-%
Air feed	70	t/h
Temperature	350	C
$N_2(g)$	77	m-%
$O_2(g)$	23	m-%
Stop time	8	hours
Time step	150	s
Calculation nodes	31	#
Initial temperature	25	C
Initial charge	Lime mud feed	

Figure 13 shows the calculated bed temperatures as function of axial position of the kiln and time step number (time step numbers cover period from zero to eight hours).
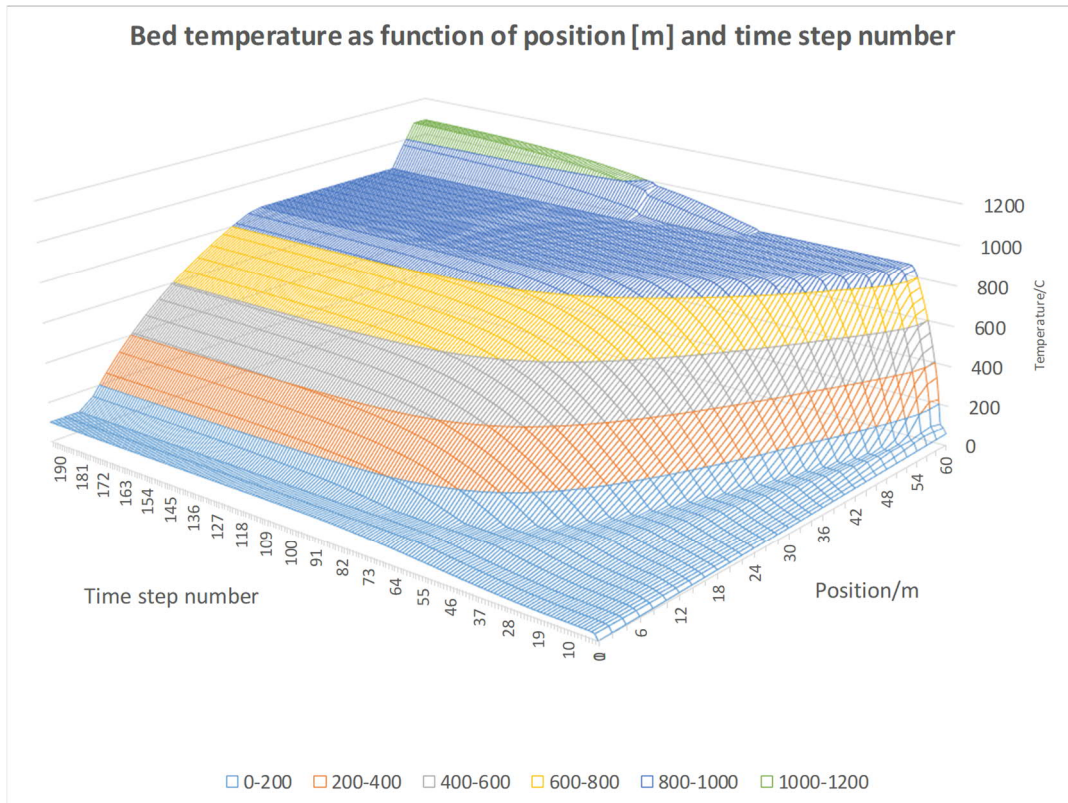
Figure 13. Bed temperature as function of position [m] and time step number (from zero to eight hours).

Figure 14 shows the calculated temperature profiles in axial direction at eight hours (at the end of the simulation).
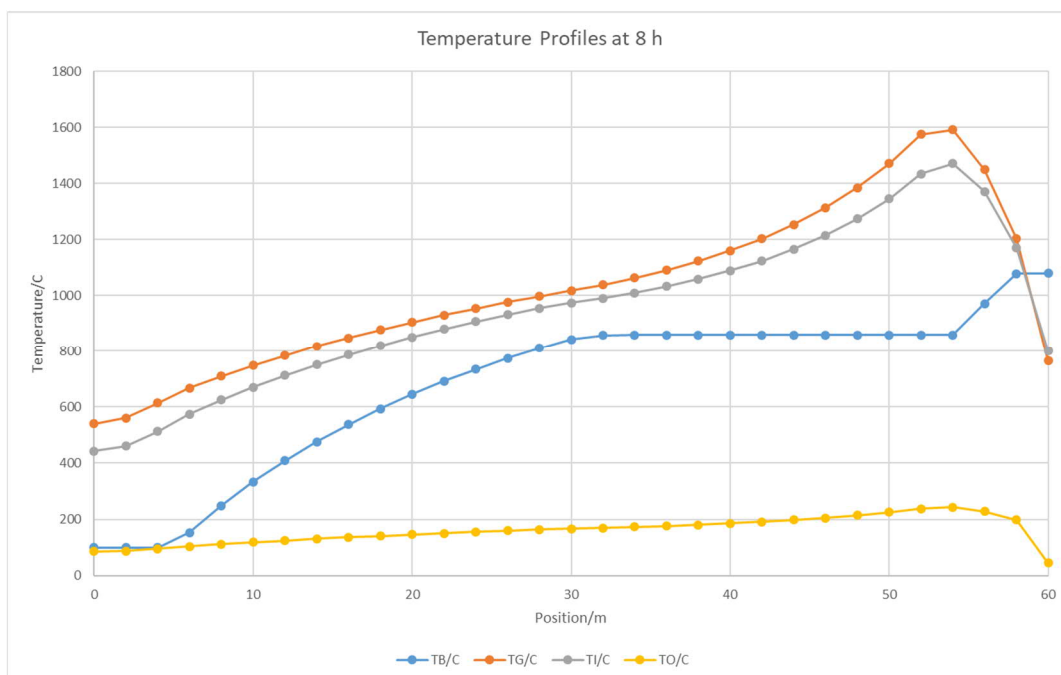
Figure 14. Calculated temperature profiles in axial direction at eight hours.

Figure 15 shows the calculated bed composition profiles for the main phases in axial direction at eight hours (at the end of the simulation). Lighter green curve is limestone in lime

mud and dark green curve is the formed the lime. Water (yellow curve) in the lime feed is vaporised in the first three nodes. Residual limestone in the product is 6 mass-%.
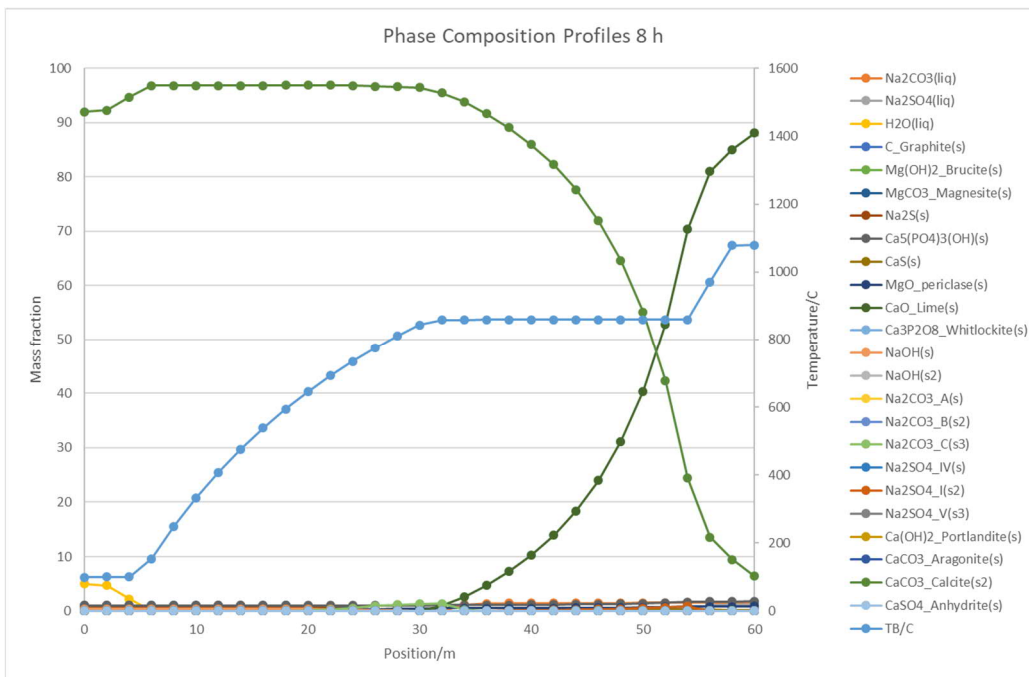
Figure 15. Calculated bed composition profiles for the major phases in axial direction at eight hours.

Figure 16 shows the calculated bed composition profiles for the minor phases in axial direction at eight hours (at the end of the simulation).
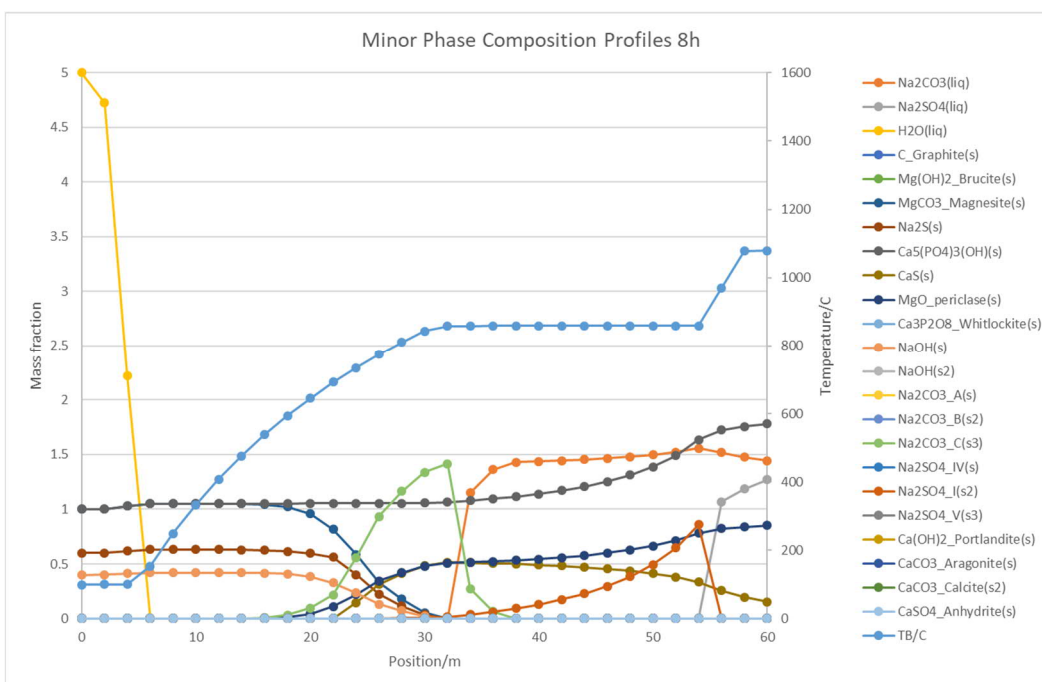
Figure 16. Calculated bed composition profiles for the minor phases in axial direction at eight hours.

Hydroxyapatite (dark grey curve) is the most prominent of the minor phases and it is practically stable throughout the kiln. Magnesite (blue curve) is decomposed to magnesium oxide (dark blue curve) and carbon dioxide gas. Sodium sulphide (red brown curve) and sodium hydroxide (yellow brown curve) seem first to react to solid and then to liquid sodium carbonate (light green and orange brown curves) and finally to sodium sulphate (dark red brown curve) as the temperature is increased. In addition, some calcium sulphide is formed (dark yellow brown curve) but this may be incorrect, and it can be prevented by eliminating it from the set of stable phases. The thermodynamic model did not contain any liquid slag or salt solution phases, and this could have affected the formation of liquids.

Figure 17 shows temperature and limestone/lime profiles calculated with the steady-state version of KilnSimu as a reference for a similar case also using natural gas as fuel.
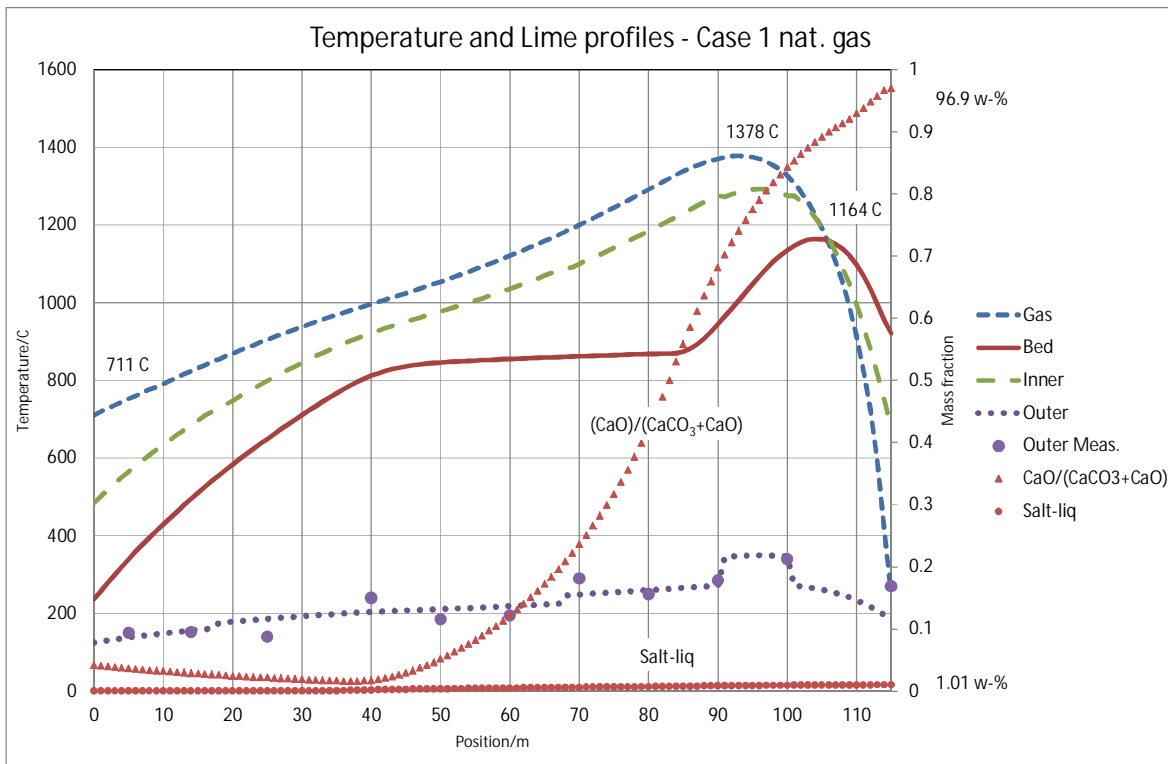
*Figure 17. Temperature and limestone/lime profiles calculated with the steady-state version of KilnSimu.*

3.3.4   Conclusions

Dynamic version of the KilnSimu has been made and used to simulate a general lime kiln in the chemical recovery of the Kraft process. This first version of the dynamic model was primarily used to solve the temperatures and reactions for the main components in the lime mud feed. However, in the future the dynamic algorithm will be improved so that also large number of minor NPEs could be included so that their enrichment in the process could be studied as function of time. Moreover, other low temperature, aqueous processes in the recovery cycle such as the smelt dissolver, the slaker and the causticizer will be included.

3.4 Phase diagrams using affinity and extent of reaction as axis variables

Pertti Koukkari and Risto Pajarre

A method where conjugate pair of the driving force (affinity, D) and extent of reaction (EOR, ξ) are used as axis variables to present non-equilibrium conditions of multiphase systems as phase diagrams is introduced. An aqueous sorption-precipitation system is given as an example, yet the method is fully generic and can be applied in typical non-equilibrium systems where the major constraining reaction(s) can be identified.

For non-equilibrium systems with internal entropy producing processes the combined first and second law of thermodynamics includes the driving force (D) as an intensive state variable, in conjunction with the advancement of the internal change (ξ), which is then the respective extensive property (Hillert, 2007; Liu and Wang, 2016). As for chemical reactions, the terms Affinity for D and Extent of Reaction for ξ are customarily used, such as they were introduced by De Donder. (De Donder and Van Rysselberghe, 1936). While both Liu & Wang and Hillert insinuate that there is a possibility of utilizing the correspondence of D and ξ with the equilibrium properties in Gibbs'ian (phase diagram) calculations for non-equilibrium systems, an appropriate methodology for this has not been presented. On the other hand, in the Constrained Gibbs Free energy minimization (CFE) method (Koukkari & Pajarre, 2006a) the conjugate pair of D, ξ appears as one key concept for the calculation procedure. In the non-equilibrium applications of the CFE method the driving force may be either given as a target input or is received as the non-equilibrium 'constraint potential' - *i.e.* the affinity of the internal change - as the result of the calculation. The advancement of the internal process is then either given as an external constraint, being an independent variable of the non-equilibrium system or becomes defined from the internal conditions of a metastable state and acts as a dependent variable of the system. Then, it is obvious that these features of CFE method together with the conjugate properties D and ξ can be used to construct phase diagrams for such systems, where partial equilibria exist during a relatively slow chemical or phase change.

3.4.1 Theory

Following Hillert, there is for the energy, entropy and volume scheme:

$$dU = TdS - PdV + \sum \mu_j dN_j - Dd\xi \tag{30}$$

$$-dS = -\left(\frac{1}{T}\right)dU - \left(\frac{P}{T}\right)dV + \sum \left(\frac{\mu_j}{T}\right)dN_j - \left(\frac{D}{T}\right)d\xi \tag{31}$$

$$dV = \left(\frac{T}{P}\right)dS - \left(\frac{1}{P}\right)dU + \sum \left(\frac{\mu_j}{P}\right)dN_j - \left(\frac{D}{P}\right)d\xi \tag{32}$$

where N_j refers to the amounts of components in the thermodynamic system. The conjugate pair variables become as listed in the Table 5 (see *e.g.* Hillert, 2007, p. 54):

Table 5. Typical sets of conjugate pairs of state variables.

U	T, S	$-P, V$	μ_j, N_j	$-D, \xi$
$-S$	$-1/T, U$	$-P/T, V$	$(\mu_j/T), N_j$	$-D/T, \xi$
V	$T/P, S$	$-1/P, U$	$(\mu_j/P), N_j$	$-D/P, \xi$

where $-D$ and ξ are also regarded as a pair of conjugate properties, $-D$ being a potential which is obtained as

$$-D = \left(\frac{\partial U}{\partial \xi}\right)_{X^a} \tag{33}$$

where X^a represents all conjugate $X-$variables in equations (1-3). The extent of reaction is then regarded as an independent variable and the respective conjugate potentials are defined for the frozen-in state (HIllert p 22-23).

The Gibbs energy is then respectively

$$dG = -SdT + VdP + \sum \mu_j dN_j - Dd\xi \tag{34}$$

In equations 1-2 and 5 the last term $Dd\xi$ drops off at equilibrium ($D = 0$ or $d\xi = 0$) and ξ is a dependent variable of the system, determined by the equilibrium conditions and mass balance. With $dx = 0$ and $D > 0$ the system is under constrained state or 'frozen-in-condition' and ξ remains an independent variable. In the latter case, the $min(G)$ calculation provides the composition and state properties of the 'frozen-in' system at given conditions defined by the mass balance, T, P and ξ , (Liu & Wang, 2016 p 4-5).

In general, for $min(G)$ problems there is conservation of system components b_j

$$b_j - b_j^\circ = 0 \quad ; \; j = 1, \ldots NC \tag{35}$$

The amounts of components b_j are connected with the amounts of chemical constituents n_k via the stoichiometric conservation matrix, the elements of which are denoted as c_{kj}:

$$b_j = \sum_{k=1}^{N} c_{kj} n_k \tag{36}$$

Similarly, using immaterial reaction constraints for extents of reaction (ξ_r) there is

$$\xi_r - \xi_r^t = 0 \; ; \; r = 1, \ldots NR \tag{37}$$

where superscript t relates to incremental time and subscript r to each reaction (total number of reactions is NR). The extent of reaction obviously is deduced from the molar amounts of constituents participating in each reaction. Thus:

$$\xi_r = \sum_{k=1}^{N} c_{kr} n_{kr} \tag{38}$$

The constraints related to the advancement of the internal processes must be incorporated into the conservation matrix of the Gibbs'ian system as massless (virtual) system components and respective virtual phases. Accordingly, *e.g.* for paraequilibrium solidification systems the constraints are deduced from the ratio of substitutional components in the mother phase and defined along this ratio as virtual components affecting each stoichiometric phase that may be appear stable in the Gibbs energy minimization calculation (Pelton et al., 2014). For systems with chemical reactions, the reaction matrix is transformed into an enlarged conservation matrix that includes both mass balance and reaction constraints, where the latter apply to explicit (kinetically slow) reactions. The driving force is inherently solved by the Gibbs'ian procedure as the chemical potential of the introduced virtual component, typically assigned for a single slow reaction.

Using the Lagrange method of undetermined multipliers the objective function to be minimised includes in addition to the NC conventional mass balance constraints (equations 6-7), the NR new constraints (equations 8-9) as follows:

$$L = G - \sum_{j=1}^{NC} \lambda_j \left(b_j - b_j^\circ \right) + \sum_{j=NC+1}^{NC+NR} \lambda_j \left(\xi_r - \xi_r^t \right) \qquad (39)$$

The solution gives the chemical potentials of the system components in terms of the Lagrange multipliers

$$\lambda_j = \left(\frac{\partial G}{\partial b_j}\right) \equiv \mu_j \; ; \; j = 1, \ldots NC \qquad (40)$$

in analogy with the definition of the component potentials, one obtains then:

$$\lambda_j = \left(\frac{\partial G}{\partial \xi_r}\right) \equiv A_r \; ; \; j = NC + 1, \ldots NC + NR \qquad (41)$$

where $A_r = D_r$ is the affinity (driving force) of each constrained reaction in the system. Note that from (39) and (41) it is obvious that each reaction constraint represents another immaterial component in the Gibbs'ian system and thus subscripts j and r could formally be replaced by just one index symbol (Pajarre et al., 2016). It is yet often practical to distinguish between the two entities and follow number of components and reactions separately.

With the virtual constraints incorporated into a phase diagram software, such as FactSage (Bale et al., 2002), the corresponding diagrams for non-equilibrium conditions can be produced in terms of D and ξ. The conjugate properties applicable for potential diagrams listed in Table 5 indicate that the driving force is then equivalently comparable with the component potentials (μ_j). As for molar phase diagrams, the conditions analogous to conventional equilibrium phase diagrams apply. Non-equilibrium affinity ($D = A_r$) will appear as a potential, ξ as an extensive variable that must be related to some other quantity. The latter condition is in conformance with the conventional tradition of chemical reaction kinetics, where a proportional figure ($0 \leq \xi \leq 1$) for the advancement of a given reaction is commonly used, *e.g.* representing the fraction of a reactant consumed. Using such premises, examples of diagrams constructed for some non-equilibrium reactive systems are introduced below.

The virtual components and virtual species have been used *e.g.* in ChemSheet software for quite some time (Koukkari et al., 2001, 2000). The $\min(G)$ algorithm for ChemSheet is provided by the well-known ChemApp library (Petersen and Hack, 2007) in which it is possible to use arbitrary names for both the virtual components and constituents. However, in FactSage, which was here used for calculating and drawing the phase diagrams, such freedom in its nomenclature is currently not available. This technical problem was circumvented by using the idents of chemically inert elements (such as noble metals of gases) for the virtual components with the input data files prepared for ChemSheet. To avoid any confusion, the variable names r_i for species and v_j for components were however used in the graphs that were produced. Reactions were indexed as $i = 1,2$ and used repeatedly for each case as there are no odds for confusion.

3.4.2 Absorption of carbon dioxide to the aqueous Na_2CO_3 solution

As recently shown by Hack (Hack, 2008) and published in detail by Pelton et al., (2018), true phase diagram sections for aqueous systems can be calculated thermodynamically with currently available software and databases. In FactSage, the aqueous phase diagrams can be calculated with various axis variables under a wide variety of constraints for real (*i.e.* non-

ideal) solutions and for any number of components. Iso-Eh and iso-pH lines may optionally be plotted in the diagrams. Use of affinity-extent of reaction approach for axis variables then provides an interesting technique to analyse the conditions in aqueous solutions, which often appear in near-equilibrium or metastable ('freezing-in') conditions, for which however *e.g.* temperature and pH can be measured with reasonable accuracy. To illustrate this approach, the chemistry of carbon dioxide absorption to caustic soda solution is here briefly considered in terms of the aqueous phase diagrams, presented both for equilibrium and non-equilibrium conditions.

The immersion of carbon dioxide to solutions with elevated pH is well-known and applied for several practical purposes. Most applications deal with gas sorption to carbonate solutions of moderate concentrations in two-phase gas-liquid systems *e.g.* (Cents et al., 2005; Ghosh et al., 2009) where precipitation of solid carbonates is avoided. The example chosen here is however the absorption of carbon dioxide to concentrated Na_2CO_3 solutions, applied in commercial sodium bicarbonate $NaHCO_3$ production, studied experimentally *e.g.* by Wylock et al., (2008), who also constructed a mechanistic reaction model to calculate time-dependent pH-development in the brine absorbing carbon dioxide at atmospheric conditions. Another bulk application of the Na_2CO_3 -absorption is natural gas purification where dissolving CO_2 to a carbonate brine also allows for the simultaneous removal of acid gas impurities, typically H_2S (Wallin and Olausson, 1993). In the latter application both CO_2 and the H_2S impurity will remain in the brine solution, methane is recovered as gaseous product and can be deported to further use. Gas purification is concurrently gaining new interest *e.g.* for biogas cleaning. The leftover bicarbonate solution can be regenerated (to produce pure CO_2) and recycled in such process (Melin, 2009). The capacity of the technique is affected both by the overall rate of CO_2 absorption and the solubility of sodium bicarbonate, which is the precipitating solid in the sorption system.

The solubility of $NaHCO_3$ increases with temperature and *e.g.* Knuutila et al., (2010) have recently performed vapour–liquid equilibrium (VLE) measurements of the carbon dioxide loaded sodium carbonate– water system in the temperature range 40–80 °C and for sodium carbonate concentrations 8-12 wt% (Knuutila et al., 2010). Equation-of-state (VLE) calculations were also performed by using the electrolyte-NRTL model. In Figure 18 the results published by Knuutila et al., (2010) (40 and 60 °C) are compared with respective ChemSheet equilibrium calculations for temperatures 40-80C, with one result (40 °C) from the e-NRTL model. In ChemSheet, temperature-dependent Pitzer parameters are typically used (Pajarre et al., 2018); in this case both models agree reasonably well with each other and with measurements.

A respective aqueous phase diagram for the equilibrium system is shown in Figure 19 in terms of the partial pressure of CO_2 and Na_2CO_3 molality. In such diagram, the temperature dependent solubility of $NaHCO_3$ becomes clearly visible and the iso-pH-lines (only shown for 32 °C) will serve as an additional guideline *e.g.* when used to support practical purposes. The multicomponent diagram calculation may, of course, also comprise impurities, here included as hydrogen disulphide, H_2S, the equilibrium distribution of which between gas and liquid may directly be read from the data at each point of the diagram.
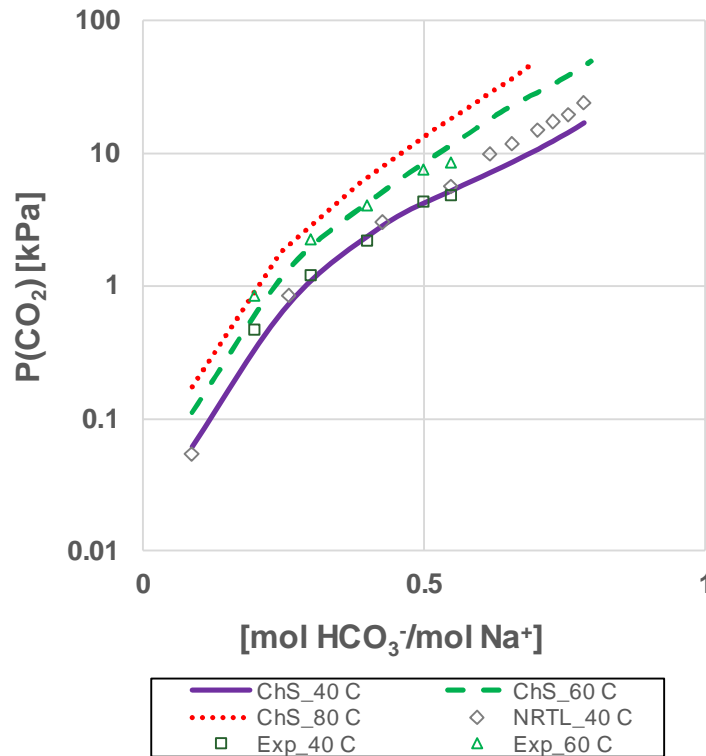
Figure 18. The partial pressure of CO_2 as function of Na_2CO_3 conversion to bicarbonate in 12 Na_2CO_3 % ☒ solution. The lines show ChemSheet equilibrium results, measured data and NRTL-model points are from Knuutila et al., (2010).
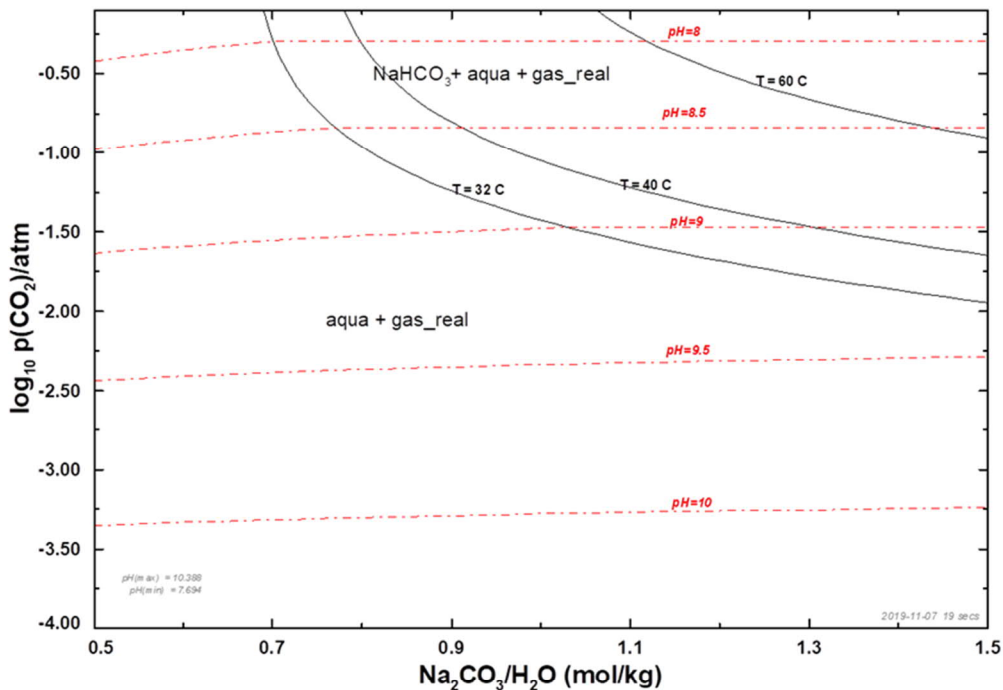
Figure 19. Aqueous phase diagram for the $H_2O - Na_2CO_3 - H_2S$-N_2- –system. H_2S /H_2O (mol/kg)=3.0e-8, N_2 /H_2O (mol/kg)=1.2; 32-60 °C, 1 atm. Superimposing of three temperatures shows the increasing solubility of $NaHCO_3$ with increase of temperature. Iso-pH curves shown merely for T= 32 °C.

To illustrate the usage of affinity- extent of reaction -diagrams for such aqueous system the constraints were set for the absorption of CO_2 and precipitation of bicarbonate, as shown in Table 6.

Table 6. Extended matrix for the aqueous carbon dioxide - sodium carbonate absorption system

N	O	C	H	Na	EA	$v(CO_2)$	$v(NaHCO_3)$	
2	0	0	0	0	0	0	0	$N_2(g)$
0	2	0	0	0	0	0	0	$O_2(g)$
0	2	1	0	0	0	1	0	$CO_2(g)$
0	1	0	2	0	0	0	0	$H_2O(g)$
0	1	0	2	0	0	0	0	H_2O
0	0	0	1	0	−1	0	0	H^+
0	1	0	1	0	1	0	0	OH^-
0	2	1	0	0	0	0	0	$CO_2(aq)$
0	3	1	1	0	1	0	0	HCO_3^-
0	3	1	0	0	2	0	0	CO_3^{2-}
0	0	0	0	1	−1	0	0	Na^+
0	3	1	0	2	0	0	0	$Na2CO_3^{\circ}$
0	1	0	1	1	0	0	0	$NaOH$
0	3	1	1	1	0	0	1	$NaHCO_3$
0	0	0	0	0	0	1	0	r_1^+
0	0	0	0	0	0	−1	0	r_1^-
0	0	0	0	0	0	0	1	r_2^+
0	0	0	0	0	0	0	−1	r_2^-

| Constraints set for the reactions:	
$CO_2(g) \rightarrow CO_2(aq)$	(r_1^+)
$Na^+ + HCO_3^- \rightarrow NaHCO_3$	(r_2^+)

In Figure 20 (left), the equilibrium diagram is presented in using molalities of CO_2 and Na_2CO_3 as axis variables. Then in Figure 20 (right) the affinity of reaction r_2^+ has been used for the Y-axis, while the reaction r_1^+ is assumed to be in equilibrium. The effect of temperature on the solubility of sodium bicarbonate is shown equally when compared with Figure 19. The affinity of $NaHCO_3$ precipitation is positive at 32 C in the region where the molality of Na_2CO_3 exceeds 0.442 m, while the same limit for the precipitation equilibrium at 60 C is observed at 0.732 m. The zero phase fraction line crosses the zero affinity line at these points, equally recognised in the left equilibrium diagram when following 1 m CO_2 dashed line.
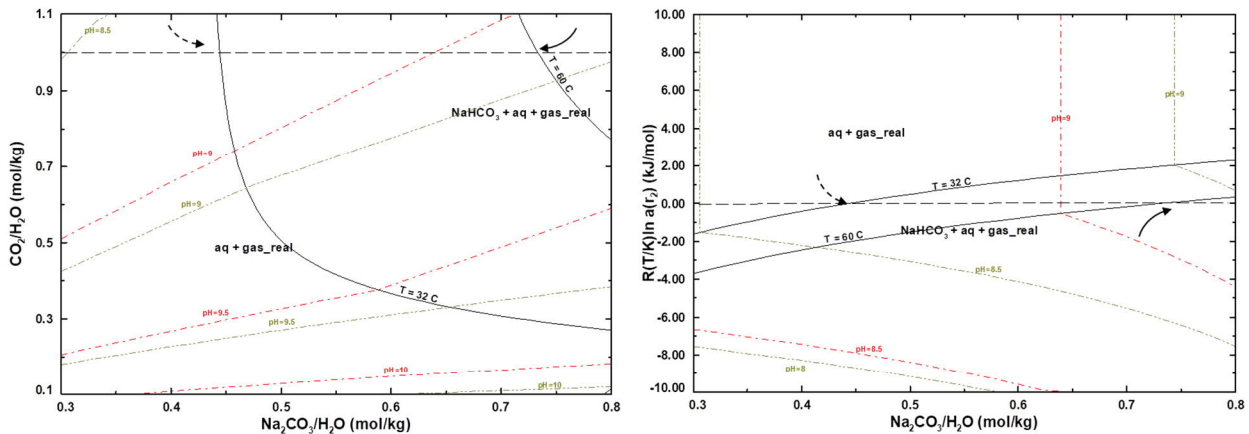
Figure 20. Aqueous phase diagram for the $H_2O - Na_2CO_3 - CO_2$- N_2- –equilibrium system (left) compared with the potential diagram where the affinity of CO_2 absorption is assumed to be zero and Y-axis shows the driving force of $NaHCO_3$ precipitation (right). N_2/H_2O (mol/kg) = 4; pH colour code: olive dash-dot-dot – 32 C; red dash-dot - 60 °C. The corresponding equilibrium points at 1.0 mol CO_2 /kg H_2O are marked with dotted (32 °C) and solid (60 °C) arrows.

In Figure 21 the affinity of $NaHCO_3$ precipitation is assumed to be zero and, instead the extent of reaction r_1^+ has been used for the x-axis variable. For the time being FactSage only allows the use of positive integers as virtual constraints and thus the constraint was actually set for all carbonaceous species in the aqueous solution as well as in condensed phases - *i.e.* regarding all these as products of constrained CO_2 absorption, yet in mutual equilibrium with each other. Then, the zero point for the EOR-X-axis must be set for the amount of constraint (r_1^+ phase) in the feed, while FACTSAGE, of course, performs the calculation using the total amount of this component. In Figure 21 the amount of feed Na_2CO_3 is 0.3435 m and a system containing 0.4027 m of r_1^+ gives a condition of 0.283 m Na_2CO_3 and 0.226 m $NaHCO_3$ in the solution, corresponding the condition in the experiment of Wylock et al., (2008). , performed at 293 K, 1 atm (m used here as the symbol of molality, mol/kg H_2O).

The *T,ξ*-diagram maps the reaction process, indicating the also conditions for $NaHCO_3$ - precipitation and the equilibrium limit for CO_2 absorption. As the work of Wylock et al., (2008) was entirely based on concentration variables, their reported pH-values were adjusted to correspond the respective hydrogen ion activities to compare with the iso-pH-lines in the FactSage diagram at 293 K, shown in the diagram on this isotherm. The respective ChemSheet model associated with the same experimental data is shown in the insert of Figure 21. One must keep in mind that no kinetic rate parameters are involved and thus while the pH values for the initial condition and the final equilibrium in each temperature are well defined, the intermediate region is subject to the assumption of local chemical equilibrium, as the EOR-constraint by necessity does not include any mechanistic assumptions. Thus, the iso-pH lines in the intermediate region remain somewhat approximate. The graphs yet indicate that the EOR- diagram method allows for a robust approach to foresee the reaction conditions within a relevant pH range, including pH-dependent formation of solids which often is omitted when using kinetic modelling procedures (*e.g.* Wylock et al., 2008).
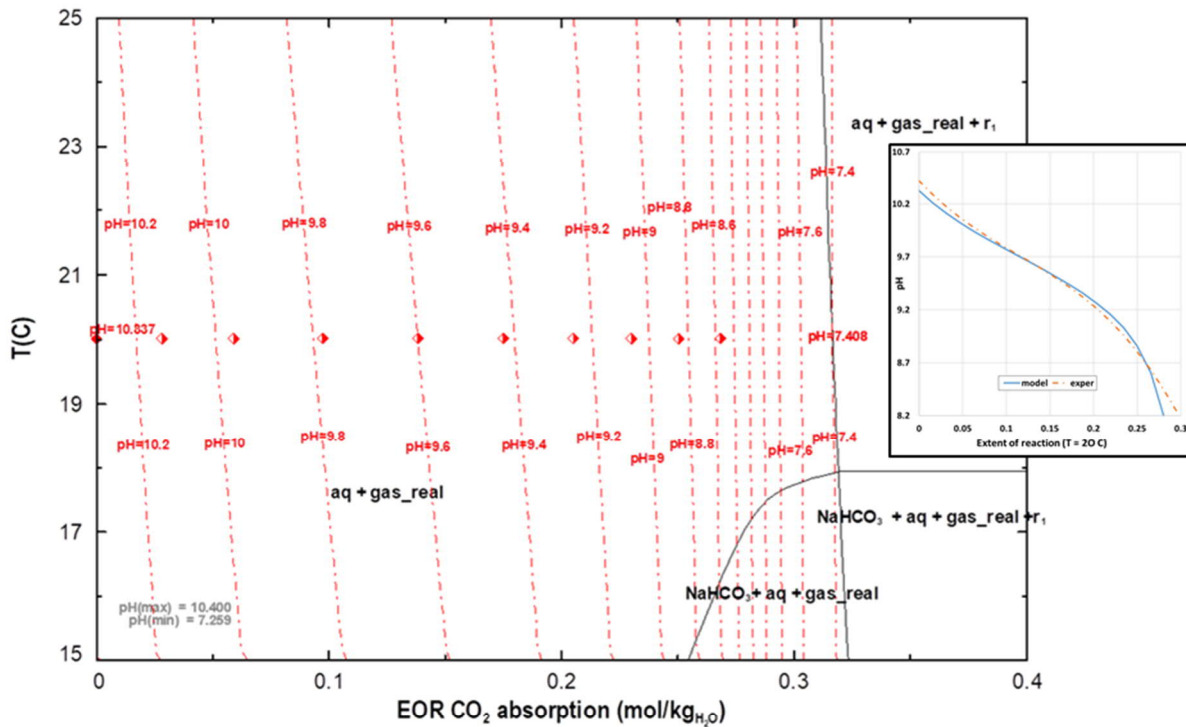
Figure 21. Temperature – extent of reaction diagram for the $H_2O - Na_2CO_3 - CO_2 - N_2$-system at 1 atm. Affinity of NaHCO₃ precipitation is set to zero. Extent of the absorption reaction is assumed to follow the constraint set for carbonaceous species in the liquid and solid phases. Experimental points of Wylock et al (2008) as adjusted to the FactSage activity scale shown at the 'isotherm' of 293K, each value shows measured pH of the nearest calculated iso-pH line at given EOR (end points with their pH -values shown separately). Na_2CO_3 0.3425 m; r_1^+ 0.4027 m; CO_2 1.0 mol/kg H_2O. The insert shows the respective ChemSheet model result at 20 °C.

3.4.3 Conclusions

The driving force (affinity, D) and extent of reaction (EOR, ξ) were used as axis variables to produce phase diagrams for non-equilibrium conditions by using the Calphad multiphase method. Particular focus was in studying the thermodynamic validity of the suggested technique, which is pursued to be consistent with the methodology that is used for conventional equilibrium phase diagrams. An aqueous system absorbing CO_2 into a Na_2CO_3 solution with possible precipitation of $NaHCO_3$ was used as an example.

The results indicate that the proposed affinity-EOR-diagrams are generically applicable for various multiphase problems. The new method can be applied for 'mapping' reaction conditions in terms of thermodynamic potentials and concentration variables.

Aqueous processes often appear in non-equilibrium states that involve slow reaction kinetics or in metastable conditions, for which however *e.g.* temperature, pH and redox potential (Eh) as well as molar amounts of given ionic species can be measured with relative ease and with reasonable accuracy. It may be anticipated that computational studies of the 'freezing-in-conditions' for these systems will have practical significance both in model-based design of experiments as well as in interpreting measured results.

The thermodynamics-based diagrams also provide a practicable technique to approximate reaction conditions when/if no kinetic data is available, being thus related with techniques extensively used in materials technology *e.g.* for Scheil solidification and paraequilibrium studies (Koukkari and Pajarre, 2021). While the use of D, ξ-diagrams is by necessity restricted with the limited number of assumptions, the respective CFE approach of course can further be developed to kinetic-thermodynamic process models, which then include the necessary mechanistic assumptions as well as time-dependent rate parameters

4. Concentrates and Brines

4.1　Multicomponent aqueous solution model based on BET / GAB approach

Risto Pajarre

Aqueous solutions are one of the main application areas of equilibrium thermodynamics. However, when it comes to highly concentrated solutions the most widely used non-ideal solution model, the Pitzer model (Pitzer, 1991), is typically valid only up to concentrations about 6 mol/kg. Model extensions are possible (Pajarre et al., 2018), but usually require significant number of additional fitting parameters.

An alternative to traditional solution models for highly concentrated aqueous solutions are the Brunauer–Emmett–Teller (BET) and the related Guggenheim–Anderson–De Boer (GAB) models (Stokes and Robinson, 1948). They both are based on the idea that the highly concentrated solution could be modelled as water adsorbing on the solute salt. They have been shown to work in solutions that are beyond the validity range of the Pitzer model but do not work in dilute and moderately dilute solutions. Purpose of this study was to extend the earlier work (Pajarre and Koukkari, 2018) on the application of BET / GAB model within a multiphase equilibrium solvers and test its usage with a number of highly soluble salts in a combination with the standard Pitzer model to create a model that would be valid from dilute solutions to the solubility limit.

4.1.1　Methodology

For the general model framework of the highly concentrated solutions the GAB model with the model specific parameter K having a value less unity was chosen. This makes a phase applying the model thermodynamically unstable in the dilute range compared to *e.g.* Pitzer model (Figure 22). Therefore, it becomes feasible to use a free energy minimiser with a combined thermodynamic model so, that the equilibrium description is always the one suitable for the concentration range, Pitzer model in dilute and moderately concentrated solutions and the GAB adsorption model in the highly concentrated range (Figure 23)
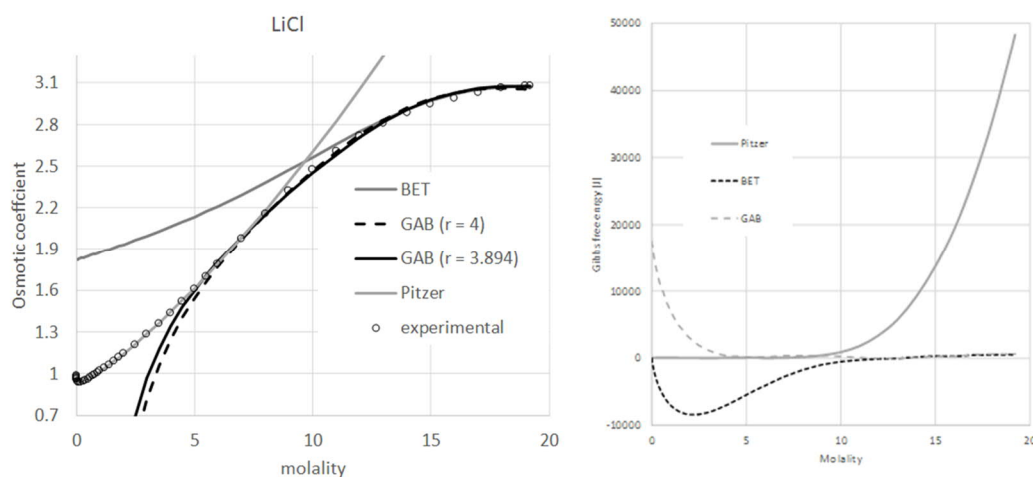

Figure 22. Higher osmotic coefficient (Pajarre and Koukkari, 2018) *(left) and the corresponding Free energy* (Pajarre and Koukkari, to be published) *(right) shown with GAB model in the dilute range and Pitzer model in the highly concentrated range in LiCl model solution.*
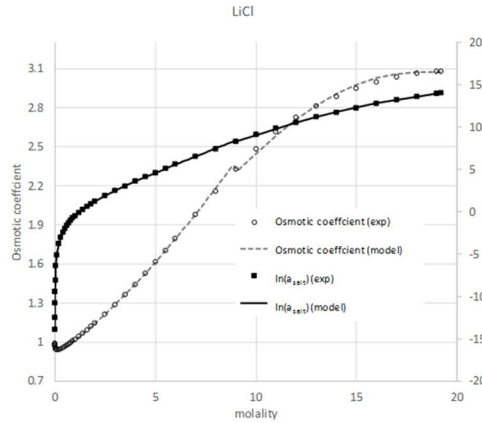
Figure 23. Modelled solute salt activity and osmotic coefficient using combined Pitzer – GAB model. The small kink around 9 mol/kg is an artefact caused by model phase transition between the dilute and concentrated range.

It was estimated that acceptable fit with experimental data could be obtained by using one constant value (the same for all systems) for the GAB parameter K and two salt specific parameters r and E that were assumed to vary linearly in respect to temperature.

For mixed electrolyte solutions, if sufficient data is available, the model structure enables inclusion of interaction parameters for better fit. If they are lacking, the multicomponent system follows the Zdanovskii-Stokes-Robinson relationship (Stokes and Robinson, 1966) for mixtures (Pajarre and Koukkari, 2018; Pajarre and Koukkari, n.d.).

4.1.2 Results

Experimental water activity data in concentrated range was fitted to the GAB model to derive the model parameters. Example model fits are shown in Figure 24. During the work it was observed that GAB model fit became noticeably worse if the water activity was less than 0.05. Also, the chosen model framework did not seem to work in temperatures above 100°C, possibly because the relationship of the chosen (constant) K parameter and vaporisation energy of water.

Figure 24. GAB model function (Stokes and Robinson, 1948) *as a function of water activity in NaOH (left) and CaCl₂ solution (right)*

Obtained parameter values for the salts under study are shown in Table 7.

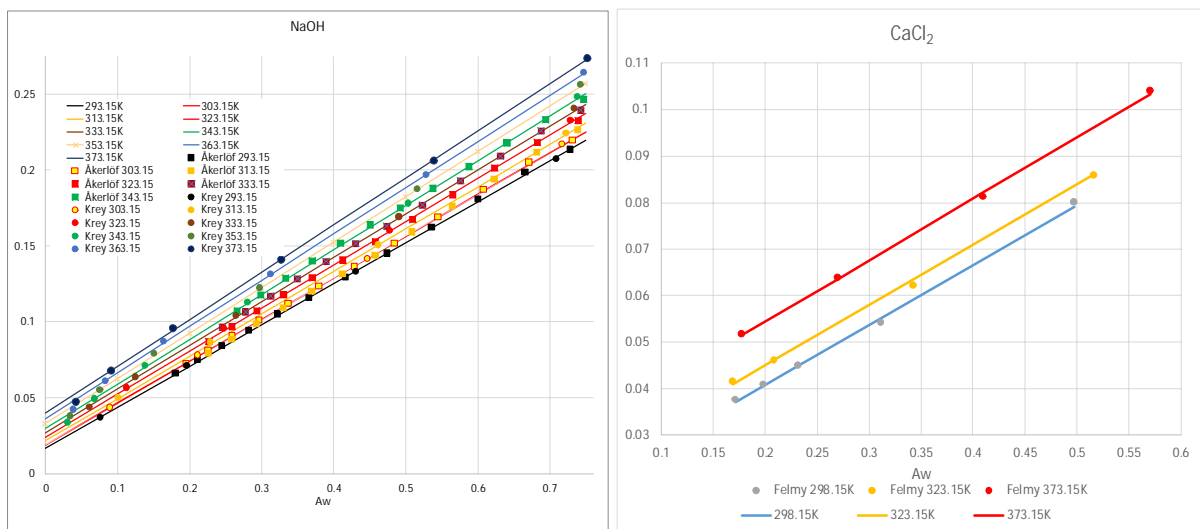*Table 7. Parameters for the GAB model. K is constant in all systems*

		a	b	at 298.15 K
	Ek	639.697262	-0.9903817	344.41
	K = exp(-E/RT)			0.870
CaCl2	r	9.655591564	-0.00878782	7.04
	E	6447.271737	-1.95364767	5864.79
KOH	r	8.289930409	-0.00799447	5.91
	E	1128.226566	19.92731251	7069.55
LiCl	r	6.09973796	-0.0072459	3.94
	E	5087.644587	6.171240917	6927.60
NaOH	r	5.790522161	-0.00778864	3.47
	E	8139.737426	-3.08755544	7219.18
LiNO3	r	3.605827292	-0.00163126	3.12
	E	6118.680172	-4.38889511	4810.13
NaNO3	r	4.849837707	-0.00191836	4.28
	E	9655.277311	-7.34262151	7466.07
KNO3	r	5.882853139	-0.00230165	5.20
	E	11914.6122	-10.1695308	8882.57
Ca(NO3)2	r	6.571146956	-0.00218956	5.92
	E	14929.00909	-14.3288689	10656.86
KCl	r	8.326142316	-0.00269535	7.52
	E	7387.259941	-20.7911888	1188.37
NaCl	r	9.67017201	-0.00356864	8.61
	E	10044.43598	-23.1198019	3151.27
LiOH	r	7.611901413	-0.00476056	6.19
	E	14280.99952	-12.484693	10558.69
Ca(OH)2	r	5.460917258	-0.01218704	1.83
	E	12938.0716	-19.2264273	7205.71

Full report of the results of the study will be included in the upcoming paper "CALPHAD aqueous solution model based on the BET approach: Multicomponent solutions", to be submitted to the CALPHAD journal in 2021.

4.2 LIFAC -electrolyte model

Karri Penttilä

Various industrial and natural processes require the knowledge of the real behaviour of aqueous electrolyte solutions, because the salt that is present in the liquid phase may influence the phase equilibrium behaviour significantly. Even small amounts of salt may have an appreciable impact on the boiling points, the mutual solubility, or the relative volatility of solvents. The main solvent found in bioprocesses, which is water, is highly polar and has the capability to dissolve large amounts of electrolytes. The ions resulting from dissociated electrolytes pose a problem for thermodynamic modelling, as electrolytic solutions behave highly non-ideally even in small concentrations (Hautala, 2016). A reliable knowledge of the phase equilibria of electrolyte systems is essential for the design and simulation of different chemical processes, including wastewater treatment, extractive distillation, various extraction processes, extractive and antisolvent crystallization of salts, petroleum refining, coal gasification, environmental protection, petroleum and natural gas exploitation, formation of gas hydrates, and various absorption and gas scrubbing processes. The quality of the description of the phase equilibrium behaviour for electrolyte systems is strongly dependent on the thermodynamic model (gE model, group contribution concept, equation of state (EOS), EOS + gE mixing rules) and the quality of the parameters used (Kiepe et al., 2006).

In this work, LIQUAC (Li et al., 1994) and LIFAC (Yan et al., 1999) models are implemented and added as user defined models to ChemSheet (Koukkari et al., 2000) and ChemApp (Petersen and Hack, 2007). Furthermore, a separate Excel based tool was developed to be able to fit various activity model parameters by using Solver Add-in. Mean ionic activity coefficients for strong electrolytes in pure water can be calculated accurately with these models. By assuming total dissociation of the salt, these models are generally applicable for the reliable prediction of arbitrary systems with strong electrolytes up to high salt concentrations. With ChemApp and its global Gibbs energy minimization algorithm it becomes possible to combine LIQUAC and LIFAC electrolyte models with various vapour and solid phase models in order to solve vapour/liquid/liquid equilibrium (VLLE) including complex chemical reactions, solid dissolution and precipitation. Moreover, it also becomes possible to combine equilibrium and kinetically controlled reactions by using constrained free Gibbs energy (CFE) approach (Koukkari and Pajarre, 2006).

4.2.1 LIFAC Model

In the LIQUAC and LIFAC models, the excess Gibbs energy for single- or mixed-solvent electrolyte systems is calculated as the sum of three contributions (Figure 25):

$$G^E = G^E_{LR} + G^E_{MR} + G^E_{SR} \tag{42}$$

The first term represents the long-range (LR) interaction contribution and it takes into account direct charge effects like attraction and repulsion between ions and the formation of a solvate shell in solution. The second term describes the middle-range (MR) interaction contribution caused by charge dipole and charge-induced dipole interactions. The third term (SR) expresses the contribution of the non-charge interactions (UNIQUAC and UNIFAC).
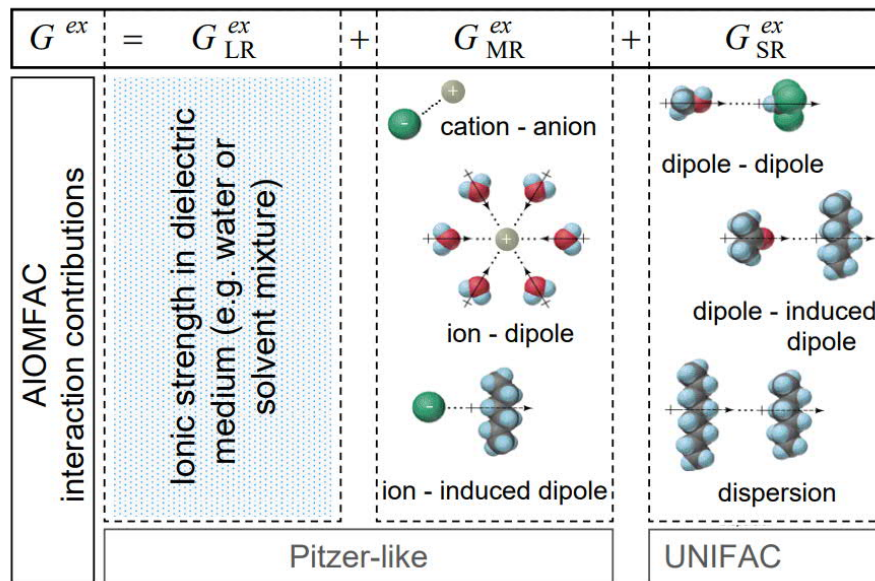
Figure 25. LIQUAC and LIFAC contributions (Zünd, 2007)*.*

In UNIFAC model (Fredenslund et al., 1977), the functional groups of a chemical species are divided into (functional) main groups and subgroups. For example, the alkyl groups CH_3, CH_2, CH and C are different subgroups of the main group CH_2 (Figure 26).

Main group	Sub group	Name	R	Q	Sample molecule
	1	CH_3	0.9011	0.848	Hexane
1	2	CH_2	0.6744	0.540	=2*(1)+4*(2)
(CH_2)	3	CH	0.4469	0.228	
	4	C	0.2195	0.000	
	5	CH_2=CH	1.3454	1.176	2-Methyl-1-butene
2	6	CH=CH	1.1167	0.867	=2*(1)+1*(2)+1*(7)
(C=C)	7	CH_2=C	1.1173	0.988	
	8	CH=C	0.8886	0.676	
	70	C=C	0.6605	0.485	

Figure 26. Examples of UNIFAC and LIFAC main and subgroups.

The group contribution components consist of volume contribution (R_k), surface area contribution (Q_k), and interaction parameter between the functional groups ($a_{i,j}$), which are obtained from wide range of experimental measurements. In LIFAC model, the UNIFAC group contribution method is generalised to water and inorganic ions but their main groups, subgroups, and chemical species are in each case identical. Figure 27 shows currently published groups.

4.2.2   LIFAC Activity Model

According to the thermodynamics relation:

$$\ln \gamma_i = \frac{1}{RT} \frac{\partial G^E}{\partial n_i} \tag{43}$$

Since for ions and for solvents a different reference state and a different concentration scale is used (molality), the three terms are calculated differently for ions and solvents. As

reference state for the ions the infinite diluted solution is chosen. This means that for the calculation of the activity coefficient two different equations are used:

$$\ln \gamma_{solv}^{x} = \ln \gamma_{solv}^{x,LR} + \ln \gamma_{solv}^{x,MR} + \ln \gamma_{solv}^{x,SR} \tag{44}$$

$$\ln \gamma_{ion}^{*,m} = \ln \gamma_{ion}^{*,m,LR} + \ln \gamma_{ion}^{*,m,MR} + \ln \gamma_{ion}^{*,m,R} \tag{45}$$

The indexes *solv* and *ion* indicate the activity coefficient of the solvent or the ion, the indexes *x* and *m* stand for the concentration scale that is used, mole fraction (*x*) or molality (*m*). The asterisk indicates the reference state of the infinite diluted solution for the ions.

For solvents and ions, the long-range (LR) part of the activity coefficient is calculated as:

$$\ln \gamma_i^{x,LR} = \left(\frac{2AM_{solv}d_{mix}}{b^3 d_{solv}} \right) \left(1 + b\sqrt{I} - \frac{1}{(1+b\sqrt{I})} - 2\ln\left(1 + b\sqrt{I} \right) \right) \tag{46}$$

$$\ln \gamma_{ion}^{LR} = \frac{z_{ion}^2 A\sqrt{I}}{1+b\sqrt{I}} \tag{47}$$

where z_{ion} stands for the charge number of the regarded ion, M_{solv} is the molar mass of the solvent in kg/mol, d_{solv} is the density of the regarded solvent in kg/mol, d_{mix} is the density of the solvent mixture and I is the ionic strength given as follows:

$$I = \frac{1}{2}\sum_{ion} z_{ion}^2 m_{ion} \tag{48}$$

where m_{ion} is the molality of the ions in solution in mol/kg. A and b are the Debye-Hückel parameters dependent on the absolute temperature and the relative dielectric constant of the solvent mixture. A polynomial equation has been fitted for number of organic solvents to calculate it. Parameters of these polynomials and equations for the middle-range (MR) part of the activity coefficients and the for interaction functions $B_{i,j}(I)$ can be found in Mohs (Mohs and Gmehling, 2013).

For the calculation of the short-range term of the LIQUAC/LIFAC model UNIQUAC/UNIFAC is used. In both cases the part consists of a combinatorial (C) and a residual (R) part.

For both the solvents and the ions, the Combinatorial term in short-range (SR) part of the activity coefficient is calculated as:

$$\ln \gamma_i^{SR} = \ln \gamma_i^{C} + \ln \gamma_i^{R} \tag{49}$$

$$\ln \gamma_i^{C} = 1 - V_i + \ln i - 5q_i \left(1 - \frac{V_i}{F_i} + \ln \frac{V_i}{F_i} \right) \tag{50}$$

$$V_i = \frac{r_i}{\sum_j x_j r_j} \tag{51}$$

$$F_i = \frac{q_i}{\sum_j q_j} \tag{52}$$

where x_i is the mole fraction of the regarded species (including the ions) while r_i and q_i stands for the relative van der Waals volume and surface area of the species, respectively.

For UNIQUAC and LIQUAC models these are fitted for number of species, but for LIFAC and UNIFAC model these are calculated using the subgroup structure of the molecule representing the species:

$$r_i = \sum_k n_k R_k \tag{53}$$

$$q_i = \sum_k n_k Q_k \tag{54}$$

where n_k is the number of subgroups of type k in molecule i and R_k and Q_k are the van der Waal volume and surface area of subgroup k, respectively.

In the UNIQUAC and LIQUAC model the Residual term in short-range (SR) part of the activity coefficient is calculated as:

$$\ln \gamma_i^R = q_i \left(1 - \ln \sum_j \theta_j \Psi_{j,i} - \sum_j \frac{\theta_j \Psi_{i,j}}{\sum_k \theta_k \Psi_{k,j}} \right) \tag{55}$$

$$\theta_i = \frac{x_i q_i}{\sum_j x_j q_j} \tag{56}$$

In the UNIFAC and LIFAC model the Residual term in short-range (SR) part of the activity coefficient depends on the group structure of the molecule representing the species:

$$\ln \gamma_i^R = \sum_k n_k \left(\ln \Gamma_k - \ln \Gamma_k^{(i)} \right) \tag{57}$$

where Γ_k is the group residual activity coefficient, and $\Gamma_k^{(i)}$ is the residual activity coefficient of group k in a reference mixture containing only all molecules of type i:

$$\ln \gamma_k^R = Q_k \left(1 - \ln \sum_m \theta_m \Psi_{m,k} - \sum_m \frac{\theta_m \Psi_{k,m}}{\sum_n \theta_n \Psi_{n,m}} \right) \tag{58}$$

where θ_m is the area fraction of group m and X_m is the fraction of group m in the mixture:

$$\theta_m = \frac{Q_m X_m}{\sum_n Q_n X_n} \tag{59}$$

$$X_m = \frac{\sum_i n_m^{(i)} X_m}{\sum_i \sum_k n_k^{(i)} X_i} \tag{60}$$

The group interaction parameter $\Psi_{i,j}$ is given as:

$$\Psi_{i,j} = exp\left(\frac{a_{i,j}}{T}\right) \tag{61}$$

where T is the absolute temperature. There are two parameters for each group-group interaction, $a_{i,j}$ and $a_{j,i}$, where $a_{i,j} \neq a_{j,i}$.

Since for ions the infinite diluted mixture is chosen as reference state, the residual and combinatorial term have to be normalised to this reference state. See Mohs and Gmehling, (2013) for the equations.

Number of LIQUAC and LIFAC parameters have been published in the literature. Kiepe et al., (2006) tabularizes number of calculated Relative van der Waals Group Volume (R) and Surface Area (Q) of solvents, solvent groups and Ions for mod. LIQUAC and mod. LIFAC. It also tabularizes number of fitted MR parameters $b_{s,ion}$ and $c_{s,ion}$ between solvents and ions and for solvent groups and Ions, and number of fitted MR parameters $b_{c,a}$ and $c_{c,a}$ between cations and anions for modified LIQUAC and LIFAC. Also used UNIQUAC and UNIFAC parameters $a_{i,j}$ and $a_{j,l}$ are tabularized for the main groups.

Mohs and Gmehling, (2013) has refitted large number of solvent group and ion parameters for a revised LIQUAC and LIFAC model, which enables the user to describe mean activity coefficients, osmotic coefficients and also vapour–liquid equilibria reliably. Furthermore, the prediction of salt solubilities in aqueous solutions and mixed solvents can be performed successfully. These parameters are also used in this work. User defined model as well as the Excel tool both have internal data tables containing their values. There is also possibility to enter user defined parameters either to overwrite existing values or to enter parameters for new solvent and ion groups.

Figure 27 shows parameter matrix for currently published LIFAC groups and ions: Red boxes refer to existing UNIFAC interaction parameters ($a_{i,j}$ and $a_{j,i}$) between the solvent groups. Blue and green boxes refer to existing LIFAC interaction parameters ($b_{i,j}$ and $c_{i,j}$) between solvent groups and ions and cations and anions, respectively. It can be seen that many interactions are still missing and need to be fitted.
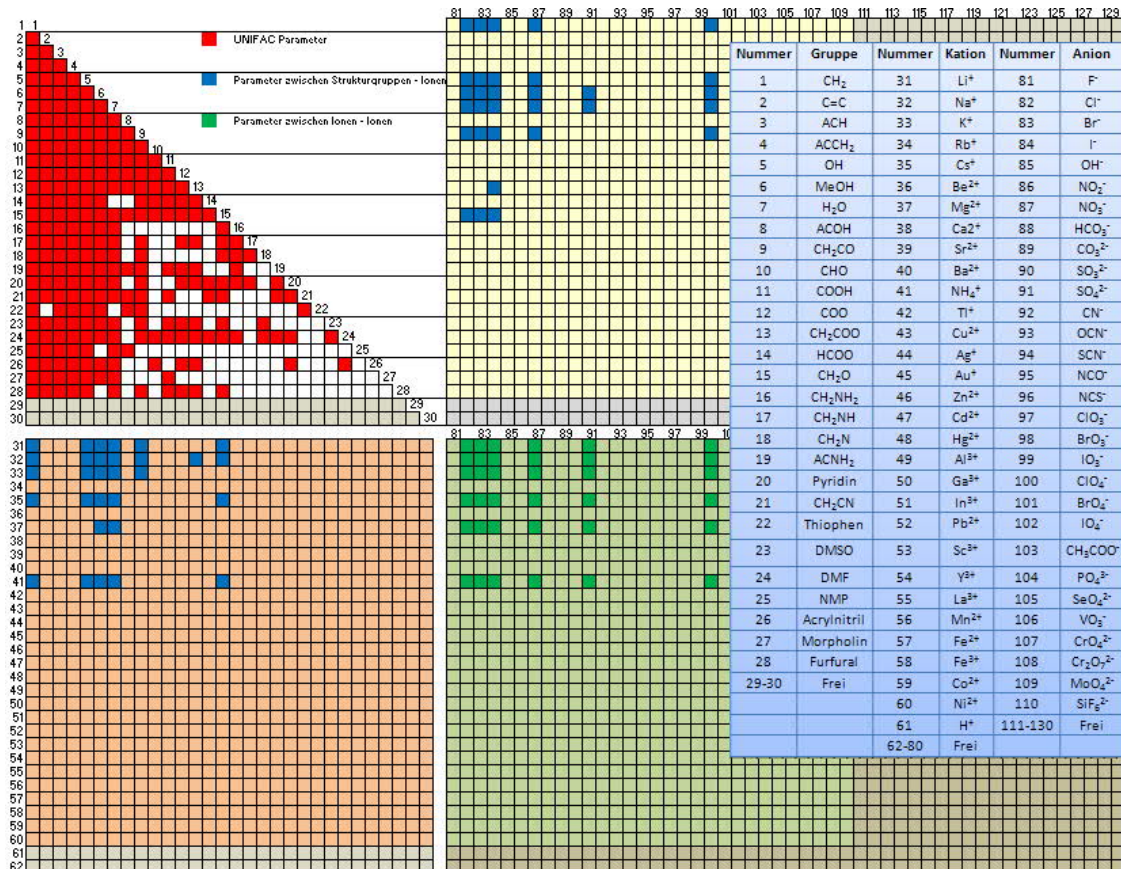
Figure 27. Parameter matrix for LIFAC solvent groups and ions (Mohs, 2011).

4.2.3 ChemSheet and ChemApp

ChemSheet (Koukkari et al., 2000) is Excel Add-in for ChemApp. It provides intuitive, easy-to-use interface for ChemApp and its thermodynamic routines. A special user defined model compatible version of ChemApp calls specific routines in an external usermod.dll file when it encounters a certain phase model name in ChemSage data-file (USX?). User defined routine should then calculate $\ln\gamma_i$ (partial excess Gibbs energies) for each species in the given phase at given temperature, pressure and composition. For aqueous phase model, routine USERGP is called (see Figure 28)

```
SUBROUTINE USERGP[DLLEXPORT](NTXX, ITXX1, ITXX2, ITXX3, ITXX4, WTXX, PXX, TXX,

G0XX, V0XX, XXX, CHXX, MDLXX, NCXX, APHI, SION, TMI, GINT, GXX, OSMO)
```

NTXX	= ORDER OF GIVEN INTERACTION	
IXX?	= INTERACTION PARAMETERS GIVEN IN THE DATA-FILE	
WTXX	= UNDIMENSIONAL INTERACTION ENERGY (DIVIDED BY R*T)	
PXX	= PRESSURE [bar]	
TXX	= TEMPERATURE [K]	
G0XX	= DIMENSIONLESS STANDARD GIBBS ENERGIES	
V0XX	= MOLAR VOLUMES [cm3]	
XXX	= MOLE FRACTIONS OF ALL PHASE CONSTITUENTS	
CHXX	= CHARGE OD ALL SOLUTES	
MDLXX	= MODEL NAME FOR THE PHASE	
APHI	= PARAMETER A(PHI) OF THE DEBYE-HUECKEL LIMITING LAW	
SION	= IONIC STRENGTH	
TMI	= SUM OF SOLUTE MOLALITIES	
NCXX	= NUMBER OF SPECIES IN THE PHASE	
GINT	= CONTRIBUTION TO THE EXCESS PARTIAL GIBBS ENERGY FROM THE DEBYE-HUECKEL TERM AFTER THIS HAS BEEN DIVIDED BY A SOLUTE CHARGE SQUARED	
GXX	= CONTRIBUTION TO THE EXCESS PARTIAL GIBBS ENERGY OF ALL PHASE CONSTITUENTS FROM THE GIVEN INTERACTION	
OSMO	= CONTRIBUTION TO THE OSMOTIC COEFFICIENT FROM THE DEBYE-HUECKEL TERM (NTXX = 0) OR FROM THE GIVEN INTERACTION (NTXX > 0)	

Figure 28. Entry point in usermod.dll to calculate the contributions to the excess partial Gibbs energies in an aqueous phase.

Already several EOS and group contribution models have been implemented in earlier projects (Leppävuori and Koukkari, 2012). These include:

- Unifac (liquid phase)
- Original VLE
- Original LLE
- Dortmund modified
- Lyngby modified
- NRTL(liquid phase)
- Dortmund PSRK (used with PSRK only)
- Dortmund VTPR (used with VTPR only)
- SRK (for only vapour phase or vapour+liquid phases)
- PR (for only vapour phase or vapour+liquid phases)
- PSRK (for vapour+liquid phases using PSRK Unifac)
- VTPR (for vapour+liquid phases using VTPR Unifac)

In this work LIQUAC and LIFAC models were added to the usermod.dll. User defined model project has been implemented with Visual Studio and coded with Intel Visual Fortran (Intel Parallel Studio XE 2017). At the time of writing LIQUAC and LIFAC models are being tested and debugged.

4.2.4   Excel Tool

A separate Excel based tool to calculate the activities of various EOS and group contribution methods has also been made and LIFAC and LIQUAC models were added to it. Currently it supports the following models:

- SRK (vapour phase or vapour+liquid phases)
- PR (vapour phase or vapour+liquid phases)
- NRTL (liquid only)
- UNIFAC (liquid, original VLE + LLE, Dortmund + Lyngby modified)
- LIQUAC + LIFAC (aqueous/electrolyte)

ChemApp User-defined models compiles as a dynamic-link library (DLL), which is not easiest to debug during the model coding and development. Thus, there was a need for a separate Excel based model for calculating/debugging the activity models with VBA modules and comparing calculated values against the literature values. Moreover, Excel Solver Add-in can be used with the Excel tool for parameter fitting (see Figure 29).

Excel tool contains one macro that is used as entry point for all model calculations.

FUNCTION MODEL_GET(Mode as Variant, Temp as Variant, Pres as Variant, Comp as Variant, Units as Variant, Parameters as Variant, Variables as Variant) as Variant

Mode	Model and mode ("NRTL",… and "HEA", "LIQ", "VAP", "LVE", "LLE")
Temp	Temperature (constant or range containing the temperature)
Pres	Pressure (constant or range containing the pressure)
Comp	Composition (constant array or range array containing the composition values)
Units	Units for T, P and X (constant array or range array containing the unit names)
Parameters	Model parameters (range array containing the values)
Variables	Variable(s) (constant names or range array containing the names)

MODEL_GET returns and saves the calculated values as array formula. An array formula is a formula that can perform multiple calculations on one or more items in an array. Array formula must be entered by pressing Ctrl+Shift+Enter. Figure 29 shows an example of using MODEL_GET with Excel Solver to fit parameters of the NRTL model for a ternary LLE case (extraction of levulinic acid from water with 2-MTHF).
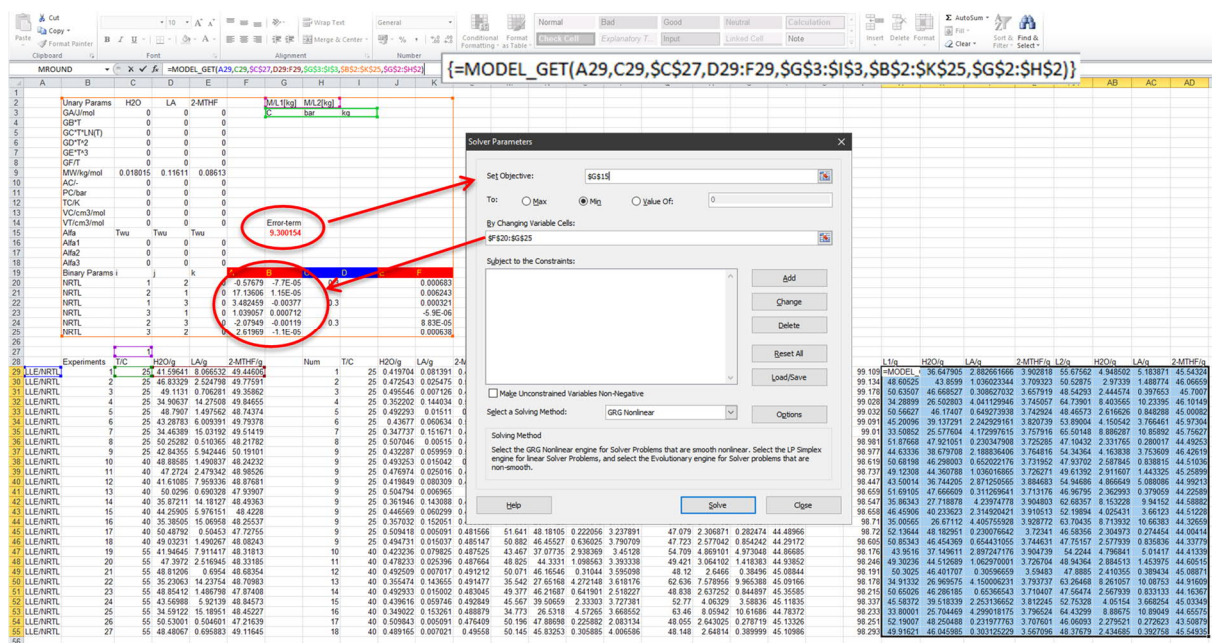

Figure 29. Fitting NRTL model parameters with Excel tool and Solver Add-in.

4.2.5   Application

Extraction of ZnSO₄ with kerosene and CYANEX (see Figure 30) was selected as a test application for the LIFAC model. This is a common test system for extraction and also set of measurements have been conducted at VTT during 2019/2020 in a separate project to find out the compositions of the two components in the aqueous and the organic phases.
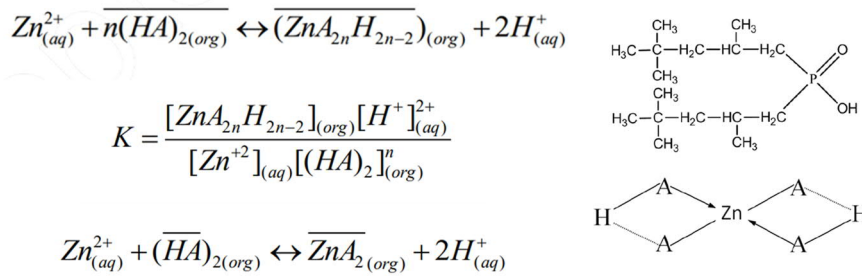
$$Zn_{(aq)}^{2+} + \overline{n(HA)_{2(org)}} \leftrightarrow \overline{(ZnA_{2n}H_{2n-2})}_{(org)} + 2H_{(aq)}^{+}$$

$$K = \frac{[ZnA_{2n}H_{2n-2}]_{(org)}[H^{+}]_{(aq)}^{2+}}{[Zn^{+2}]_{(aq)}[(HA)_2]_{(org)}^{n}}$$

$$Zn_{(aq)}^{2+} + \overline{(HA)}_{2(org)} \leftrightarrow \overline{ZnA_{2}}_{(org)} + 2H_{(aq)}^{+}$$

Figure 30. Extraction of ZnSO₄ with kerosene and CYANEX® 272.

Thermodynamic system of the extraction process consists of an aqueous (H_2O) and an organic solution phase kerosene, which is not a pure phase but very similar to dodecane $C_{12}H_{26}$. CYANEX 272 is a dialkyl phosphinic acid extractant widely used especially for the separation of cobalt from nickel to produce high purity cobalt salts and cobalt metal. Since the active component of CYANEX 272 extractant is a phosphinic acid, metals are extracted through a cation exchange mechanism. It can be dimerized through hydrogen bonding in the non-polar organic diluent (Begum et al., 2012). The LIQUAC and LIFAC models were not ready yet for parameter fitting or calculating the test case at the time of writing the report.

4.2.6   Conclusions

Mean ionic activity coefficients for strong electrolytes in pure water can be calculated accurately with LIQUAC and LIFAC models. By assuming total dissociation of the salt, these models are generally applicable for the reliable prediction of arbitrary systems with strong electrolytes up to high salt concentrations. With the corrected reference state for the ion activity coefficient, mean ionic activity coefficients in non-aqueous or mixed-aqueous systems that contain strong electrolytes can also be predicted. But at the same time there is lack of experimental data for organic activities in all solutions and electrolyte activities in organic-electrolyte solutions. There is also lack of parameters for standard thermodynamic properties like enthalpy for many organic molecules that are needed in solubility calculations.

With ChemApp and its global Gibbs energy minimisation algorithm it is possible to combine LIQUAC and LIFAC electrolyte models with various vapour and solid phase models in order to solve vapour/liquid/liquid equilibrium (VLLE) including complex chemical reactions, solid dissolution and precipitation. Moreover, it also possible to combine equilibrium and kinetically controlled reactions by using constrained free Gibbs energy (CFE) approach. However, further work is necessary to verify how well these models can be applied to multicomponent systems as they have conventionally been tested for ternary systems.

4.3 Non process elements in aqueous database for modelling industrial processes

4.3.1 Data evaluation for concentrated sulphide containing systems

Risto Pajarre

The data obtainable from VTT's aqueous database (Pajarre & al 2018) gives a fair basis for simulation of the aqueous processes occurring in the lime cycle of Kraft pulping. However, reliable data for sulphide solubility for the lime cycle conditions has been missing. In late 1990's Jarmo Heinonen working for KCL (Keskuslaboratorio) did series of solubility measurements (Heinonen, 1999) on concentrated Na_2S solutions within temperature range of 25°C-90°C. The data was but partially disclosed in a conference presentation(Heinonen, 1998). Within the DeepCleanTech task related to concentrated aqueous solutions and modelling of non-process elements (NPE) in Kraft pulping, this data could be used a part of the VTT aqueous solution database.

The KCL measurements had been done with Na_2S-KCl, Na_2S-K_2CO_3 and Na_2S-K_2SO_4 binary aqueous salt systems. Additionally, a data for the aqueous Na_2S-NaCl, Na_2S-Na_2CO_3, Na_2S-NaOH and Na_2S-Na_2SO4 systems had been collected from literature. While the original work included evaluated Pitzer parameters as fixed temperatures, in preliminary check it was found out that the thermodynamic standard state values and speciation were not compatible with the other data in the newer VTT database (Pajarre et al., 2018). Therefore, the parameters were reassessed applying the Pitzer formalism using the original experimental (by Heinonen and from referenced literature).

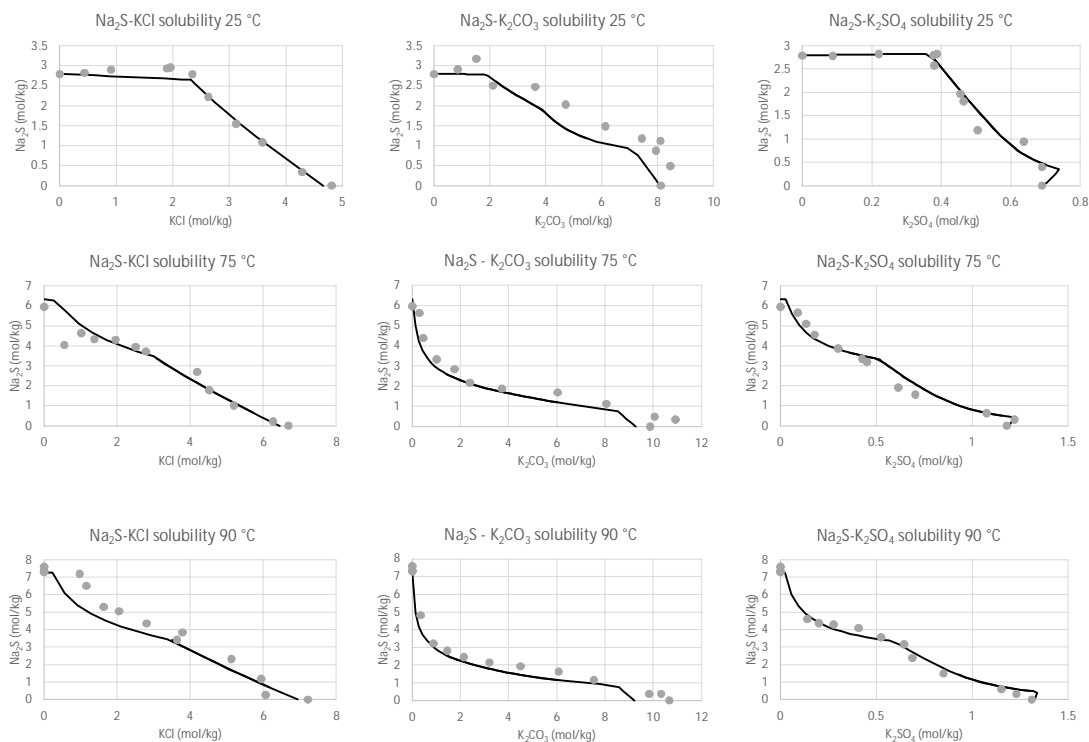Model results together with experimental data from (Heinonen, 1999) are shown in Figure 31.

Figure 31. Experimental data together with model curves for binary systems of Na_2S with KCl, K_2CO3 and K_2SO_4 at temperatures 25, 75 and 90 °C.

Additional model results are compared with data collected by Heinonen for systems containing Na_2S with NaCl, Na_2CO_3, NaOH and Na_2SO_4 in Figure 32.
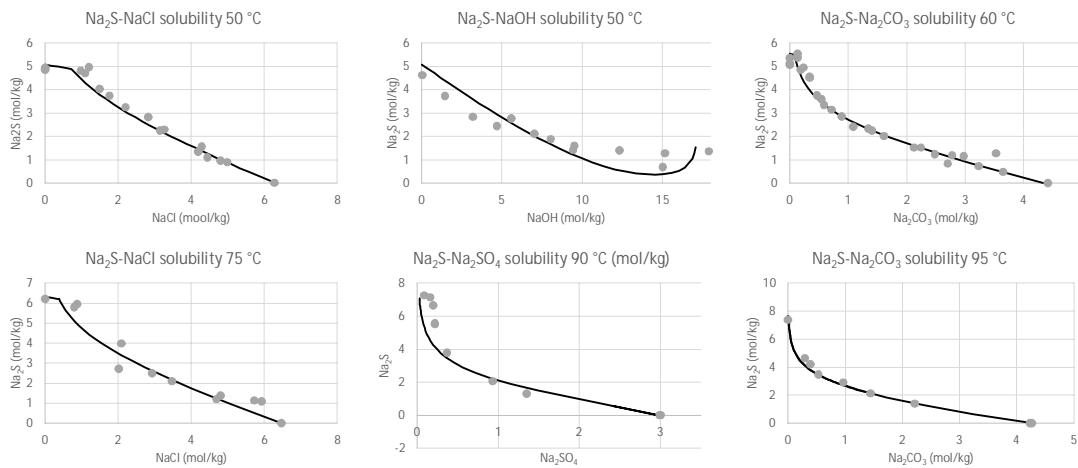
Figure 32. Literature data together with model curves for binary systems of Na_2S with NaCl, NaOH, Na_2CO_3 and Na_2SO_4 within temperature range 50-90 °C.

Thermodynamic parameters for the model are included in the updated database compiled during the project.

4.3.2 Updated database for aqueous modelling

As a part of the project a FactSage (Bale et al. 2016) version of the VTT aqueous solution database was constructed. This was done both for future database maintenance and to offer a product usable directly with other Factsage databases for thermochemical simulation. The work was based on the solution database created during the earlier Multirec project (Pajarre, Koukkari, and Kangas 2017). Due to restriction in allowed phase names in FactSage, most of the existing pure solid phases had to be renamed while phase descriptions containing first order phase transformations had to split to separate phases to be compatible with the FactSage standard. During the project number of new solid precipitates and some solution species were added to the data while some adjustments to the non-ideal aqueous solution model were made in order to improve the solubility predictions for Si and Al containing solutions. The newly evaluated sulphide systems were added to the database. The new database contains elements Al, Ba, C, Ca, Cl, Cu, Fe, H, K, Mg, Mn, N, Na, O, P, S, Si, Sr and Zn with gas and aqueous solution phases and two solid solutions (non-stoichiometric burkeite and glaserite). The total number of chemical species in the database is approximately 250.

Figure 33. View of the database species listing within FactSage

The database is an equilibrium database without reaction constraint options as the constraints are not supported by the current version of FactSage.

5. Modelling of bioreactor systems

Industrial biotechnology, bioremediation, and biohydrometallurgy increasingly generate thermodynamic models for processes that include biological phenomena. Gibbs energy minimization enable model construction with much less effort than a purely kinetic model due to the availability of thermodynamic parameters and the relatively rapid equilibration of acid-base reactions in aqueous solutions. However, biochemical systems tend to have dependent reactions, thus making the constraint selection challenging.

The solution space of a CFE model is a simplex (convex hull) spanned by a set of basis vectors. Every active constraint is a hyperplane touching one side of the simplex. The addition of a reaction constraint adds a hyperplane to split the solution space into two non-empty subspaces (reactants on one side and products on the other). Therefore, the maximum number of linearly independent reaction constraints is the number of linearly independent basis vectors. The selection of one reaction constraint limits the set of alternatives for the other reaction constraints. Therefore, the full set of constraints may need to be modified when adding a new reaction constraint to a system with reaction constraints.

Biochemical systems tend to have many reactions, sometimes more reactions than species. The generation of a thermodynamically consistent set of constraints and the mapping from deterministic reactions to these linearly independent constraints is essential for the development and utilization of these models.

5.1   MatriMa for generating reaction constraints

Peter Blomberg

MatriMa (Blomberg and Koukkari, 2011) is a tool for calculating a reasonably sparse null space of a numerical matrix and can be applied to a) any element or entity-conservation matrix, b) to any reaction matrix, and c) with or without an earlier/partial solution. When the output is an entity conservation matrix, a matrix where all non-zero matrix elements are positive can be constructed. Such a matrix is required *e.g.* when plotting phase diagrams in FactSage. Reasonable sparsity is sufficient for most purposes (*e.g.* ChemSheet).

The algorithm computes a new entity conservation matrix containing all pertinent reaction constraints from a known reaction matrix. Any additions and removals of reactions must occur by modifying the reaction matrix before the algorithm is run.

The algorithm computes the entity conservation matrix by iterating a linear program for solving one row at a time. Each new row must a) satisfy the null space equation, b) be perpendicular to all previous rows, have as few non-zero elements as possible, and if required have only positive non-zero elements. Splitting the forward and reverse reaction directions into separate unidirectional reactions is the key for a successful implementation of the algorithm. Having separate binary variables for the forward and reverse reactions means twice the number of binary variables, but the resulting constraints are much easier to solve because they are completely linear. There is no need to create saddle-constraints (binary multiplied with continuous) or dynamically modify boundaries of continuous variables. A solution vector is accepted only if it increases the rank of the resulting entity constraint matrix, thus guaranteeing that the correct number of basis vectors are generated and knowing when to terminate the iteration. The algorithm also features exclusion of zero solutions, numerical rounding, and numerical robustness considerations.

5.1.1 Parallel reactions

A hypothetical system where A becomes D via intermediates B or C can be described with a single conserved entity, thus leaving 3 degrees of freedom left for reaction constraints. However, the system contains 4 reactions. Whenever a reaction in one of the branches is constrained, thereby separating A from D, a reaction in the other branch will also have to be constrained. Thus, there are four possible constraints when assuming a thermodynamically feasible direction from A to D.

A	B	C	D	r
1	1	1	1	
	1	1	1	1

A	B	C	D	r
1	1	1	1	
		1	1	1

A	B	C	D	r
1	1	1	1	
	1		1	1

A	B	C	D	r
1	1	1	1	
			1	1

Reactions A→B and A→C are constrained in the leftmost matrix. Reactions B→D and A→C are constrained in the second matrix. Reactions A→B and C→D are constrained in the third matrix. Reactions B→D and C→D are constrained in the rightmost matrix.

5.1.2 Consecutive reactions

The dissolution of $CO_2(g)$ in aqueous base is hypothesised to occur via two consecutive reactions, both of which are kinetically rate-limiting; a) the phase transfer of CO_2 from gas to liquid, and b) the hydration of CO_2 to bicarbonate (Cents et al., 2005; Wylock et al., 2008). Water autoprotolysis (R1) and acid-base equilibria (R2, R3) are assumed. Thus, the reaction matrix has five linearly independent reactions as shown in Table 8.

Table 8. Reaction matrix for dissolution and equilibration of CO_2 in water.

	R1	R2	R3	R4	R5
$CO_2(g)$				-1	
$CO_2(aq)$				1	-1
$H_2CO_3(aq)$		-1			1
$HCO_3^-(aq)$		1	-1		
$CO_3^{2-}(aq)$			1		
$H^+(aq)$	1	1	1		
$HO^-(aq)$	1				
$H_2O(l)$	-1				-1
$Na^+(aq)$					

According to the rank-nullity theorem, the algorithm should find 9 - 5 = 4 linearly independent entity constraints. The entities can be chosen as the elements (H, C, O, Na) or a combination of these as shown below. In simple cases such as the case here, the charge accompanies the elements and is not a linearly independent constraint. The augmented entity conservation matrix having two explicit reaction constraints is shown in Table 9. Although sparser versions exist, this version of the matrix was selected due to pedagogical purposes.

Table 9. Entity conservation matrix for the dissolution and equilibration of CO_2 in water. The two reaction constraints limit two consecutive reactions; dissolution and hydration of CO_2.

	$CO_2(g)$	$CO_2(aq)$	$H_2CO_3(aq)$	$HCO_3^-(aq)$	$CO_3^{2-}(aq)$	$H^+(aq)$	$HO^-(aq)$	$H_2O(l)$	$Na^+(aq)$	r1	r2
Na^+									1		
H^+			2	1		1	1	2			
O^{2-}			1	1	1		1	1			
CO_2	1	1	1	1	1						
R4		1	1	1	1					1	
R5			1	1	1						1

The column for $CO_2(aq)$ is now the sum of the columns for $CO_2(g)$ and r1. This corresponds to reaction R4 with the following modification: $CO_2(g) + r1 \rightarrow CO_2(aq)$. Assuming that the forward direction is thermodynamically feasible, the amount of r1 in the system now limits the extent of reaction R4. A similar statement is true for reaction $CO_2(aq) + H_2O(l) + r2 \rightarrow H_2CO_3(aq)$. The product of this reaction can be any of the carbonate species (as long as all reactions are properly balanced) because the carbonate species will be in equilibrium among themselves as assumed earlier. Biochemical pseudoisomer groups are often convenient reactants because of the built-in equilibration of protonation species, thus reducing the matrix size.

Wylock et al., (2008) measured pH and the amount of CO_2 in the aqueous phase as a function of time for CO_2-absorption into a $NaHCO_3$-Na_2CO_3 brine. The total salt concentration was 10 g/kg. The amount of CO_2 in the liquid directly determines the extent of reaction R4, thus fixing the amount of entity r1 entered into the system. Since the pH was measured, the amount of entity r2 needed at any given time point can be fitted. As shown in Figure 34, reaction R5 lags behind reaction R4 measurably at these conditions.

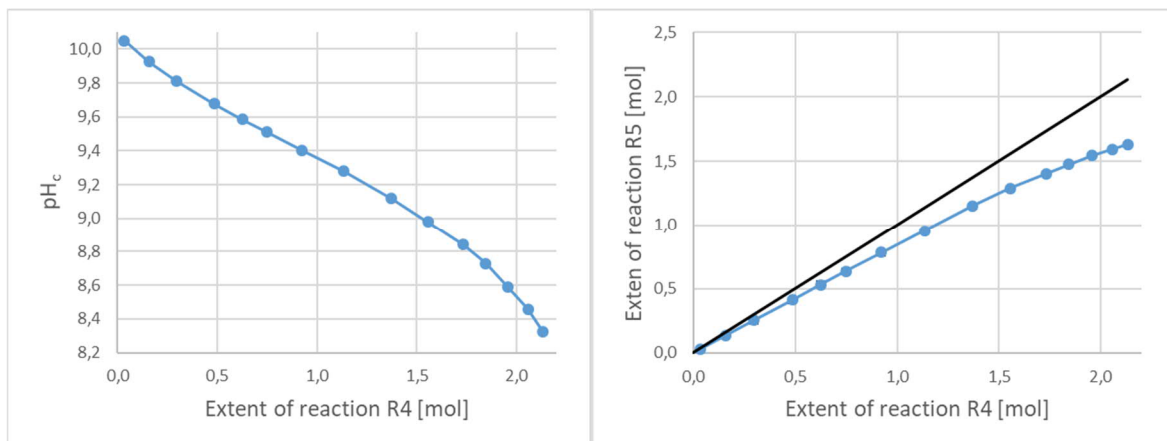*Figure 34. On the left: Measured pH_c versus the measured extent of reaction R4. On the right: Fitted extent of reaction R5 versus measured extent of reaction R4. The line supporting visual interpretation goes through origo and has a unit slope.*

5.2 Tools for modelling bioreactors

Peter Blomberg, Marja Nappa, Petteri Kangas†

Biochemical reactions use pseudoisomer groups as reactants to describe the reactions independently of the pH. The approach assumes protonation equilibria and has been formalised via Legendre transforms (Alberty, 2003). The chemically distinct species H_3PO_4, $H_2PO_4^-$, HPO_4^{2-}, and PO_4^{3-} achieve equal Gibbs energies during the Legendre transform and can thus be grouped into one pseudoisomer group to be used for thermodynamic calculations relating to biochemical reactions. This is readily interpreted as having a fixed equilibrium distribution of chemical species at each particular pH. The average number of protons bound by chemical species within one pseudoisomer group can thus be calculated as a function of pH. The next subchapter presents an application of such a calculation for modelling a particular bioreactor, followed by an example of computing equilibria in a system having biochemical reactions. Subsequent chapters demonstrate various software tools available for modelling biochemical processes.

Microbial sulphate reduction was selected as the main application focus regarding bioreactor modelling in this report. Due to the combined removal of acidity, metals, and sulphate, microbial sulphate-reduction appears to be the most promising process for acid mine drainage treatment (Kaksonen, 2004). This process is also developed by Sulfator and Savonia.

5.2.1 Legendre transforms for process design

The average number of protons n_H bound to the molecules of a pseudoisomer group can be calculated by equations (62) and (63) for pseudoisomer groups having one pKa and two pKa values, respectively. The value is fixed by the *pH* of the aqueous solution (Figure 35).

$$n_H = n_0 + \frac{1}{1 + 10^{pH - pKa}} \tag{62}$$

$$n_H = n_0 + \frac{1 + 2 * 10^{pKa1 - pH}}{1 + 10^{pH - pKa2} + 10^{pKa1 - pH}} \tag{63}$$

where n_0 is the number of hydrogen atoms in the least protonated pseudoisomer and the *pKa* with indexes are acid dissociation constants.
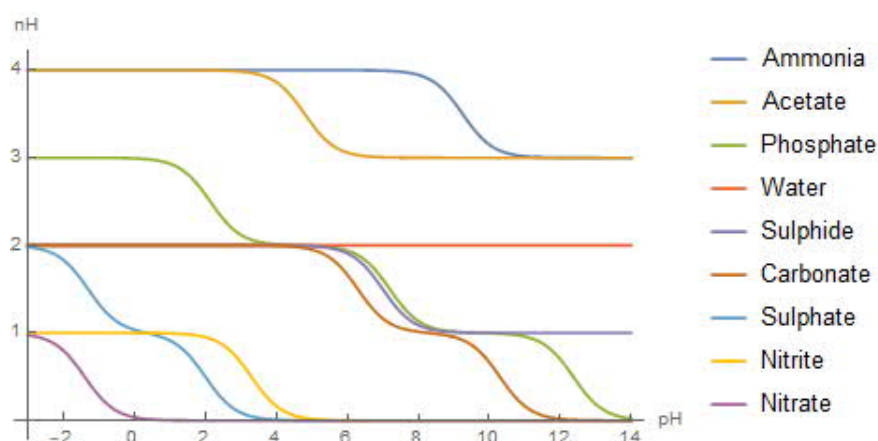

Figure 35. Average number of hydrogen atoms bound to molecules within pseudoisomer groups for select small biochemical species as a function of pH.

When applied to the biological reduction of sulphate to sulphide with acetate as the electron source, acetate + sulphate → sulphide + 2 carbonate, n_H shows that steady-state operation occurs near pH 8.3 or requires a constant source of protons (Figure 36). In this case, luckily the acetate feed can be in the form of acetic acid, which supplies the protons needed to operate at a lower pH. The lower pH is desired because a) the hydrogen sulphide product is more easily extracted at pH nearer to or below its pK_a value near 7 and b) the cell catalyst is sensitive to high pH.
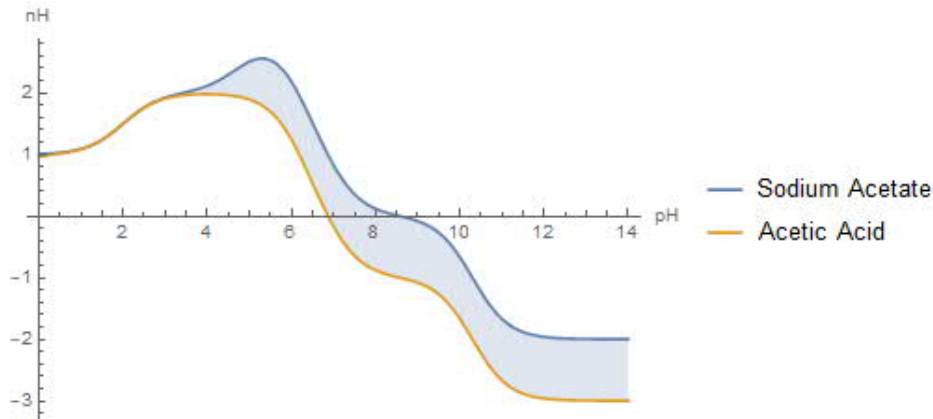

Figure 36. The average number of protons bound by the biological reduction of sulphate that consumes acetate and acetic acid as feed.

In Figure 36, a positive n_H means that the reaction consumes protons, while a negative n_H means that the reaction releases protons. Thus increasing or decreasing the pH. The graph reveals two possible states with constant pH and that the system pH tends to approach these values with time, no matter what the pH was in the beginning.

5.2.2   Equilibrium thermodynamics with biochemical reactions

The biological reduction of sulphate to sulphide with acetic acid as the source of electrons is conveniently described by the biochemical equation: "Sulphate + Acetate → Sulphide + 2 Carbonate", where "Carbonate" is the pseudoisomer group for $CO_2(aq)$, $H_2CO_3(aq)$, $HCO_3^-(aq)$, and $CO_3^{2-}(aq)$. This reaction expression is independent of pH since it is a biochemical reaction where pH-equilibration occurs within each pseudoisomer group.

Biochemical reaction constraints can be added to biochemical systems (Blomberg and Koukkari, 2009) in the same way as chemical reaction constraints are added to chemical systems. However, the two cannot be mixed directly. A hydrogen- and electron-balanced chemical reaction is needed for adding a biochemical reaction to a chemical system. The conversion from a biochemical reaction to a chemical reaction is ameliorated by the fact that the proton can take part of the chemical reaction with an undetermined stoichiometry. For the great majority of reactions, choosing any pseudoisomer from a pseudoisomer group is acceptable because the proton will balance the equation. Carbonate is the one known exception since choosing the unhydrated/hydrated form when the other form is required results in an imbalance of water. This imbalance cannot be rectified by any amount of protons. Nevertheless, in most cases, the task is to find the number of protons that balances the reaction.

For this particular case, the species most abundant between pH 7 and 8 are chosen; *i.e.* $SO_4^{2-}(aq)$, $CH_3COO^-(aq)$, $HS^-(aq)$, and $HCO_3^-(aq)$. Fortuitously, the resulting chemical equation $SO_4^{2-}(aq) + CH_3COO^-(aq) = HS^-(aq) + 2\ HCO_3^-(aq)$ balances perfectly. Figure 37 shows the evolution of pH in a batch reactor where sulphate in acid mine drainage is reduced with acetic acid to sulphide. The calculation was done by adding a specified amount of acetic acid to the mixture and computing the equilibrium composition of the solution using

ChemSheet. Eventually, sulphate would run out and excess acetic acid would be left unreacted, thus demonstrating the use of a biologically-catalyzed reaction in a thermodynamic data file.
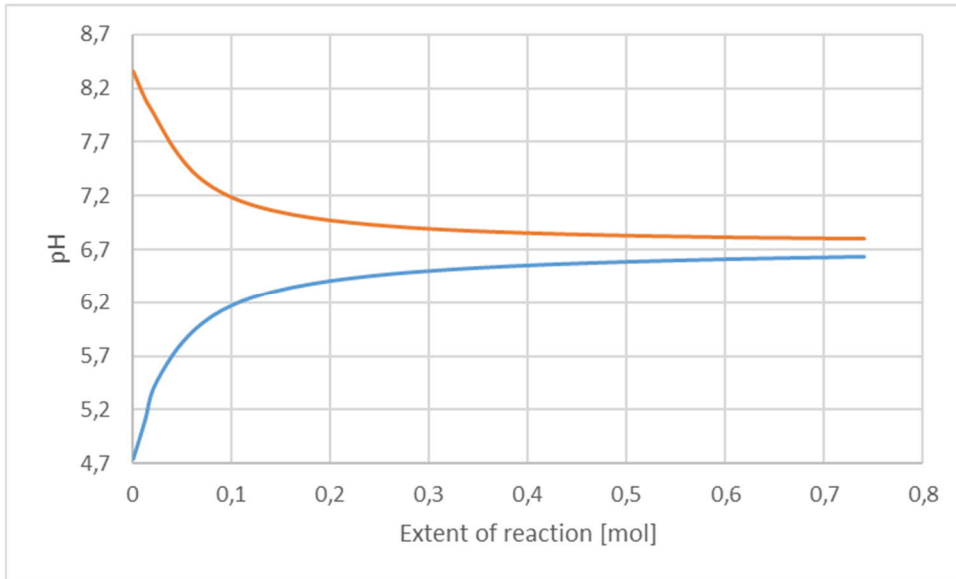
Figure 37. Evolution of pH with extent of reaction for sulphate reduction using acetic acid as the electron source. The pH converges to the steady-state value calculated in Figure 36.

5.2.3   Dynamic SRB -model

A dynamic model for sulphate reduction by bacteria was constructed. The reactor model accounts for continuous feeds (electron source, sulphate source) and product outlets (gas, liquid, solid). Initially, the reactor at Savonia was thought to be a plug-flow reactor (PFR), but the circulation flow rate $\dot{v}_{Kierto}$ was sufficient (experimentally confirmed, data not shown) to model the reactor as a continuously-stirred tank reactor (CSTR), modelled by equations (64-67).

$$\frac{\partial c_R}{\partial t} = \frac{c_{BR}\dot{v}_{BR} - c_R\dot{v}_{RD}}{V_R} - kc_R \tag{64}$$

$$c_{BR}\dot{v}_{BR} = c_{IN}\dot{v}_{IN} + c_R\dot{v}_{Kierto} \tag{65}$$

$$\dot{v}_{BR} = \dot{v}_{IN} + \dot{v}_{Kierto} \tag{66}$$

$$\dot{v}_{RD} = \dot{v}_{OUT} + \dot{v}_{Kierto} \tag{67}$$

, where c_R is the substrate concentration in the reactor, V_R is the reactor volume, and k is the apparent rate constant. In steady-state, the volumetric flow into the reactor $\dot{v}_{BR}$ equals the volumetric flow out from the reactor $\dot{v}_{RD}$.

Substrate uptake is often limited by saturation of the permeability mechanism at high substrate concentrations, thus resulting in the experimentally-derived Monod-equation (68). Microbes do not catalyse the reverse reaction in any measurable amount since they do not grow under such conditions.

$$\frac{r_{\text{Metabolism}}}{c_{\text{Cells}}} = k_{\max} \left[\frac{c_{\text{Sulphate}}}{K_{\text{Sulphate}} + c_{\text{Sulphate}}} \right] \left[\frac{c_{\text{RedEq}}}{K_{\text{RedEq}} + c_{\text{RedEq}}} \right] \tag{68}$$

Both the growth rate of the bacteria and the metabolic activity of the bacteria are sensitive to pH and often well-enough modelled by a Bell-shaped curve (69).

$$r(pH, \cdots) = r(\cdots) \left[\frac{1}{1 + 10^{pH-A} + 10^{B-pH}} \right] \tag{69}$$

, where the parameters A > B define the range of optimal pH values.

Although the exact values may differ from strain to strain and from one community to another, sulphate-reducing bacteria are generally inhibited 50% by H_2S-concentrations between 2 and 15 mmol L^{-1} (Koschorreck, 2008). The neutral H_2S-molecule is highly membrane-permeable and ionizes inside the cell, thereby reducing the membrane potential essential for survival and growth. The same mechanism explains the toxicity of small organic acids. Hydrogen sulphide is also toxic inside the cell because it interferes with the stability (disulphide bonds) and catalytic activity (cysteines, iron-sulphur clusters) of enzymes. The reversible inhibition by H_2S can be described by the non-competitive inhibition model (70) (Reis et al., 1992). This expression underestimates the level of inhibition at low H_2S concentrations and cannot be used for concentrations exceeding 530 mg L^{-1} simply due to numerical issues.

$$r\left(c_{H_2S}, \cdots\right) = r(\cdots) \left[1 - \frac{c_{H_2S}}{547} \right]^{0.401} \tag{70}$$

, where the concentration of undissociated H_2S is given in mg L^{-1}.

Due to the mechanism of action, well-growing cells tend to tolerate higher concentrations of inhibitors than poorly growing cells. This can be modelled by the simple, yet effective differentiation of metabolism and growth (71). This allows survival without growth and metabolic activity while dying. It has been experimentally observed that both the rate of growth and the yield of growth decline independently as the pH is lowered (Reis et al., 1992). The yield of growth is reduced as more energy is diverted toward maintaining the membrane potential than toward growth. Diffusive flux across a membrane is proportional to the concentration difference across the membrane (72).

$$r_{\text{Cells}} = Y_{\text{Cells}}[r_{\text{Metabolism}} - r_{\text{Maintenance}}]$$

$$growth \; if \; r_{\text{Cells}} > 0 \tag{71}$$

$$death \; if \; r_{\text{Cells}} < 0$$

$$J_{\text{Flux}} \propto \Delta c$$

$$\frac{r_{\text{Maintenance}}}{c_{\text{Cells}}} = \tau_0 [10^{pH_{\text{IN}} - pH_{\text{OUT}}} - 1] + \frac{\tau_{\text{HA}} c_{\text{HA}}}{K_{\text{HA}} + c_{\text{HA}}} + \frac{\tau_{H_2S} c_{H_2S}}{K_{H_2S} + c_{H_2S}} \tag{72}$$

, where H_2S is specifically the undissociated H_2S and HA is the undissociated form of acid.

The full model derived above was not used in the project because there was no need for it. The applications were satisfactorily modelled using applicable parts of it. The following two chapters present two applications in which parts of the above model was used.

5.2.4   Process flowsheeting

A flowsheet model for a process including an SRB-reactor was assembled. The model was used to study the efficacy of reactor effluent on the removal of Calcium from the reactor influent. The study included optional concentration of effluent by reverse osmosis and supplementary chemicals.

The HSC Chemistry 9.8 (Outotec, 2018) was used for the computational assessment. The process streams were modelled using a multi-phase approach. Gaseous phase, aqueous phase, and pure solid phases were included in the model. Thermodynamic equilibria were computed for illustrating the effects of precipitation and dissolution as well as the evolution of pH. Thermodynamic data was obtained from HSC Chemistry 9.8 database for flowsheet simulation. The Pitzer formalism (Aqua module) was used as the activity model for the aqueous suspensions. In addition, the SRB-reactor was modelled using biochemical reaction equations. The entire process was assumed to operate at steady state even though an actual process might operate partly as a batch process. A snapshot of the flowsheet is shown in Figure 38.
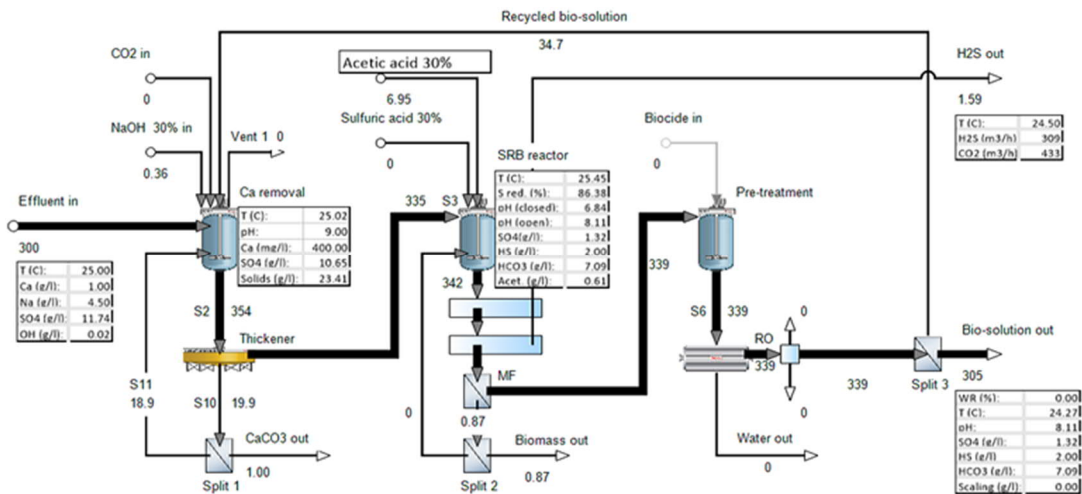
Figure 38. SRB process modelled using HSC Sim9.

The influent contained 1100 mg Calcium, 110 mg Magnesium, 630 mg Sodium, 15 mg Potassium, and 4420 mg sulphate in 1000 g water and its pH was adjusted to pH 9 by using approximately 1 mg NaOH. Thereafter, the model was quickly tested by adding a) an equimolar mixture of NaOH and $NaHCO_3$, b) an equimolar mixture of $Ca(OH)_2$ and $NaHCO_3$, concerning hydrogen and carbonate and c) only $NaHCO_3$. (See Figure 39)

The target for residual calcium was 400 mg L^{-1} and it was met by adding 18 mmol L^{-1}, 27 mmol L^{-1}, and 60 mmol L^{-1} reagents in cases a), b), and c), respectively. Case b) required approximately 50% larger chemical feeds than case a) because the feed itself contained calcium. In case c), the pH decreased rapidly to pH 6.5, where after it slowly increased to pH 7 due to the buffering capacity of the solution. Computational assessment thus suggested that all three treatments were capable of reducing calcium to the desired level. The needed chemical amounts were the lowest when caustic soda and bicarbonate were utilised.

Replacing the solid NaHCO₃ reagent with the effluent mixture increases the amount of fluid passing through the unit operations. While this may dilute some of the calcium, effluent alone in any amount would not be sufficient for lowering the calcium concentration to the desired level. Here, one must weigh the cost of purchasing pure chemical feed versus the increased costs of larger equipment sizes and operating the reverse osmosis unit.
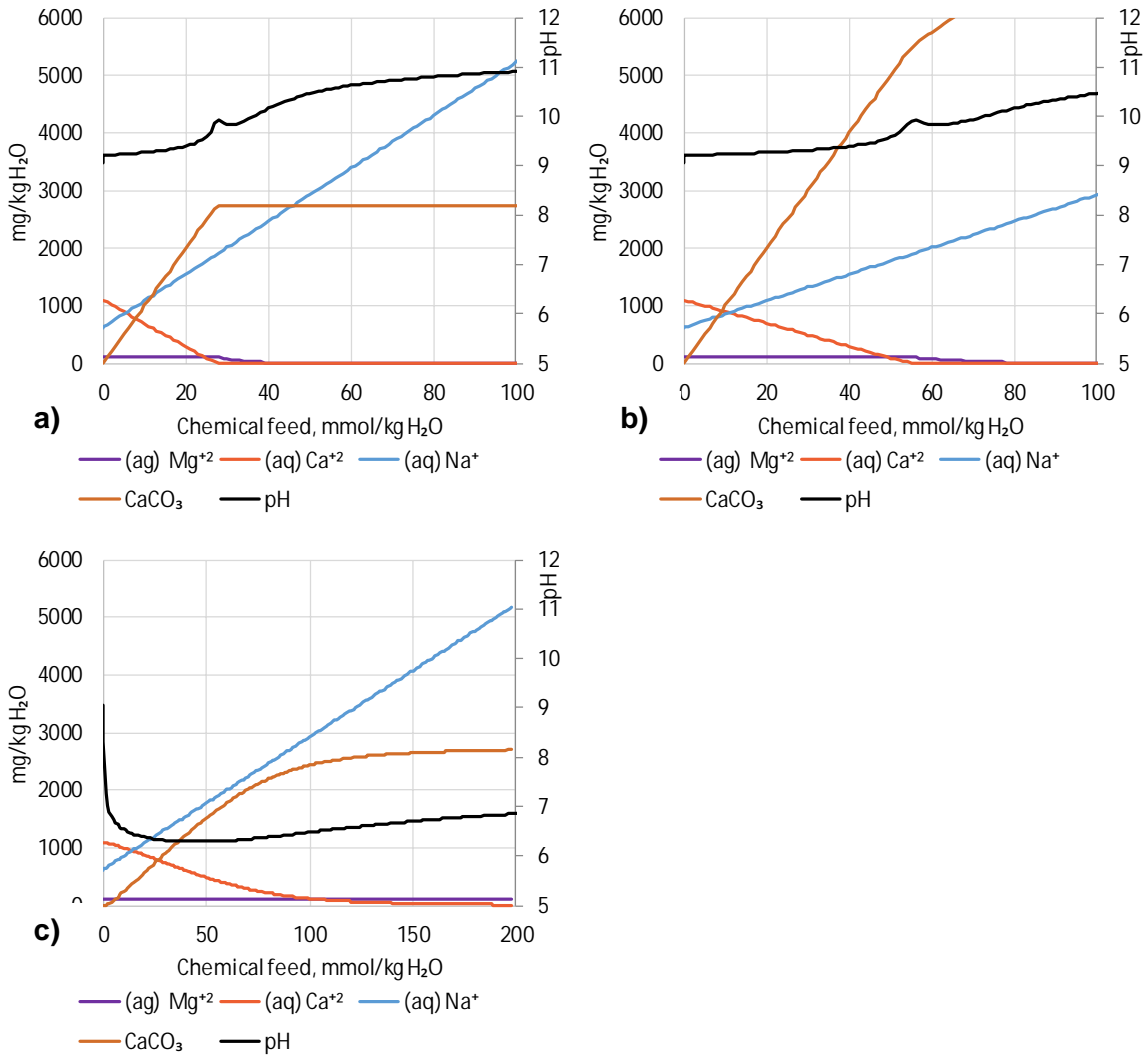
Figure 39. Pre-treatment of the influent to remove calcium, three treatments a) NaOH and NaHCO₃, b) Ca(OH)₂ and NaHCO₃ and c) NaHCO₃. Amounts in aqueous phase and precipitate (primary axis) and pH (secondary axis) as a function of chemical feed (mmol of bicarbonate and hydroxide each per kg H₂O).

5.2.5   Deriving biochemical kinetics from process data

This example shows that process measurements can in some cases be used to compute reaction kinetics even for complex biochemical reactions.

The process performance data measured by Savonia during the development of the SRB process was analysed using parts of the dynamic SRB model developed in this project. After having confirmed that the reactor operated sufficiently similar to a continuously stirred tank reactor, the corresponding reactor design equations were used to reverse engineer the reaction rates needed to incur the observed changes in the process measurements. After studious examination of the observed special events and changes to the operating

conditions, a surprisingly accurate calculation of the reaction rate for the main biochemical reaction was obtained (Figure 40). Further details are in the confidential technical report.
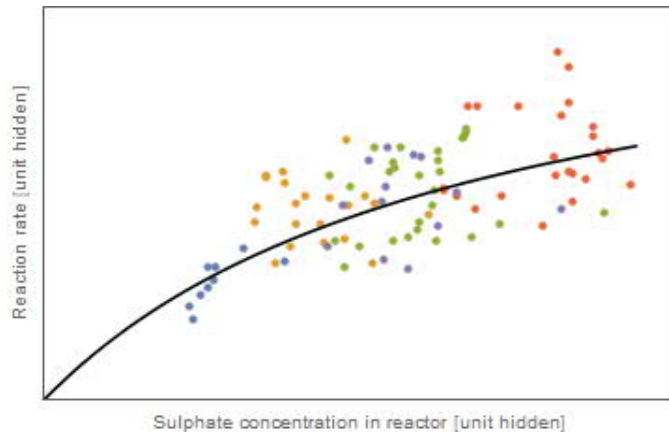
Figure 40. Apparent reaction rate versus substrate concentration for the main biochemical reaction in the SRB process.

While the reactor was operated in more or less steady-state, the momentary behaviour of the reactor spanned a conveniently large portion of the substrate concentration range to visualise the shape of the curve. Similar plots (not shown) were obtained for key inhibitory compounds. Being able to recognise the shape of the curve implies that the reactor model sufficiently captures the phenomena needed to model the reactor. Since these calculations do not differentiate the individual protonation states of the reactants, this is an example where biochemical reactions expressed in terms of pseudoisomer groups are handy.

5.3　　　Uncertainties in models

Risto Pajarre and Karri Penttilä

Thermochemical process modelling is typically deterministic. A given set of input parameters combined with specified model parametrization gives certain specific numerical output values as result. The practical problems being modelled however contain uncertainties in the input parameters, which result in uncertainties in the predicted outputs. A study of ways to test and visualise these uncertainties was performed.

It is not possible to calculate by regular free energy minimisers truly continuous states; however, it is possible to discretise the variables and the states being studied. As the number of sates needed to be solved is approximately proportional to a^N, where N is the number of parameters with uncertainty, it is typically preferable to use as small number of parameters as possible and probably never larger number than N=3.

In the study the simulation window was scanned with equally spaced data points, with a given minimum and maximum parameter value. After that, probability functions were used to generate weight factors corresponding to individual parameter values and calculated results.

The equilibrium calculation results do not need to be repeated if the weight factors are changed as the result for any individual equilibrium calculation does not change. Also, if the applied are deemed to be not independent, as long as the underlying chemical model is valid, the dependency will be implicitly shown only in the formulas used to generate the weight factors.

The work done here concentrates in uncertainties in used input values such as molar amounts, temperature or pressure and not in those in the applied thermodynamic data. It can be noted though that within the framework of CFE equilibrium calculations, non-equilibrium reaction affinity is a valid input parameter, similar to fixed partial pressure of gaseous component, and therefore could be applied here as well. On the other hand, non-zero affinity can be equated with system in equilibrium but different chemical potential standard states (equilibrium constant) related to that reaction, and therefore with an uncertainty related to value. The proposed method is not applicable in its current form to uncertainties in the applied activity coefficient models.

5.3.1　　　Model example

The necessary equilibrium calculations were done using ChemSheet, and the resulting data was handled by regular worksheet functions. Chemical system applied the VTT aqueous database with the following inputs (Table 10)

Table 10. Input values for the model chemical system

	value	min	max
H_2O/kg	1		
Na_2CO_3/mol	2	1.5	2.5
Na_2SO_4/mol	2	1.6	2.5
T/°C	50	48	52
$MgCl_2$/mol	0.05		
$CaSO_4$/mol	0.05		
$FeCl_3$/mol	0.01		

Input amounts of Na_2CO_3, Na_2SO_4 and temperature were considered variable parameters, while the other inputs had one fixed value. For the amounts of Na_2CO_3, Na_2SO_4, 21 equally spaced input values were used for both, while temperature was varied with 7 steps, resulting with a calculation model with a total of 3087 model points to be generated.

The modelled output values were divided 20 to equally spaced groups within calculated minimum and maximum values. In Figure 41 the calculated equilibrium pH, burkeite and soluble Mg amounts are shown using the original equal spaced, equal probability distribution of input parameters. Blue curves show the calculated probability distribution, the red bar the value corresponding to the average composition.
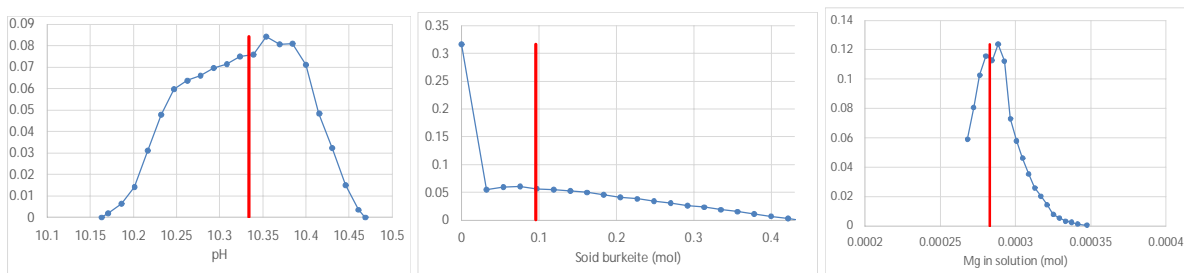
Figure 41. Calculated probability distributions of solution pH, formed burkeite and magnesium in solution.

As can be seen the pH shows fairly smooth distribution around the value that would be obtained using the average inputs. Regarding burkeite, about the third of the states are below the solubility limit and then show a fairly steadily reducing probability of finding more salt up to a certain maximum value corresponding to optimal conditions, while dissolved magnesium shows a maximum close to the value corresponding to the average input parameter values.

Using the same calculated equilibrium distribution, but assuming a truncated normal distribution (normal distribution, but with hard cut off at the applied minimum and maximum parameter values) around the mean with standard deviations 0.05 mol/kg for the Na_2CO_3 and Na_2SO_4 inputs, while maintaining the original temperature distribution, results with the curves shown in Figure 42.
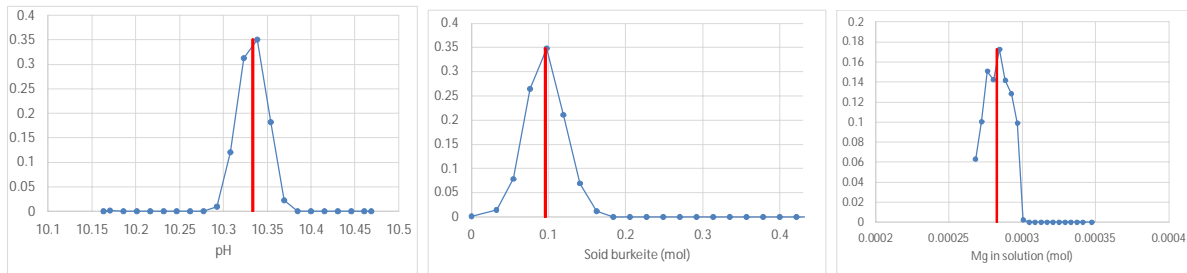
Figure 42. Calculated probability distributions with the truncated normal distribution for the feed input parameters assumed.

The pH distribution is now much sharper while the probability of no burkeite being precipitated is close to zero. A more detailed analysis would be needed to determine if the double peak with dissolved Magnesium is due to data artefact and the limited precision of the distribution calculation or due to two different basic Mg salts being precipitated partly simultaneously.

5.3.2   Conclusions

Reasonable distribution presentation for analysis and data visualization can be created with a moderate number of model points that for most systems can be generated fairly fast with present computational routines. After the necessary model data for the desired parameter values has been generated, various probability distributions within that parameter space can be evaluated without redoing the time consuming equilibrium calculations. For faster more automatized data generation a custom made ChemApp-application could be constructed, also supporting cross tabulation of various calculated quantities.

6. Hybrid systems and methods in thermodynamic modelling

6.1 Machine learning for predicting Pitzer parameters based on ion specific properties

Petteri Kangas† and Risto Pajarre

The use of technology metals in the ICT sector has increased tremendously since the 1990s. Improved efficiency, cameras, touchscreens, and wireless connectivity have been achieved by innovative usage of different elements. In 1990, the manufacturing of computers and mobile phones used approximately 10 metals. Now the number exceeds 50. The fractionation, concentration, recovery and refining of these elements require fundamental material property data, particularly so for their mixtures appearing in the respective extraction processes.

Although much of the fundamental property measurements were conducted in the first half of the twentieth century, there are still many metals and ion pairs for which there is too little experimental data available, thus hampering the development of new process concepts. Conduction of such fundamental measurements with conventional techniques is elaborate and time-consuming, which has led to scarce practicing in this field.

The exponential growth of computational power has introduced new possibilities for computational science. Data-based machine learning algorithms have been developed and deployed to many impressive solutions, such as computer games, machine vision, and drug discovery. The aim of this work package was to evaluate whether these new machine learning algorithms could be applied for predicting properties of non-ideal electrolyte solutions when experiment based data evaluations are not available, the expected applications areas including hydrometallurgy, water purification, and the treatment of industrial concentrates and brines.

6.1.1 Methodology

Mean activity coefficients of cation-anion pairs in aqueous solution were predicted using a neural network trained on data from (Pitzer and Mayorga, 1973). This data describes Pitzer parameters (Pitzer, 1991) for calculating mean activity coefficients for over 200 different cation-anion pairs covering 50 different cations and 54 different anions. This parameter set was considered as proxy for a evaluated experimental data within the stated validity range, which varied but in most cases extended up to 6 M. Mean activity coefficients acted as labels (outputs) for the neural network. These labels were connected to features (inputs) of each particular cation and anion. The features included i) molecular weight, ii) charge, iii) hydratation number, iv) enthalpy of hydratation, v) entropy of hydratation, vi) Gibbs' energy of hydratation, vii) softness, viii) partial molar volume, and ix) radius. The x) molality was used as an additional input for the neural network. The size of dataset was approximately 5000 data points. 80 % of the data was used for training and the remaining part for validation.

Based on preliminary screening of different neural network structures, a feed-forward neural network was chosen. It suited better for estimating continuous mean activity coefficients as functions of molality compared to *e.g.* regression trees. Machine learning studies were conducted using the Keras (Chollet and others, 2015) framework as it allows rapid development of neural network based models. Tensorflow (Abadi et al., 2015) and PlaidML (plaidML, 2019) were used as Keras backends. The hyper-parameters of the neural network model were optimised using the Scikit-learn (Pedregosa et al., 2011) toolbox. Model development was conducted using the Jupyter (Kluyver et al., 2016) notebook environment within the Anaconda (Anaconda, n.d.) Python toolbox. Calculations were run on a laptop computer (Windows 10, Intel quad core, 1900 MHz) with separate graphics processing unit (AMD Radeon RX550).

6.1.2 Results

The model for predicting mean activity coefficients was divided into two parts. The first part described an average mean activity coefficient based solely on the charge of the cation and the charge of anion (1-1,1-2, 2-1,2-2,1-3,3-1,4-1,5-1). The second part represented the deviation of the mean activity coefficient for a specific cation-anion pair with respect to the average mean activity coefficient for ions of corresponding charges. This deviation was estimated based on the neural network model trained using above mentioned cation-anion specific features and labels obtained from literature.

The over-fitting of the neural network model was avoided using hyper-parameter optimisation. The following hyper-parameters were optimised: i) number of epochs, ii) batch size, iii) applied activation function, iv) number of neurons in each layer, v) number of hidden layers, vi) loss function, and vii) training algorithm. Based on the optimisation of hyper-parameters, it was concluded that a two hidden layer network topology with about 20 neurons in the first layer and about 5 neurons in the second layer was sufficient. A special characteristic of this feed-forward neural network topology was the fact that molality was fed as a feature to both layers. Other features were supplied only to the first layer of network. This allowed accurate modelling of diluted suspensions as described by Debye-Hückel limiting law (Huckel and Debye, 1924).

80% of the data was used for training and 20% for model validation. The accuracy of predicting mean activity coefficients using the final neural network model was improved for 65% of the cation-anion pairs when compared to charge specific average values. The model failed to improve accuracy in cases were the original data for certain anions were scattered. Some polyatomic organic anions were only participating in one or two ion pairs. In addition, some features used for machine learning were not defined for these polyatomic organic anions. On the other hand, predicting mean activity coefficients for cation-anion pairs with inorganic anions (such as SO_4, CO_3, NO_3) was successful in many cases.
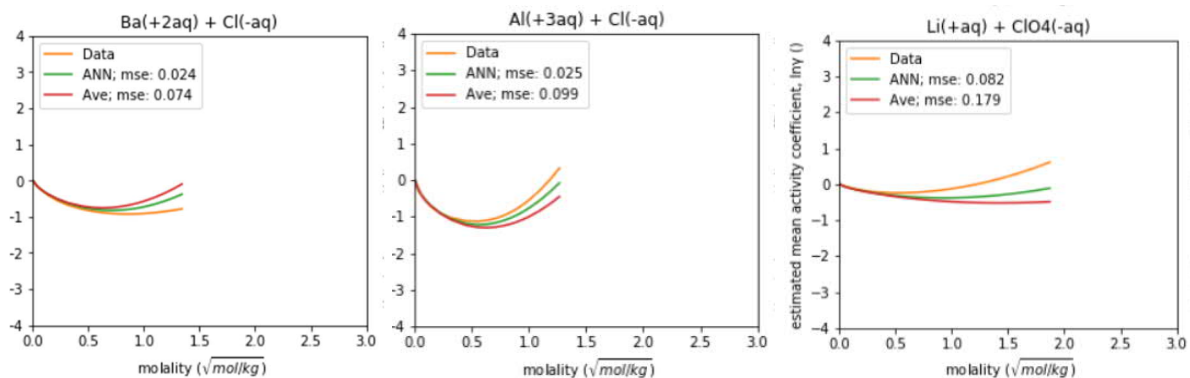
Figure 43. Example comparisons of mean activity coefficients as function of square root of molality. Orange: Experimental data based Pitzer model; Green: Neural network model; Ionic charge based comparison model. Ion pairs are from the data validation set.

Figure 44. Comparison of the predicted and experimental mean activity coefficients within the training and validation test sets.

Table 11. Comparison fit errors between the neural Network model and the Ionic charge based comparison model. Green colour denotes the cases (133 out of 203) where the neural network model work better than the ionic charge based model. Relatively poor performance was found with Na(+) and K(+) where large part of the dataset was with interaction with large anions that had little data with other cations.

Since the finalization of this work package, the datasets and analysis has been used as a basis for further work in a candidate thesis at Aalto University (Kattelus, 2020).

6.1.3 Summary

Machine learning was applied for predicting mean activity coefficients for ion pairs in concentrated aqueous solutions. The developed model was able to improve the predicted mean activity coefficients for two thirds of the cases compared to using only ion charges for prediction. Predictions were most successful when modelling metal cations and inorganic anions. The training data for polyatomic organic anions was too scarce.

6.2 Surrogate models for faster thermodynamic calculations in chemical flowsheet simulation

Andreas Roth and Risto Pajarre

6.2.1 Introduction

Surrogate models are an engineering approach mostly used to replace systems that are complex or unknown. The main idea is to view the system as a black box and mimic the output of the system. They are mathematically simple models that map, or regress, the input-output relationships of a more complex, computationally demanding model. In this work, applicability of neural networks based surrogate models were studied for replacement of unit operation models in HSC Chemistry 10 software (Metso Outotec, 2020) and as a replacement for a thermodynamic non-ideal solution model for modelling activity coefficients.

6.2.2 Methods

The neural network modelling was performed using both HSC inbuilt tools and the Tensorflow open source program (Abadi et al., 2015). For the unit operation calculations a system with one hidden layer with 45 neurons was used with the number of input and output nodes depending on the number of input and output values in the case system. For the activity coefficient modelling, the best results were obtained by three hidden layers combined with dropout layers. The short description of the modelling work and results are given here, full description is included in the Masters Thesis of Andreas Roth (Roth, 2020).

6.2.3 Unit operation model

Neural Networks based surrogate models have potential application area in accelerating complex thermodynamic and process calculations in systems were similar calculations need to repeated a large number of times, *e.g.* for optimization tasks or in digital twins. As a test case, autoclave model within the Outotec HSC 10 simulation software was converted to a surrogate model (Figure 45).
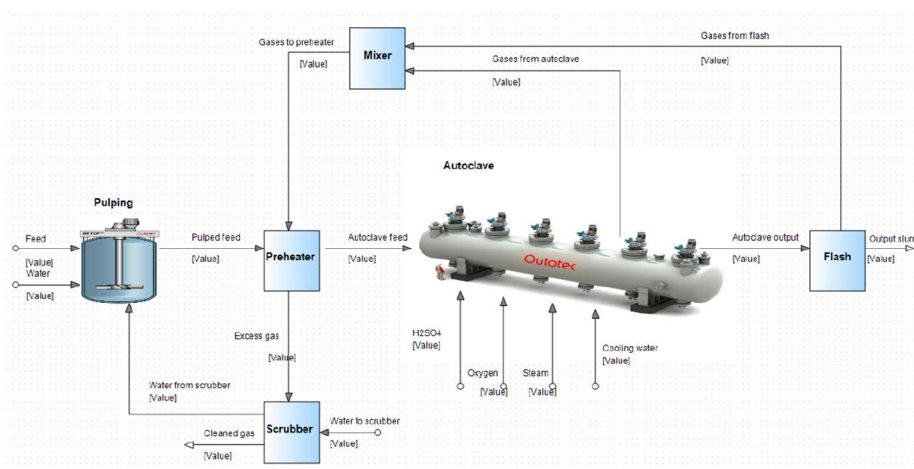

Figure 45. Autoclave system.

The HSC model contained in addition to the autoclave itself the surrounding pulping, preheater, scrubber, mixer and flash units. The chemical system in the model contained the H_2O, O_2, N_2, H_2SO_4, $H(+a)$, $Co(+2a)$, $SO4(-2a)$, CoS, Fe_2O_3, FeS_2, S and SiO_2 species. Two

versions of the surrogate modelling were tested. In one, only the autoclave unit only was converted to a surrogate model, in the other, the whole larger system in Figure 45. Because of the large number of internal streams and relatively small number of streams exiting the balance area of Figure 45, the larger model area has smaller number of stream inputs and outputs to model; Indeed, the larger model area had only three input values (CoS, FeS_2 and SiO_2 inputs) that were considered to variables.
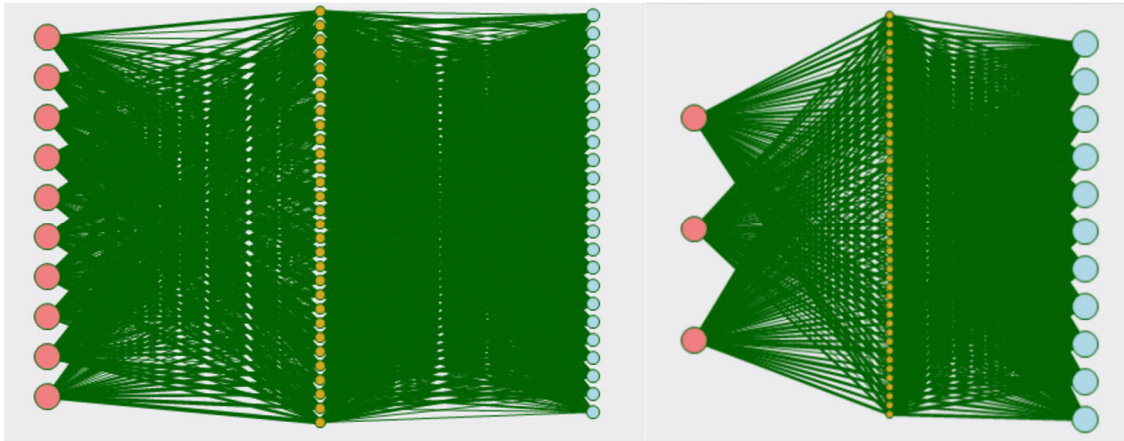

Figure 46. Neural network schemas for the autoclave unit (left) and the whole balance area (right)

Training data was generated for 2000 cases, varying the feed amounts uniformly by 50% from their original values.

For the autoclave unit the Mean Square Error (MSE) was 2.54e-4 while the largest relative error was 0.04. For the larger model area MSE was 4.15e-8 and the largest relative error 0.001. The dependency of accuracy on the number of data sets used for network training was tested for the larger model. Approximately 1000 data sets were found to be enough for sufficient accuracy.
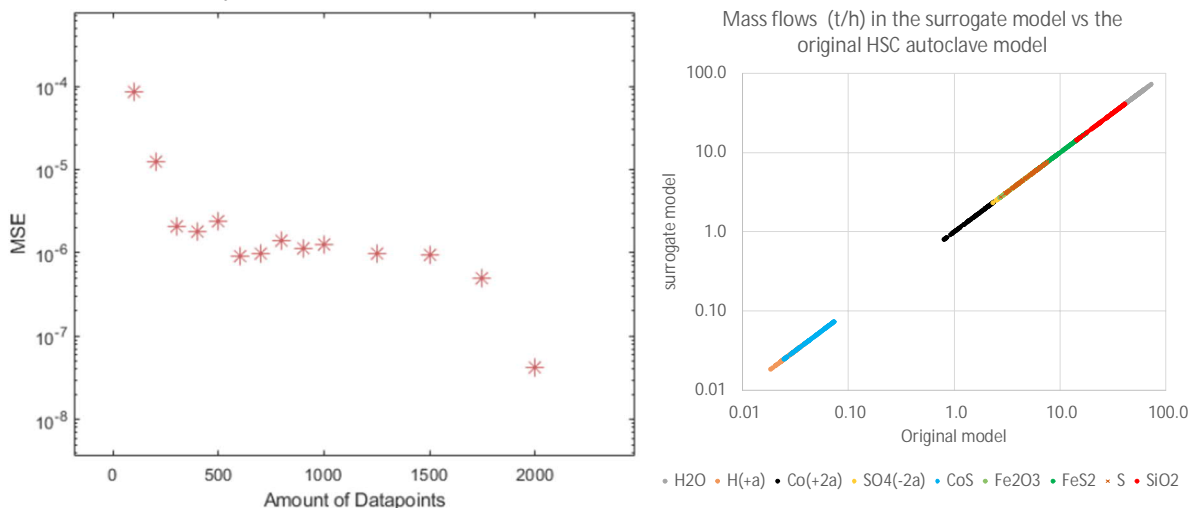
Figure 47. Achieved MSE as a function of data points (left). Comparison of the surrogate model mass flow rates with the original model for the autoclave unit (right).

The model run times are presented in Table 12. Given are the simulation times for 100 model runs for the original non-neural network case, surrogate model were only the actual autoclave model has been replaced, surrogate model were the whole flowsheet in Figure 45 has been replaced by a neural network and finally a 'blanco' model to give an estimate of the constant computational overhead not dependent of the model type used.

Table 12. Effect of a neural network on the simulation time

	Original model	Unit NN	Model area NN	Blanco
time/s	125.2	103.2	10.5	6.6

6.2.4 Activity coefficient model for mixtures

The ability of neural networks to find patterns in complex data could potentially be used to estimate non ideal solution properties in thermochemical systems that are not properly assessed. As a concept test of the capabilities of a neural network based modelling for simulating activity coefficients in a non-ideal multicomponent systems, a study based on aqueous solution mixture properties as evaluated by the HSC 10 program was performed. The test system contained 22 aqueous species whose activity was modelled in mixtures of varying concentrations, taking account their solubility relative to corresponding major solids in the HSC 10 database. After training the model it was tested against a validation dataset. Comparison of the surrogate activity coefficients vs. the original ones are shown in Figure 48.
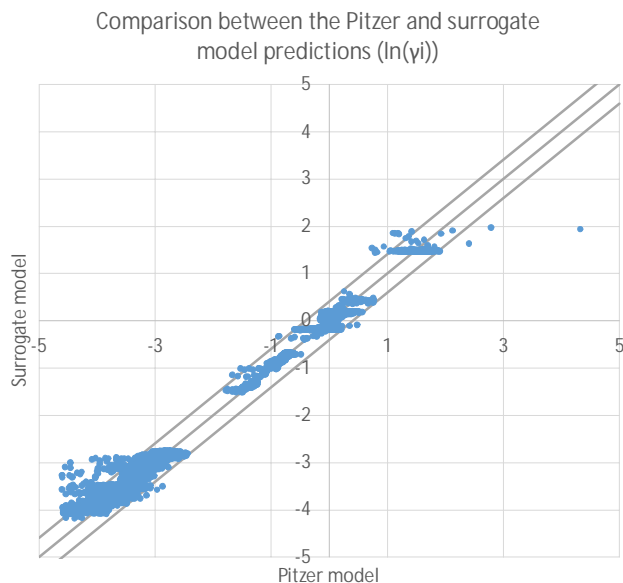

Comparison between the Pitzer and surrogate model predictions (ln(γi))

Figure 48. Comparison of the original Pitzer model based estimates for the activity coefficients ($ln\gamma_i$) from the HSC 10 program and the corresponding surrogate model. Also shown are the error limits corresponding to 50% relative error in activity coefficients.

6.2.5 Conclusions

The accuracy of the unit operation surrogate model was excellent. The time savings obtained for a single relatively simple unit were small but noticeable. With a large model area replaced by neural network model the time savings increased rapidly.

The largest errors in the activity coefficient model were encountered in cases of very small or very high activity coefficients in highly concentrated solutions. While the surrogate model is not directly affected by the lack of physical realism of the training data, it is possible that the data was qualitatively different in a region were the applied Pitzer model is not properly valid anymore. Elsewhere, the surrogate model predictions were generally within 50% of those derived from the original model. If roughly corresponding results could be obtained in poorly

studied system with sparse data, they would be adequate for many purposes. This would be need to be shown in a further study.

7. Industrial perspective and future challenges

7.1 Benefits to Finnish process industry

The exponential growth of computational power has introduced new possibilities for computational science. In process industry, this can be seen by the on-going global digitalization, which provides new opportunities for the process modelling, design, control and other expert systems even though digitalization has been part of this industry for a long time.

Research institutes VTT and Savonia, industrial companies Valmet, Outotec and Finnish Minerals Group and SMEs Langis and Sulfator were involved in the DeepCleanTech consortium. The focus of the research at VTT has been thermodynamic modelling and especially the applying the constrained equilibrium calculations, AI tools and biochemical modelling in industrial processes.

Valmet has practiced long-term development work in which the know-how and utilisation of chemistry through multi-phase programs, particularly VTT's ChemSheet, has created a unique and internationally recognised competitive advantage to the company. In the future, special attention will be paid on the control of contaminant behaviour in forest industry by innovative means to control of the chemistry of non-process elements and help the customers to make their processes greener. The research of both topics has been the key focus in DeepCleanTech.

Outotec actively utilises the models in the development of new process concepts and their further marketing to customers. Digital twin models are also increasingly used for dynamic process control as well as in practical process commissioning and operator training. Physical and chemical models describing the process phenomena combined with black-box models is an interesting development tendency that has an important role in digitalization and has been also an interest in DeepCleanTech.

Modelling reduces the risks in new process solutions. Finnish Minerals Group focusses on developing new holistic methods for metals recovery, using the multi-phase models to support development of optional process concepts. The usage of modelling is often cost-effective way to evaluate the viability of new process options. Certainly, the models need to be validated through experimental work.

SME companies will benefit on the computational root cause analysis of new monitoring techniques, in developing novel remote sensors for environmental analysis and when designing new innovative bioactive processes. Good understanding of phenomena helps avoiding the problems and fastens the trouble shooting. The computational results can be further connected to experimental knowledge with the help of new expert systems, soft-sensor solutions and artificial intelligence algorithms utilising machine learning.

A comprehensive set of concurrent industrial applications were also presented in the **Latest in Modelling symposium** which was organised under the auspices of the DeepCleanTech project at VTT on September 12th 2019 (Kangas et al., 2019), (see Figure 49 to Figure 51). The symposium speakers represented a broad range of expertise from both academia and industry from Finland, France, Germany and Russia. Multicomponent chemical modelling was widely applied for various circular economy processes for their design and problem solving. Computational physics and multiphase chemistry had been successfully connected for chemical reactors, power plant modelling, rotary kilns and other industrial furnaces as well as for hydrometallurgical precipitators and digesters. At best, the new process concepts introduced have reached 50-60% reductions in process energy consumption and CO_2-release.

Figure 49. The Latest in Modelling symposium September 12th, 2019 was arranged to honour the 65th birthday of professor Pertti Koukkari. The international symposium gathered ca 80 modelling experts from both academia and industry.

Figure 50. Speakers of the Latest in Modelling 2019 symposium. Top left prof. Antti Vasara, CEO of VTT, seminar opening, Prof. Tapio Salmi, Academy of Finland, Dr. Susanna Kuitunen, Neste Engineering Oy, from left Ass.prof. Daniel Lindberg Aalto University, Prof. Irina Zvereva, Prof. Alexander Toikka St. Petersburg State University below Dr Ville-Valtteri Visuri Univdrstiy of Oulu and Dr. Timo Kankaanpää, Freeport Cobalt.

Figure 51. Speakers of the Latest in Modelling 2019 symposium. Top left prof. Pertti Koukkari, Dr. Alexander Pisch, CNRS Grenoble, Dr. Sonja Enestam, Valmet Oyj, from left Dr Jukka Rantamäki, Metsä Fibre Oyj, Dr. Keijo Salmenoja, Andritz Oyj, Dr. Antti Roine Outotec Oyj, below Karri Penttilä VTT, Eemeli Hytonen VTT with prof. Klaus Hack and Dr. Stephan Petersen of GTT Technologies.

7.2　Future challenges

The on-going global digitalization of process industry provides new opportunities and brings new challenges for the thermodynamic methodology.

The utilisation of both measured and simulated thermochemical state properties in the information networks is an interesting task of the future web-controlled industrial practice. The multi-phase models of unit processes can be further coupled with the control system for the entire process and process-specific time constants, which in addition allows the thermodynamic models to be used as components in the automation software.

To speed up the calculations, hybrid models combining the thermochemical data with empirical or machine learning techniques is a forthcoming opportunity. It has also been suggested that the ample data received from thermochemical calculations would be well suited for training expert systems and algorithms using methods of artificial intelligence.

Thermodynamic simulation is based on the thermodynamic property data. In addition to properties of pure substances, a process chemist will also need the data on how the elements and compounds behave when mixing and reacting with each other. The same basic data is then applicable to various processes - *e.g.* the mining water simulation tools developed by VTT include properties for approximately ten metal cations and five anions and the data is equally applicable in pulp and paper industry and wastewater management (Pajarre et al., 2018).

The aim for sustainable circular economy however creates new challenges. While interest to manage the non-process and trace elements in process industries has proliferated during the last few years, in the field of materials technology several tens of chemical elements have been adapted for commercial use both in industry and in consumer products. For the great

majority of their compounds only the property data of pure substances have been determined while the mixing model parameters are for most part unknown. A typical concurrent example are the lithium species, both in high temperature salt and slag mixtures as well as in aqueous solutions. The lack of adequate property data hampers both the design of primary extraction processes and the development of recycling technologies.

To a fair extent the elaborate thermodynamic experimental measurement can be replaced by computational methods. First principles or ab initio calculations combined with thermodynamic continuum models are already applicable to relatively simple high temperature systems. More complex cases such as aqueous solutions may be subjected to machine learning and artificial intelligence methods for deducing interaction parameters for new systems based on previously studied conditions of familiar systems. The obvious challenges for future research in this field are to overcome the discontinuities of some of the thermochemical data at phase transformation points and finding ways to select the appropriate training sets when developing parameters for unknown mixtures.

Supplying thermodynamic data for new unmeasured systems has traditionally been possible only by added experimental research, which is costly and time-consuming. In the new circular economy, the in-depth research of property data for the freshly adapted chemical elements and compounds in industrial use yet appears as an up-to-date task. While physicists and material scientists have harnessed the properties of the novel substances for various high-tech products, the process chemists must accept the challenge to quantify the interactions of these species when recovering and recycling them.

References

Abadi, M., Agarwal, A., Barham, P., Brevdo, E., Chen, Z., Citro, C., Corrado, G.S., Davis, A., Dean, J., Devin, M., Ghemawat, S., Goodfellow, I., Harp, A., Irving, G., Isard, M., Jozefowicz, R., Jia, Y., Kaiser, L., Kudlur, M., Levenberg, J., Mané, D., Schuster, M., Monga, R., Moore, S., Murray, D., Olah, C., Shlens, J., Steiner, B., Sutskever, I., Talwar, K., Tucker, P., Vanhoucke, V., Vasudevan, V., Viégas, F., Vinyals, O., Warden, P., Wattenberg, M., Wicke, M., Yu, Y., Zheng, X., 2015. TensorFlow: Large-scale machine learning on heterogeneous systems.

Abd-El-Khalek, D.E., Abd-El-Nabey, B.A., Abdel-kawi, M.A., Ebrahim, S., Ramadan, S.R., 2019. The inhibition of crystal growth of gypsum and barite scales in industrial water systems using green antiscalant. Water Supply. https://doi.org/10.2166/ws.2019.094

Alberty, R.A., 2003. Thermodynamics of Biochemical Reactions. John Wiley & Sons, Inc., Hoboken, NJ, USA. https://doi.org/10.1002/0471332607

Anaconda, n.d. Anaconda Software Distribution. Computer software.

Bale, C.W., Chartrand, P., Degterov, S.A., Eriksson, G., Hack, K., Ben Mahfoud, R., Melançon, J., Pelton, A.D., Petersen, S., 2002. FactSage thermochemical software and databases. Calphad 26, 189–228. https://doi.org/10.1016/S0364-5916(02)00035-4

Begum, N., Bari, F., Jamaludin, S.B., Hussin, K., 2012. Solvent extraction of copper, nickel and zinc by Cyanex 272. International Journal of Physical Sciences 7, 2905–2910. https://doi.org/10.5897/IJPS12.116

Blomberg, P.B.A., Koukkari, P., 2011. A systematic method to create reaction constraints for stoichiometric matrices. Computers & Chemical Engineering 35, 1238–1250. https://doi.org/10.1016/j.compchemeng.2010.07.024

Blomberg, P.B.A., Koukkari, P., 2009. The combination of transformed and constrained Gibbs energies. Mathematical Biosciences 220, 81–88. https://doi.org/10.1016/j.mbs.2009.04.004

Cents, A.H.G., Brilman, D.W.F., Versteeg, G.F., 2005. CO2 absorption in carbonate/bicarbonate solutions: The Danckwerts-criterion revisited. Chemical Engineering Science 60, 5830–5835. https://doi.org/10.1016/j.ces.2005.05.020

Chollet, F., others, 2015. Keras.

De Donder, T., Van Rysselberghe, P., 1936. Thermodynamic theory of affinity. Stanford University Press, Stanford.

Doubra, P., Kamran-Pirzaman, A., Mohammadi, A.H., Hassanalizadeh, R., 2017. Thermodynamic modelling of scale (Calcite, Barite, Anhydrite and Gypsum) deposition from brine. Journal of Molecular Liquids 230, 96–103. https://doi.org/10.1016/j.molliq.2016.11.135

Francey, S., Tran, H., Jones, A., 2009. Current status of alternative fuel use in lime kilns. Tappi Journal 8, 33–39.

Fredenslund, A., Gmehling, J., Rasmussen, P., 1977. Vapor-liquid Equilibria Using Unifac, Vapor-liquid Equilibria Using Unifac. Elsevier. https://doi.org/10.1016/b978-0-444-41621-6.x5001-7

Freyer, D., Voigt, W., 2003. Crystallization and Phase Stability of CaSO4 and CaSO4 - Based Salts. Monatshefte fur Chemie 134, 693–719. https://doi.org/10.1007/s00706-003-0590-3

Ghosh, U.K., Kentish, S.E., Stevens, G.W., 2009. Absorption of carbon dioxide into aqueous

potassium carbonate promoted by boric acid. Energy Procedia 1, 1075–1081. https://doi.org/10.1016/j.egypro.2009.01.142

Guo, W., Ngo, H.H., Li, J., 2012. A mini-review on membrane fouling. Bioresource Technology 122, 27–34. https://doi.org/10.1016/j.biortech.2012.04.089

Hack, K. (Ed.), 2008. The SGTE Casebook, 2nd ed. Woodhead Publishing Limited.

Hautala, M.H., 2016. Modeling of Electrolytic Solutions and Implementation of the Models in Flowbat. University of Oulu.

Heinonen, J., 1999. Sellutehtaiden lipeiden termodynaaminen mallinnus. KCL Report, Espoo.

Heinonen, J., 1998. Thermodynamic model for predicting chloride and potassium concentrations in the kraft chemical recovery cycle, in: International Chemical Recovery Conference. Tampa.

Hillert, M., 2007. Phase Equilibria, Phase Diagrams and Phase Transformations: Their Thermodynamic Basis, 2nd ed. Cambridge University Press, Cambridge.

Huckel, E., Debye, P., 1924. Zur Theorie der Elektrolyte. I. Gefrierpunktserniedrigung und verwandte Erscheinungen. Physikalische Zeitschrift 25.

Kaksonen, A., 2004. The Performance, Kinetics and Microbiology of Sulfidogenic Fluidized-Bed Reactors Treating Acidic Metal-and Sulfate-Containing Wastewater. Publication. Tampere University of Technology.

Kangas, P., Pajarre, R., Penttilä, K., Vahala, P., 2019. Latest in modelling symposium - in honour of professor Pertti Koukkari's 65th birthday. p. 47.

Kangas, P., Vidal Vázquez, F., Savolainen, J., Pajarre, R., Koukkari, P., 2017. Thermodynamic modelling of the methanation process with affinity constraints. Fuel 197, 217–225. https://doi.org/10.1016/j.fuel.2017.02.029

Kattelus, J., 2020. Artificial Neural Networks for Predicting Pitzer Parameters Based on Ion Specific Properties. Aalto University.

Ketonen, M., Penttilä, K., Koukkari, P., 1997. Simulation studies of a calcination kiln process, in: ECC 1997 - European Control Conference.

Kiepe, J., Noll, O., Gmehling, J., 2006. Modified LIQUAC and modified LIFAC - A further development of electrolyte models for the reliable prediction of phase equilibria with strong electrolytes. Industrial and Engineering Chemistry Research 45, 2361–2373. https://doi.org/10.1021/ie0510122

Kluyver, T., Ragan-Kelley, B., Pérez, F., Granger, B., Bussonnier, M., Frederic, J., Kelley, K., Hamrick, J., Grout, J., Corlay, S., Ivanov, P., Avila, D., Abdalla, S., Willing, C., 2016. Jupyter Notebooks – a publishing format for reproducible computational workflows, in: Loizides, F., Schmidt, B. (Eds.), Positioning and Power in Academic Publishing: Players, Agents and Agendas. IOS Press, pp. 87–90. https://doi.org/10.3233/978-1-61499-649-1-87

Knuutila, H., Hessen, E.T., Kim, I., Haug-Warberg, T., Svendsen, H.F., 2010. Vapor-liquid equilibrium in the sodium carbonate-sodium bicarbonate-water-CO2-system. Chemical Engineering Science 65, 2218–2226. https://doi.org/10.1016/j.ces.2009.12.024

Koschorreck, M., 2008. Microbial sulphate reduction at a low pH. FEMS Microbiology Ecology 64, 329–342. https://doi.org/10.1111/j.1574-6941.2008.00482.x

Koukkari, P., 2009. Advanced Gibbs Energy Methods for Functional Materials and Processes – ChemSheet 1999–2009.

Koukkari, P., 1995. A physico-chemical reactor calculation by successive stationary states (Dissertation, Helsinki University of Technology). Acta polytechnica Scandinavica. Chemical technology series. The Finnish Academy of Technology, Ch 224, 60 pp.

Koukkari, P., 1993. A physico-chemical method to calculate time-dependent reaction mixtures. Computers & Chemical Engineering 17, 1157–1165. https://doi.org/10.1016/0098-1354(93)80096-6

Koukkari, P., Pajarre, R., 2021. Phase diagrams with the driving force and extent of reaction as axis variables. Calphad, in press. https://doi.org/10.1016/j.calphad.2021.102290

Koukkari, P., Pajarre, R., 2006. Calculation of constrained equilibria by Gibbs energy minimization. Calphad 30, 18–26. https://doi.org/10.1016/j.calphad.2005.11.007

Koukkari, P., Pajarre, R., Hack, K., 2001. Setting Kinetic Controls for Complex Equilibrium Calculations. Zeitschrift für Metallkunde 92, 1151–1157.

Koukkari, P., Pajarre, R., Kangas, P., 2018. Thermodynamic affinity in constrained free-energy systems. Monatshefte fur Chemie 149, 381–394. https://doi.org/10.1007/s00706-017-2095-5

Koukkari, P., Penttilä, K., Hack, K., Petersen, S., 2000. CHEMSHEET – An Efficient Worksheet Tool for Thermodynamic Process Simulation, in: Microstructures, Mechanical Properties and Processes - Computer Simulation and Modelling. Wiley-VCH Verlag GmbH & Co. KGaA, Weinheim, FRG, pp. 323–330. https://doi.org/10.1002/3527606157.ch51

Kyllönen, H., Grönroos, A., Järvelä, E., Heikkinen, J., Tang, C., 2016. Experimental Aspects of Scaling Control in Membrane Filtration of Mine Water. Mine Water and the Environment 36, 193–198. https://doi.org/10.1007/s10230-016-0415-3

Leppävuori, J., Koukkari, P., 2012. BIOSCEN Modelling Biorefinery Scenarios.

Li, J., Polka, H.M., Gmehling, J., 1994. A gE model for single and mixed solvent electrolyte systems. 1. Model and results for strong electrolytes. Fluid Phase Equilibria 94, 89–114. https://doi.org/10.1016/0378-3812(94)87052-7

Liu, Z.-K., Wang, Y., 2016. Computational Thermodynamics of Materials, Computational Thermodynamics of Materials. https://doi.org/10.1017/cbo9781139018265

Melin, K., 2009. Personal communication.

Metso Outotec, 2020. HSC Chemistry 10 simulation software.

Meyer, V., Pisch, A., Penttilä, K., Koukkari, P., 2016. Computation of steady state thermochemistry in rotary kilns: Application to the cement clinker manufacturing process. Chemical Engineering Research and Design 115, 335–347. https://doi.org/10.1016/j.cherd.2016.08.007

Mohs, A., Gmehling, J., 2013. A revised LIQUAC and LIFAC model (LIQUAC*/LIFAC*) for the prediction of properties of electrolyte containing solutions. Fluid Phase Equilibria 337, 311–322. https://doi.org/10.1016/j.fluid.2012.09.023

Møller, N., 1988. The prediction of mineral solubilities in natural waters: A chemical equilibrium model for the Na-Ca-Cl-SO4-H2O system, to high temperature and concentration. Geochimica et Cosmochimica Acta 52, 821–837. https://doi.org/10.1016/0016-7037(88)90354-7

Outotec, 2018. HSC Chemistry 9.8 simulation software.

Pajarre, R., 2016. Modelling of chemical processes and materials by free energy minimization. Doctoral thesis, Aalto University.

Pajarre, R., Koukkari, P., 2018. CALPHAD aqueous solution model based on the BET approach: General theory. Calphad 63, 1–5. https://doi.org/10.1016/j.calphad.2018.06.007

Pajarre, R., Koukkari, P., n.d. CALPHAD aqueous solution model based on the BET approach: Multicomponent solutions. to be published.

Pajarre, R., Koukkari, P., Kangas, P., 2018. Industrial and mine water chemistry Advanced aqueous database for modelling industrial processes, VTT Technology Report 321. Espoo.

Pajarre, R., Koukkari, P., Kangas, P., 2016. Constrained and extended free energy minimisation for modelling of processes and materials. Chemical Engineering Science 146, 244–258. https://doi.org/10.1016/j.ces.2016.02.033

Pajarre, R., Koukkari, P., Nappa, M., n.d. Oxidation – reduction potentials in multicomponent non-equilibrium free enrgy models. to be published.

Pedregosa, F., Varoquaux, G., Gramfort, A., Michel, V., Thirion, B., Grisel, O., Blondel, M., Prettenhofer, P., Weiss, R., Dubourg, V., Vanderplas, J., Passos, A., Cournapeau, D., Brucher, M., Perrot, M., Duchesnay, É., 2011. Scikit-learn: Machine Learning in Python. JMLR 12, 2825−2830.

Pelton, A.D., Eriksson, G., Hack, K., Bale, C.W., 2018. Thermodynamic calculation of aqueous phase diagrams. Monatshefte für Chemie - Chemical Monthly 149, 395–409. https://doi.org/10.1007/s00706-017-2094-6

Pelton, A.D., Koukkari, P., Pajarre, R., Eriksson, G., 2014. Para-equilibrium phase diagrams. The Journal of Chemical Thermodynamics 72, 16–22. https://doi.org/10.1016/j.jct.2013.12.023

Petersen, S., Hack, K., 2007. The thermochemistry library ChemApp and its applications. Zeitschrift fuer Metallkunde/Materials Research and Advanced Techniques 98, 935–945. https://doi.org/10.3139/146.101551

Pitzer, K.S., 1991. Activity coefficients in electrolyte solutions, 2nd ed. CRC Press, Boca Raton, FL.

Pitzer, K.S., Mayorga, G., 1973. Thermodynamics of electrolytes. II. Activity and osmotic coefficients for strong electrolytes with one or both ions univalent. The Journal of Physical Chemistry 77, 2300–2308. https://doi.org/10.1021/j100638a009

plaidML, 2019. plaidML.

Reis, M.A.M., Almeida, J.S., Lemos, P.C., Carrondo, M.J.T., 1992. Effect of hydrogen sulfide on growth of sulfate reducing bacteria. Biotechnology and Bioengineering 40, 593–600. https://doi.org/10.1002/bit.260400506

Roth, A., 2020. Artificial intelligence applications in chemical process models. Otto-von-Guericke-Universit at Magdeburg.

Shenvi, S.S., Isloor, A.M., Ismail, A.F., 2015. A review on RO membrane technology: Developments and challenges. Desalination. https://doi.org/10.1016/j.desal.2014.12.042

Stokes, R.H., Robinson, R.A., 1966. Interactions in Aqueous Nonelectrolyte Solutions. I. Solute-Solvent Equilibria. The Journal of Physical Chemistry 70, 2126–2131. https://doi.org/10.1021/j100879a010

Stokes, R.H., Robinson, R.A., 1948. Ionic Hydration and Activity in Electrolyte Solutions. Journal of the American Chemical Society 70, 1870–1878. https://doi.org/10.1021/ja01185a065

Wallin, M., Olausson, S., 1993. Simultaneous absorption of H2S and CO2 into a solution of sodium carbonate. Chem. Eng. Comm. 123, 43–59.

Wylock, C.E., Colinet, P., Cartage, T., Haut, B., 2008. Coupling between mass transfer and chemical reactions during the absorption of CO2 in a NaHCO3-Na2CO3 brine: Experimental and theoretical study. International Journal of Chemical Reactor Engineering 6. https://doi.org/10.2202/1542-6580.1502

Yan, W., Topphoff, M., Rose, C., Gmehling, J., 1999. Prediction of vapor-liquid equilibria in mixed-solvent electrolyte systems using the group contribution concept. Fluid Phase Equilibria 162, 97–113. https://doi.org/10.1016/S0378-3812(99)00201-0

Zeino, A., Albakri, M., Khaled, M., Zarzour, M., 2018. Comparative study of the synergistic effect of ATMP and DTPMPA on CaSO4 scale inhibition and evaluation of induction time effect. Journal of Water Process Engineering 21, 1–8. https://doi.org/10.1016/j.jwpe.2017.11.013

Zünd, A., 2007. Modelling the Thermodynamics of Mixed Organic-Inorganic Aerosols to Predict Water Activities and Phase Separations. ETH ZURICH. https://doi.org/10.3929/ethz-a-005582922